WIND-TUNNEL STUDY OF
TAIKOO SHING CITY PLAZA SITE B, HONG KONG

by

J. A. Peterka* and J. E. Cermak**

for

Ove Arup & Partners Hong Kong Ltd.
16th Floor East Town Building
41 Lockhart Road
Hong Kong

Fluid Mechanics and Wind Engineering Program
Fluid Dynamics and Diffusion Laboratory
Department of Civil Engineering
Colorado State University
Fort Collins, Colorado 80523

CSU Project 2-95040

July 1982

*Associate Professor
**Professor-in-Charge, Fluid Mechanics and
Wind Engineering Program

CER82-83JAP-JEC10

TABLE OF CONTENTS

LIST OF FIGURES

LIST OF TABLES

LIST OF SYMBOLS

Symbol	Definition
U	Local mean velocity
D	Characteristic dimension (building height, width, etc.)
ν, ρ	Kinematic viscosity and density of approach flow
$\frac{UD}{\nu}$	Reynolds number
E	Mean voltage
A, B, n	Constants
U_{rms}	Root-mean-square of fluctuating velocity
E_{rms}	Root-mean-square of fluctuating voltage
U_∞	Reference mean velocity outside the boundary layer
X, Y	Horizontal coordinates
Z	Height above surface
δ	Height of boundary layer
T_u	Turbulence intensity $\frac{U_{rms}}{U_\infty}$ or $\frac{U_{rms}}{U}$
$C_{p_{mean}}$	Mean pressure coefficient, $\frac{(p-p_\infty)_{mean}}{0.5\ \rho\ U_\infty^2}$
$C_{p_{rms}}$	Root-mean-square pressure coefficient, $\frac{\left((p-p_\infty)-(p-p_\infty)_{mean}\right)_{rms}}{0.5\ \rho\ U_\infty^2}$
$C_{p_{max}}$	Peak maximum pressure coefficient, $\frac{(p-p_\infty)_{max}}{0.5\ \rho\ U_\infty^2}$
$C_{p_{min}}$	Peak minimum pressure coefficient, $\frac{(p-p_\infty)_{min}}{0.5\ \rho\ U_\infty^2}$
$(\ )_{min}$	Minimum value during data record
$(\ )_{max}$	Maximum value during data record

Symbol	Definition
p	Fluctuating pressure at a pressure tap on the structure
p_∞	Static pressure in the wind tunnel above the model
F_x, F_y	Forces in X, Y direction
A_R	Reference Area
CF_X	Force coefficient, X direction, $\dfrac{F_x}{A_R \; 0.5\rho \; U_\infty^2}$
CF_Y	Force coefficient, Y direction, $\dfrac{F_y}{A_R \; 0.5\rho \; U_\infty^2}$

1. INTRODUCTION

1.1 General

A significant characteristic of modern building design is lighter cladding and more flexible frames. These features produce an increased vulnerability of glass and cladding to wind damage and result in larger deflections of the building frame. In addition, increased use of pedestrian plazas at the base of the buildings has brought about a need to consider the effects of wind and gustiness in the design of these areas.

The building geometry itself may increase or decrease wind loading on the structure. Wind forces may be modified by nearby structures which can produce beneficial shielding or adverse increases in loading. Overestimating loads results in uneconomical design; underestimating may result in cladding or window failures. Tall structures have historically produced unpleasant wind and turbulence conditions at their bases. The intensity and frequency of objectionable winds in pedestrian areas is influenced both by the structure shape and by the shape and position of adjacent structures.

Techniques have been developed for wind tunnel modeling of proposed structures which allow the prediction of wind pressures on cladding and windows, overall structural loading, and also wind velocities and gusts in pedestrian areas adjacent to the building. Information on sidewalk-level gustiness allows plaza areas to be protected by design changes before the structure is constructed. Accurate knowledge of the intensity and distribution of the pressures on the structure permits adequate but economical selection of cladding strength to meet selected maximum design winds and overall wind loads for the design of the frame for flexural control.

Modeling of the aerodynamic loading on a structure requires special consideration of flow conditions in order to guarantee similitude between model and prototype. A detailed discussion of the similarity requirements and their wind-tunnel implementation can be found in references (1), (2), and (3). In general, the requirements are that the model and prototype be geometrically similar, that the approach mean velocity at the building site have a vertical profile shape similar to the full-scale flow, that the turbulence characteristics of the flows be similar, and that the Reynolds number for the model and prototype be equal.

These criteria are satisfied by constructing a scale model of the structure and its surroundings and performing the wind tests in a wind tunnel specifically designed to model atmospheric boundary-layer flows. Reynolds number similarity requires that the quantity UD/ν be similar for model and prototype. Since ν, the kinematic viscosity of air, is identical for both, Reynolds numbers cannot be made precisely equal with reasonable wind velocities. To accomplish this the air velocity in the wind tunnel would have to be as large as the model scale factor times the prototype wind velocity, a velocity which would introduce unacceptable compressibility effects. However, for sufficiently high Reynolds numbers ($>2\times10^4$) the pressure coefficient at any location on the structure will be essentially constant for a large range of Reynolds numbers. Typical values encountered are 10^7-10^8 for the full-scale and 10^5-10^6 for the wind-tunnel model. In this range acceptable flow similarity is achieved without precise Reynolds number equality.

1.2 The Wind-Tunnel Test

The wind-engineering study is performed on a building or building group modeled at scales ranging from 1:150 to 1:400. The building model

is constructed of clear plastic fastened together with screws. The structure is modeled in detail to provide accurate flow patterns in the wind passing over the building surfaces. The building under test is often located in a surrounding where nearby buildings or terrain may provide beneficial shielding or adverse wind loading. To achieve similarity in wind effects the area surrounding the test building is also modeled. A flow visualization study is first made (smoke is used to make the air currents visible) to define overall flow patterns and identify regions where local flow features might cause difficulties in building curtain-wall design or produce pedestrian discomfort.

The test model, equipped with pressure taps (200 to 600 or more), is exposed to an appropriately modeled atmospheric wind in the wind tunnel and the fluctuating pressure at each tap measured electronically. The model, and the modeled area, are rotated 10 or 15 degrees and another set of data recorded for each pressure tap. Normally, 24 or 36 sets of data (360 degrees of turning) are taken; however, when flow visualization or recorded data indicate high pressure regions of small azimuthal extent, data is obtained in smaller azimuthal steps.

Data are recorded, analyzed and processed by an on-line computerized data-acquisition system. Pressure coefficients of several types are calculated by the computer for each reading on each piezometer tap and are printed in tabular form as computer readout. Using wind data applicable to the building site, representative wind velocities are selected for combination with measured pressures on the building model. Integration of test data with wind data results in prediction of peak local wind pressures for design of glass or cladding and may include overall forces and moments on the structure (by floor if desired) for design of

the structural frame. Pressure contours are drawn on the developed building surfaces showing the intensity and distribution of peak wind loads on the building. These results may be used to divide the building into zones where lighter or heavier cladding or glass may be desirable.

Based on the visualization (smoke) tests and on a knowledge of heavy pedestrian use areas, a dozen or more locations may be chosen at the base of the building where wind velocities can be measured to determine the relative comfort or discomfort of pedestrians in plaza areas, near building entrances, near building corners, or on sidewalks. Usually a reference pedestrian position is also tested to determine whether the wind environment in the building area is better or worse than the environment a block or so away in an undisturbed area.

The following pages discuss in greater detail the procedures followed and the equipment and data collecting and processing methods used. In addition, the data presentation format is explained and the implications of the data are discussed.

2. EXPERIMENTAL CONFIGURATION

2.1 Wind Tunnel

Wind-engineering studies are performed in the Fluid Dynamics and Diffusion Laboratory at Colorado State University (Figure 1). Three large wind tunnels are available for wind loading studies depending on the detailed requirements of the study. The wind tunnel used for this investigation is shown in Figure 2. All tunnels have a flexible roof adjustable in height to maintain a zero pressure gradient along the test section. The mean velocity can be adjusted continuously in each tunnel to the maximum velocity available.

2.2 Model

In order to obtain an accurate assessment of local pressures using piezometer taps, models are constructed to the largest scale that does not produce significant blockage in the wind-tunnel test section. The models are constructed of 1/2 in. thick Lucite plastic and fastened together with metal screws. Significant variations in the building surface, such as mullions, are machined into the plastic surface. Piezometer taps (1/16 in. diameter) are drilled normal to the exterior vertical surfaces in rows at several or more elevations between the bottom and top of the building. Similarly, taps are placed in the roof and on any sloping, protruding, or otherwise distinctive features of the building that might need investigation.

Pressure tap locations are chosen so that the entire surface of the building can be investigated for pressure loading and at the same time permit critical examination of areas where experience has shown that maximum wind effects may be expected to occur. Locations of the pressure taps for this study are shown in Figure 3. Dimensions are

given both for full-scale building (in ft) and for model (in in.). The pressure tap numbers are shown adjacent to the taps.

The pressure tests are sometimes made in two stages. In the first stage measurements are made on the initial distribution of pressure taps. If it becomes apparent from the data that the loading on the building is being influenced by some unsuspected geometry of the building or adjacent structures, additional pressure taps are installed in the critical areas. The locations of the taps are selected so that the maximum loading can be detected and the area over which this loading is acting can be defined. Any added taps are also shown in Figure 3.

A circular area 750 to 2000 ft in radius depending on model scale and characteristics of the surrounding buildings and terrain is modeled in detail. Structures within the modeled region are made from styrofoam and cut to the individual building geometries. They are mounted on the turntable in their proper locations. Significant terrain features are included as needed. The model is mounted on a turntable (Figure 2) near the downwind end of the test section. Any buildings or terrain features which do not fit on the turntable are placed on removable pieces which are placed upwind of the turntable for appropriate wind directions. A plan view of the building and its surroundings is shown in Figure 4. The turntable is calibrated to indicate azimuthal orientation to 0.1 degree.

The region upstream from the modeled area is covered with a randomized roughness constructed using various sized cubes placed on the floor of the wind tunnel. Different roughness sizes may be used for different wind directions. Spires are installed at the test-section entrance to provide a thicker boundary layer than would otherwise be

available. The thicker boundary layer permits a somewhat larger scale model than would otherwise be possible. The spires are approximately triangularly shaped pieces of 1/2 in. thick plywood 6 in. wide at the base and 1 in. wide at the top, extending from the floor to the top of the test section. They are placed so that the broad side intercepts the flow. A barrier approximately 8 in. high is placed on the test-section floor downstream of the spires to aid in development of the boundary-layer flow.

The distribution of the roughness cubes and the spires in the roughened area was designed to provide a boundary-layer thickness of approximately 4 ft, a velocity profile power-law exponent similar to that expected to occur in the region approaching the modeled area for each wind direction (a number of wind directions may have the same approach roughness). A photograph of the completed model in the wind tunnel is shown in Figure 5. The wind-tunnel ceiling is adjusted after placement of the model to obtain a zero pressure gradient along the test section.

3. INSTRUMENTATION AND DATA ACQUISITION

3.1 Flow Visualization

Making the air flow visible in the vicinity of the model is helpful (a) in understanding and interpreting mean and fluctuating pressures, (b) in defining zones of separated flow and reattachment and zones of vortex formation where pressure coefficients may be expected to be high and (c) in indicating areas where pedestrian discomfort may be a problem. Titanium tetrachloride smoke is released from sources on and near the model to make the flow lines visible to the eye and to make it possible to obtain motion picture records of the tests. Conclusions obtained from these smoke studies are discussed in Sections 4.1 and 5.1.

3.2 Pressures

Mean and fluctuating pressures are measured at each of the pressure taps on the model structure. Data are obtained for 24 or 36 wind directions, rotating the entire model assembly in a complete circle. Seventy-six pieces of 1/16 in. I.D. plastic tubing are used to connect 76 pressure ports at a time to an 80 tap pressure switch mounted inside the model. The switch was designed and fabricated in the Fluid Dynamics and Diffusion Laboratory to minimize the attenuation of pressure fluctuations across the switch. Each of the 76 measurement ports is directed in turn by the switch to one of four pressure transducers mounted close to the switch. The four pressure input taps not used for transmitting building surface pressures are connected to a common tube leading outside the wind tunnel. This arrangement provides both a means of performing in-place calibration of the transducers and, by connecting this tube to a pitot tube mounted inside the wind tunnel, a means of automatically monitoring the tunnel speed. The switch is operated by means of a shaft projecting through

the floor of the wind tunnel. A computer-controlled stepping motor steps the switch into each of the 20 required positions. The computer keeps track of switch position but a digital readout of position is provided at the wind tunnel.

The pressure transducers used are setra differential transducers (Model 237) with a 0.10 psid range. Reference pressures are obtained by connecting the reference sides of the four transducers, using plastic tubing, to the static side of a pitot-static tube mounted in the wind tunnel free stream above the model building. In this way the transducer measures the instantaneous difference between the local pressures on the surface of the building and the static pressure in the free stream above the model.

Output from the pressure transducers is fed to an on-line data acquisition system consisting of a Hewlett-Packard 21 MX computer, disk unit, card reader, printer, Digi-Data digital tape drive and a Preston Scientific analog-to-digital converter. The data are processed immediately into pressure coefficient form as described in Section 4.3 and stored for printout or further analysis.

All four transducers are recorded simultaneously for 16 seconds at a 250 sample per second rate. The results of an experiment to determine the length of record required to obtain stable mean and rms (root-mean-square) pressures and to determine the overall accuracy of the pressure data acquisition system is shown in Figure 6. A typical pressure port record was integrated for a number of different time periods to obtain the data shown. Examination of a large number of pressure taps showed that the overall accuracy for a 16 second period is, in pressure coefficient form, 0.03 for mean pressures, 0.1 for peak pressures, and 0.01 for rms pressures. Pressure coefficients are defined in Section 4.3.

3.3 Velocity

Mean velocity and turbulence intensity profiles are measured upstream of the model to determine that an approach boundary-layer flow appropriate to the site has been established. Tests are made at one wind velocity in the tunnel. This velocity is well above that required to produce Reynolds number similarity between the model and the prototype as discussed in Section 1.1.

In addition, mean velocity and turbulence intensity measurements are made 5 to 7 ft (prototype) above the surface at a dozen or more locations on and near the building for 16 wind directions. The measurement locations are shown on Figure 4. The surface measurements are indicative of the wind environment to which a pedestrian at the measurement location would be subjected. The locations are chosen to determine the degree of pedestrian comfort or discomfort at the building corners where relatively severe conditions frequently are found, near building entrances and on adjacent sidewalks where pedestrian traffic is heavy, and in open plaza areas. In most studies a reference pedestrian position, located about a block away, is also tested. These data are helpful in evaluating the degree of pedestrian comfort or discomfort in the proposed plaza area in terms of the undisturbed environment in the immediate vicinity.

Measurements are made with a single hot-wire anemometer mounted with its axis vertical. The instrumentation used is a Thermo Systems constant temperature anemometer (Model 1050) with a 0.001 in. diameter platinum film sensing element 0.020 in. long. Output is directed to the on-line data acquisition system for analysis.

Calibration of the hot-wire anemometer is performed by comparing output with the pitot-static tube in the wind tunnel. The calibration

data are fit to a variable exponent King's Law relationship of the form

$$E^2 = A + BU^n$$

where E is the hot-wire output voltage, U the velocity and A, B, and n are coefficients selected to fit the data. The above relationship was used to determine the mean velocity at measurement points using the measured mean voltage. The fluctuating velocity in the form U_{rms} (root-mean-square velocity) was obtained from

$$U_{rms} = \frac{2\ E\ E_{rms}}{B\ n\ U^{n-1}}$$

where E_{rms} is the root-mean-square voltage output from the anemometer. For interpretation all turbulence measurements for pedestrian winds were divided by the mean velocity outside the boundary-layer U_∞. Turbulence intensity in velocity profile measurements used the local mean velocity.

4. RESULTS

4.1 Flow Visualization

A film is included as part of this report showing the characteristics of flow about the structure using smoke to make the flow visible. A listing of the contents of the film is shown in Table 1. Several features can be noted from the visualization. As with all large structures, wind approaching the building is deflected down to the plaza level, up over the structure and around the sides. A description of the smoke test results emphasizing flow patterns of concern relative to possible high-wind load areas and pedestrian comfort is given in Section 5.1.

4.2 Velocity

Velocity and turbulence profiles are shown in Figure 7. Profiles were taken upstream from the model which are characteristic of the boundary layer approaching the model and sometimes at the building site with building removed. The boundary-layer thickness, δ, is shown in Figure 7. The corresponding prototype value of δ for this study is also shown in the figure. This value was established as a reasonable height for this study. The mean velocity profile approaching the modeled area has the form

$$\frac{U}{U_\infty} = \left(\frac{z}{\delta}\right)^n .$$

The exponent n for the approach flow established for this study is shown in Figure 7.

Profiles of longitudinal turbulence intensity in the flow approaching the modeled area are shown in Figure 7. The turbulence intensities are appropriate for the approach mean velocity profile selected. For the velocity profiles, turbulence intensity is defined

as the root-mean-square about the mean of the longitudinal velocity fluctuations divided by the local mean velocity U,

$$Tu = \frac{U_{rms}}{U} .$$

Velocity data obtained at each of the pedestrian measurement locations shown in Figure 4 are listed in Table 2 as mean velocity U/U_∞, turbulence intensity U_{rms}/U_∞, and largest effective gust

$$U_{pk} = \frac{U + 3U_{rms}}{U_\infty} .$$

These data are plotted in polar form in Figure 8. Measurements were taken 5 to 7 ft above the ground surface. A site map is superimposed on the polar plots to aid in visualization of the effects of the nearby structures on the velocity and turbulence magnitudes. An analysis of these wind data is given in Section 5.2.

To enable a quantitative assessment of the wind environment, the wind-tunnel data were combined with wind frequency and direction information obtained at the local airport. Table 3 shows wind frequency by direction and magnitude obtained from summaries published by the National Weather Service. These data, usually obtained at an elevation of about 30-40 ft, were converted to velocities at the reference velocity height for the wind-tunnel measurements and combined with the wind-tunnel data to obtain cumulative probability distributions (percent time a given velocity is exceeded) for wind velocity at each measuring location. The percentage times were summed by wind direction to obtain a percent time exceeded at each measuring position independent of wind direction (but accounting for the fact that the wind blows from different directions with varying frequency). These results are plotted in Figure 9.

Interpretation of Figure 9 is aided by a description of the effects of wind of various magnitudes on people. The earliest quantitative description of wind effects was established by Sir Francis Beaufort in 1806 for use at sea and is still in use today. Several recent investigators have added to the knowledge of wind effects on pedestrians. These investigations along with suggested criteria for acceptance have been summarized by Penwarden and Wise (4) and Melbourne (5). The Beaufort scale (from ref. 4), based on mean velocity only, is reproduced as Table 4 including qualitative descriptions of wind effects. Table 4 suggests that mean wind speeds below 12 mph are of minor concern and that mean speeds above 24 mph are definitely inconvenient. Quantitative criteria for acceptance from reference 5 are superimposed as dashed lines on Figure 9. The peak gust curves shown in Figure 9 are the percent of time during which a short gust of the stated magnitude could occur (say about one of these gusts per hour). Implications of the data plotted in Figure 9 are presented in Section 5.2.

Because some pedestrian wind measuring positions are purposely chosen at sites where the smoke tests showed large velocities of small spacial extent, the general wind environment about the structure may be less severe than one might infer from a strict analysis of Table 2 and Figure 9.

4.3 Pressures

For each of the pressure taps examined at each wind direction, the data record is analyzed to obtain four separate pressure coefficients. The first is the mean pressure coefficient

$$C_{p_{mean}} = \frac{(p-p_\infty)_{mean}}{0.5\ \rho\ U_\infty^2}$$

where the symbols are as defined in the List of Symbols. It represents the mean of the instantaneous pressure difference between the building pressure tap and the static pressure in the wind tunnel above the building model, nondimensionalized by the dynamic pressure

$$0.5\ \rho\ U_\infty^2$$

at the reference velocity position. This relationship produces a dimensionless coefficient which indicates that the mean pressure difference between building and ambient wind at a given point on the structure is some fraction less or some fraction greater than the undisturbed wind dynamic pressure near the upper edge of the boundary layer. Using the measured coefficient, prototype mean pressure values for any wind velocity may be calculated.

The magnitude of the fluctuating pressure is obtained by the rms pressure coefficient

$$C_{p_{rms}} = \frac{\left((p-p_\infty) - (p-p_\infty)_{mean}\right)_{rms}}{0.5\ \rho\ U_\infty^2}$$

in which the numerator is the root-mean-square of the instantaneous pressure difference about the mean .

If the pressure fluctuations followed a Gaussian probability distribution, no additional data would be required to predict the

frequency with which any given pressure level would be observed. However, the pressure fluctuations do not, in general, follow a Gaussian probability distribution so that additional information is required to show the extreme values of pressure expected. The peak maximum and peak minimum pressure coefficients are used to determine these values:

$$C_{p_{max}} = \frac{(p-p_\infty)_{max}}{0.5\ \rho\ U_\infty^2}$$

$$C_{p_{min}} = \frac{(p-p_\infty)_{min}}{0.5\ \rho\ U_\infty^2}$$

The values of $p-p_\infty$ which were digitized at 250 samples per second for 16 seconds, representing about one hour of time in the full-scale, are examined individually by the computer to obtain the most positive and most negative values during the 16-second period. These are converted to $C_{p_{max}}$ and $C_{p_{min}}$ by nondimensionalizing with the free stream dynamic pressure.

The four pressure coefficients are calculated by the on-line data acquisition system computer and tabulated along with the approach wind azimuth in degrees from true north. The list of coefficients is included as Appendix A. The pressure tap code numbers used in the appendix are explained in Figure 3.

To determine the largest peak loads acting at any point on the structure for cladding design purposes, the pressure coefficients for all wind directions were searched to obtain, at each pressure tap, the largest peak positive and peak negative pressure coefficients. Table 6 lists the larger values and associated wind directions. Included in Section 5.3 is an analysis of the coefficients of Table 6 including the maximum values obtained and where they occurred on the building.

The pressure coefficients of Table 6 can be converted to full-scale loads by multiplication by a suitable reference pressure selected for the field site. This reference pressure is represented in the equations for pressure coefficients by the $0.5\ \rho\ U_\infty^2$ denominator. This value is the dynamic pressure associated with an hourly mean wind at the reference velocity measurement position at the edge of the boundary layer. In general, the method of arriving at a design reference pressure for a particular site involves selection of a design wind velocity, translation of the velocity to an hourly mean wind at the reference velocity location and conversion to a reference pressure. Selection of the design velocity can be made from statistical analysis of extreme wind data or selected from wind maps contained in the proposed wind loading code ANSI A58.1 of the American National Standards Institute (6). The calculation of reference pressure for this study is shown in Table 5. The factor used in Table 5 to reduce gust winds to hourly mean winds is given in reference (7).

The reference pressure associated with the design hourly mean velocity at the reference velocity location can be used directly with the peak-pressure coefficients to obtain peak local design wind loads for cladding design. Local, instantaneous peak loads on the full-scale building suitable for cladding design were computed by multiplying the reference pressure of Table 5 by the peak coefficients of Table 6 and are listed as peak pressures in that table. The maximum psf loads given at each tap location are the largest peak positive and peak negative values found in the tests. For ease in visualizing the loads on the structure, contours of equal peak pressures for cladding load shown in Table 6 have been plotted on developed elevation views of the structure,

Figure 10. If a data point which is taken in the basic model configuration is retaken in a resolution configuration, the data are averaged in preparing Figure 10. For control of water infiltration from outside to inside, the largest positive (inward-acting) pressure at each tap location is tabulated in Table 6.

For glass design pressures, a glass load factor is used to account for the different duration between measured peak pressures and the one minute loading commonly used in glass design charts. The design pressure used for glass is normally less than the peak pressures used for cladding design because of the static fatigue property of glass which can withstand higher pressures for short duration loads than for long duration loads. Recent research (8) indicates that the period of application of the peak pressures reported herein is about 5-10 seconds or less. If a glass design is based on these peak-pressure values, then a glass strength associated with this duration load should be used. Because glass design charts are normally based on some alternate load duration -- usually one minute -- then some reduction in peak loads should be made. An estimate of a load reduction factor can be obtained from an empirical relation of glass strength as a function of load duration. Current glass selection charts showing glass strength as a function of load duration (9) and older references (10) indicate the following load reduction factors:

	ref 9	ref 10
annealed float	0.80	0.81
heat strengthened	0.94	
tempered	0.97	0.98

Loadings appropriate for glass design can be computed by multiplying the peak-pressure loads of Table 6 by these load factors.

4.4 Forces and Moments

Force coefficients in the horizontal X and Y directions and moment coefficients about the X, Y, and Z axes with the origin at ground level at the base of the building with Z axis vertical may be computed for all wind directions tested by integration of mean pressures on the building. Overall forces and moments acting on the full-scale building due to wind loading which are useful in designing the structural framing of the proposed building may be obtained from use of these coefficients.

Force coefficients were computed for each floor for each wind direction using the equations shown below.

$$CF_X = \frac{F_X}{A_R \; 0.5 \; \rho \; U_\infty^2} \qquad CF_Y = \frac{F_Y}{A_R \; 0.5 \; \rho \; U_\infty^2}$$

Terms and symbols used in the equations are defined in the List of Symbols and the axes are defined for the building in Figure 3. Force coefficients CF_X and CF_Y were computed for the horizontal forces acting along the X and Y axes using the mean pressure coefficient at each pressure tap. A_R represents a constant reference area for nondimensionalization of the forces and moments.

The total forces acting on the full-scale building for each floor and wind direction were computed by multiplying the above coefficients by the appropriate full-scale reference area, by the reference pressure of Table 5, and by a gust load factor selected for an appropriate wind gust duration. The gust load factor, shown in Table 5, was selected to increase the loads from an hourly mean load to that of a gust whose duration would be sufficient for its effect to be fully felt by the structure. A table of gust load factors for various gust durations is

incorporated in Table 5 so that force and moment data of Table 7 may be adjusted to a different load duration if desired.

The forces obtained at each floor were used to obtain load, shear, and moment diagrams for the building for each wind direction. The shear diagram, in kips, was obtained by algebraic sum of all forces in each coordinate direction acting above the floor of interest. The load diagram, in psf, was obtained by dividing the shear values by their contributing areas (listed in Table 7). The moment diagram, in 1000 ft-kips, was obtained by integration of the shear values so that the moment due to forces acting above the floor level of interest was calculated. The sign of the moment was established by the right-hand rule about an X', Y' axis through the floor of interest. Moments about the Z axis were calculated by considering the displacement of forces in the X and Y directions from the Z axis shown in Figure 3. Eccentricities were computed such that the product of the Y force and X eccentricity minus the product of the X force and Y eccentricity equaled the Z moment. Load, shear, and moment diagrams are shown in Figure 11 for several wind directions.

5. DISCUSSION

5.1 Flow Visualization

Flow patterns identified with smoke showed that the largest pressures should be found near corners of the building. Because of the buildup of adjacent buildings to the east and west and the hill to the south, the number of locations where high pressures are observed should be less than on a structure with small adjacent buildings. Vortex formation, which can lead to very high local pressures, was not observed. Wind flow between the two towers did not appear to be particularly large implying that local cladding pressures in that region should not be larger than would exist if only one tower were present.

Wind speeds in pedestrian areas appeared to be quite low, particularly on the south side of the building in the plaza areas. Modification of the hill to the south to account for a possible future project appeared to decrease wind speeds in most areas about the building for southerly winds. The largest wind speeds in pedestrian areas about the building appeared to be at ground level near the northwest and northeast corners of the building for northerly winds.

The approach velocity profile used for the model simulation is shown in Figure 7. A 0.23 power law exponent mean velocity profile shape was used. For flow approaching the Taikoo Shing City Plaza model from the northeast through south to the northwest, the wind structure was severely modified by the surrounding buildings and hill which were modeled so that the wind characteristics at the model site were dictated primarily by surrounding roughness. For north winds, the approach profile is a reasonable approximation to wind flow over rough wave structure in the bay. Close to the model, the ground surface and near-bay

were smooth, simulating the proposed ground surface and shallow-water wave structure. The structures on the east and west provided further influence on the wind approaching from the north.

5.2 Pedestrian Winds

Figure 4 shows the 33 locations selected for investigation of pedestrian wind comfort. Location 1 was selected as a reference location which should be reasonably undisturbed by presence of the new project. It was located north of the adjacent buildings along the new shoreline so as to be exposed to winds approaching over the water. Table 2 and Figure 8 show that the largest values of mean velocity were measured at locations 4 and 25 at the northeast and northwest corners of the building with values ranging from 60 to 67 percent of U_∞, the mean velocity at the boundary-layer height. For comparison, reference location 1 experienced a largest mean velocity of 36 percent of U_∞; an open-country environment might expect a maximum value of 40 to 45 percent of U_∞.

The largest values of fluctuating velocity, U_{rms}, were in the range of 16 to 18 percent of U_∞. These values are quite moderate for a built-up environment. Reference location 1 had a maximum U_{rms} of 12 percent of U_∞ while an open-country environment might expect 10 to 12 percent of U_∞. The largest values of peak gust, represented by the mean plus 3 rms as discussed in Section 4.2, were measured at locations 4 and 25 with values ranging from 95 to 106 percent of U_∞. These values are not particularly large--reference location 1 experienced a largest effective peak gust of 67 percent while an open-country environment might experience gusts of 75 to 85 percent of U_∞.

Velocity data of Table 2 integrated with local wind data listed in Table 3 are shown in Figure 9. Based on the data of this figure, the windiest location is predicted to be location 4 which should be uncomfortable for walking 6 to 8 percent of the time. This location will be very similar in windiness to reference location 1 for 95 percent of the time. Five percent of the time it will be slightly windier. Most areas about the building have low wind speeds suitable for long exposure activities for a significant percentage of the time. It is anticipated that no remedial action will be necessary for pedestrian winds about the building and that the wind environment will be considered to be pleasant.

5.3 Pressures

Table 6 shows the largest peak pressure coefficients and corresponding loads measured on the building for each pressure tap location. Data identified as Configuration A in Table 6 and Appendix A represent data obtained at all tap locations for 36 wind directions in 10-degree increments for the unmodified hill configuration. Configuration B represents data obtained at selected taps at 2-degree azimuthal increments near azimuths where large pressure peaks were observed in Configuration A to ensure that the largest peaks were obtained. The largest peak pressure coefficient measured on the building was -2.95 measured at tap 917 near the roof on the east elevation. This largest pressure coefficient represents, using the 50-year recurrence wind reference pressure of Table 5, a peak cladding pressure of -6400 Pa. Figure 10 shows that most areas of the structure had peak negative (outward-acting) cladding loads of -2000 to -3000 Pa. Peak positive pressures (inward-acting) were generally less than 2300 Pa with a few locations up to 2600 Pa.

Figure 11 shows load, shear and moment diagrams for each tower and the base structure separately for wind directions giving the largest shears in each of the X and Y directions. These plots were made using data from Table 7. Maximum shear in one coordinate direction is accompanied by a significant loading in the other coordinate direction.

REFERENCES

1. Cermak, J. E., "Laboratory Simulation of the Atmospheric Boundary Layer," AIAA Jl., Vol. 9, September 1971.

2. Cermak, J. E., "Applications of Fluid Mechanics to Wind Engineering," A Freeman Scholar Lecture, ASME Jl. of Fluids Engineering, Vol. 97, No. 1, March 1975.

3. Cermak, J. E., "Aerodynamics of Buildings," Annual Review of Fluid Mechanics, Vol. 8, 1976, pp. 75-106.

4. Penwarden, A. D., and Wise, A. F. E., "Wind Environment Around Buildings," Building Research Establishment Report, HMSO, 1975.

5. Melbourne, W. H., "Criteria for Environmental Wind Conditions," Jl. Industrial Aerodynamics, Vol. 3, pp. 241-247, 1978.

6. American National Standards Institute, "American National Standard Building Code Requirements for Minimum Design Loads in Buildings and Other Structures," ANSI Standard A58.1, 1972, or the revised ANSI Standard A58.1 to be published.

7. Hollister, S. C., "The Engineering Interpretation of Weather Bureau Records for Wind Loading on Structures," Building Science Series 30--Wind Loads on Buildings and Structures, National Bureau of Standards, pp. 151-164, 1970.

8. Peterka, J. A., and Cermak, J. E., "Peak-Pressure Duration in Separated Regions on a Structure," U.S.-Japan Research Seminar on Wind Effects on Structures, Kyoto, Japan, 9-13 September 1974; Report CEP74-75JAP-JEC8, Fluid Mechanics Program, Colorado State University, September 1974.

9. PPG Glass Thickness Recommendations to Meet Architects' Specified 1-Minute Wind Load, Pittsburgh Plate Glass Industries, April 1979.

10. Shand, E. B., "Glass Engineering Handbook," Second Edition, McGraw-Hill, New York, p. 51, 1958.

FIGURES

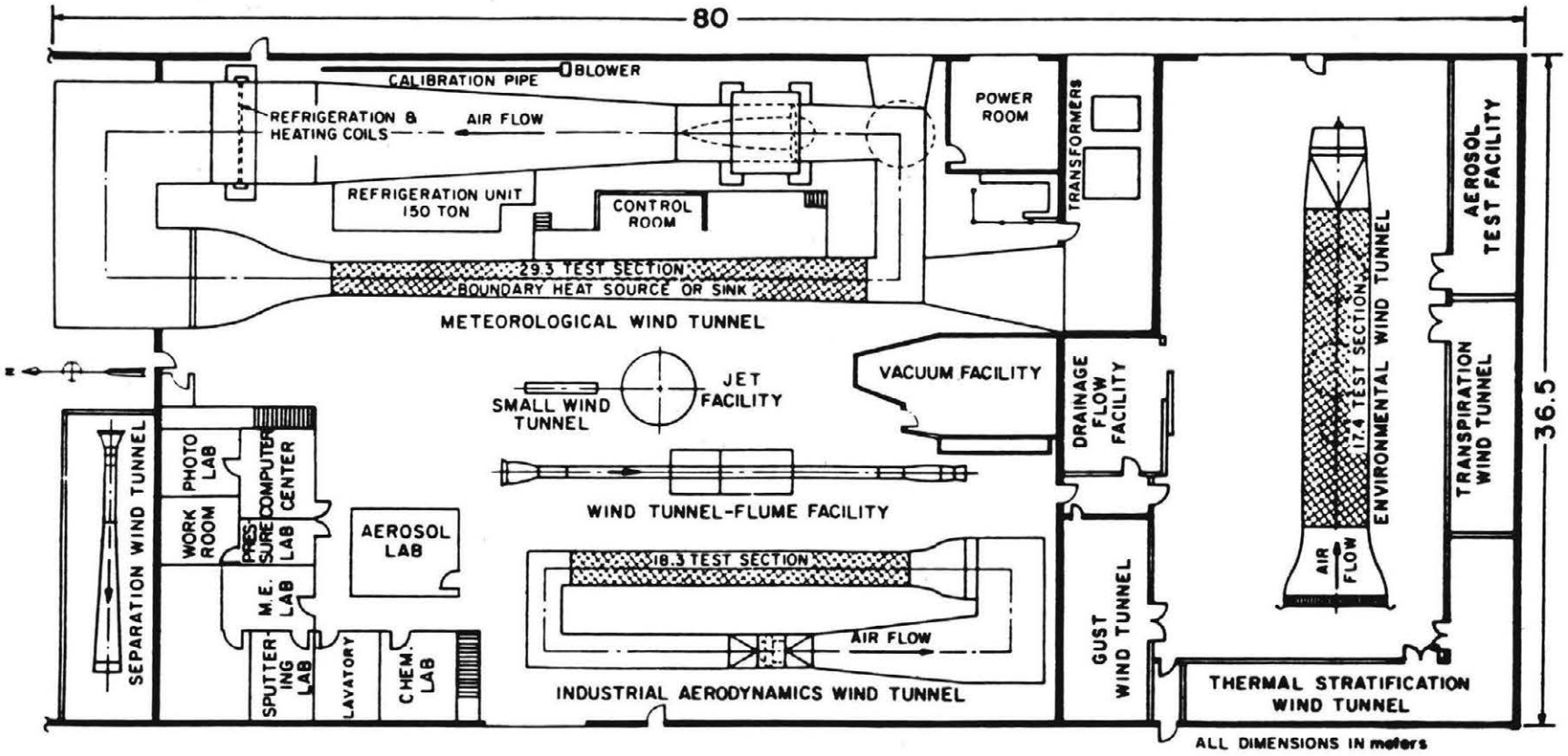

Figure 1. **FLUID DYNAMICS AND DIFFUSION LABORATORY COLORADO STATE UNIVERSITY**

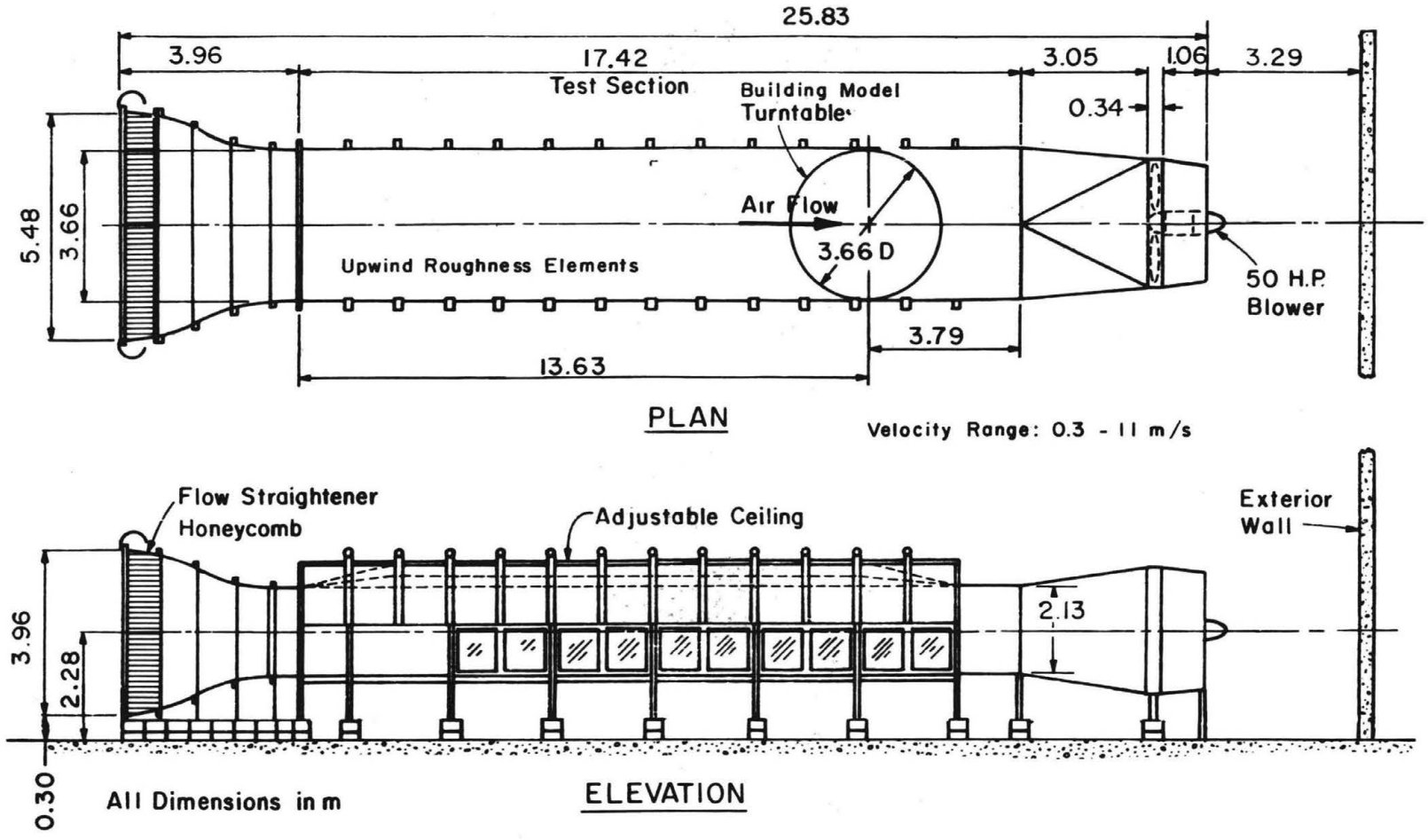

ENVIRONMENTAL WIND TUNNEL

Figure 2. Wind-Tunnel Configuration

Note:

- ● = *soffit taps; 1200 series*
- ○ = *taps on roof of breezeway(plaza level); 1300 series*
- ○ = *roof taps; 1400 series*

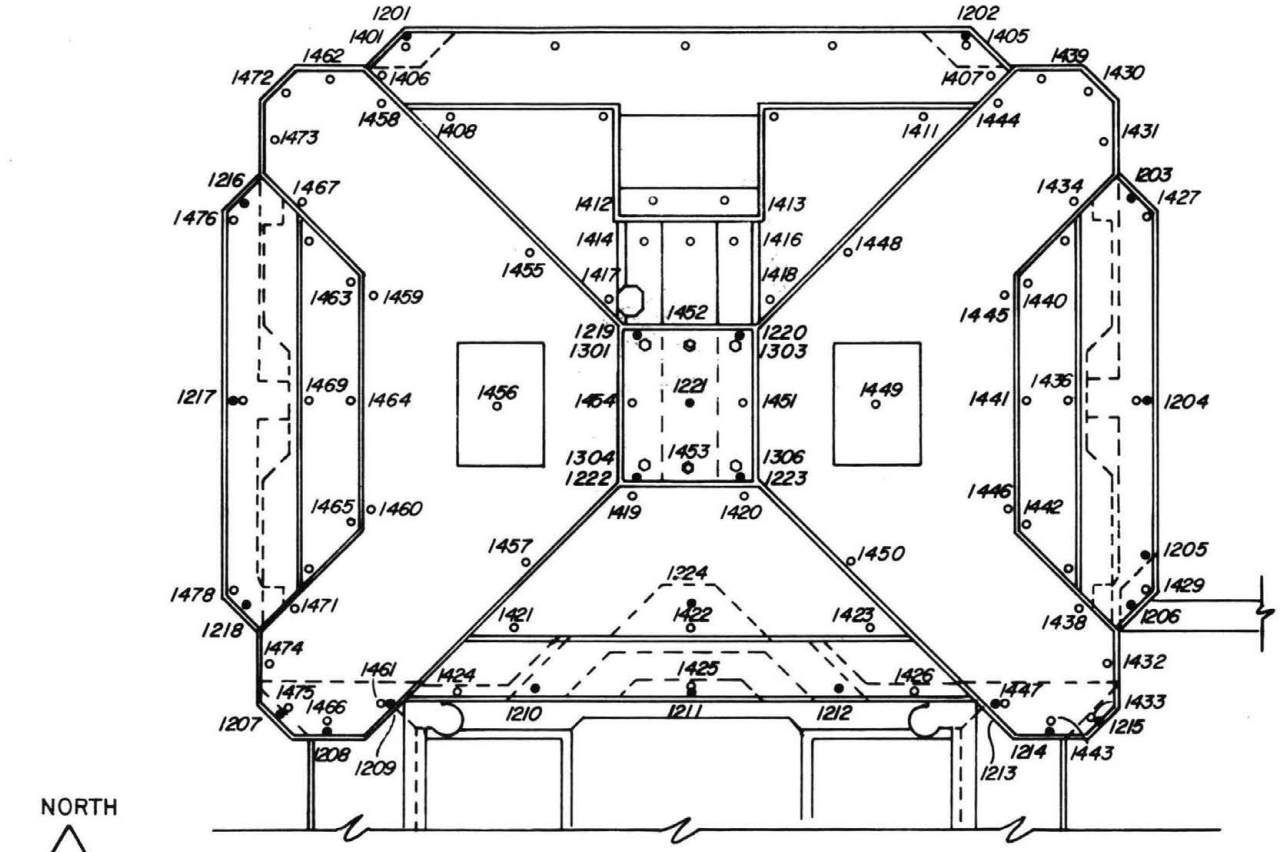

NORTH

Figure 3a. Pressure Tap Locations

Model scale = 1/250
Total taps = 894
Dimension in full scale feet and model inches.

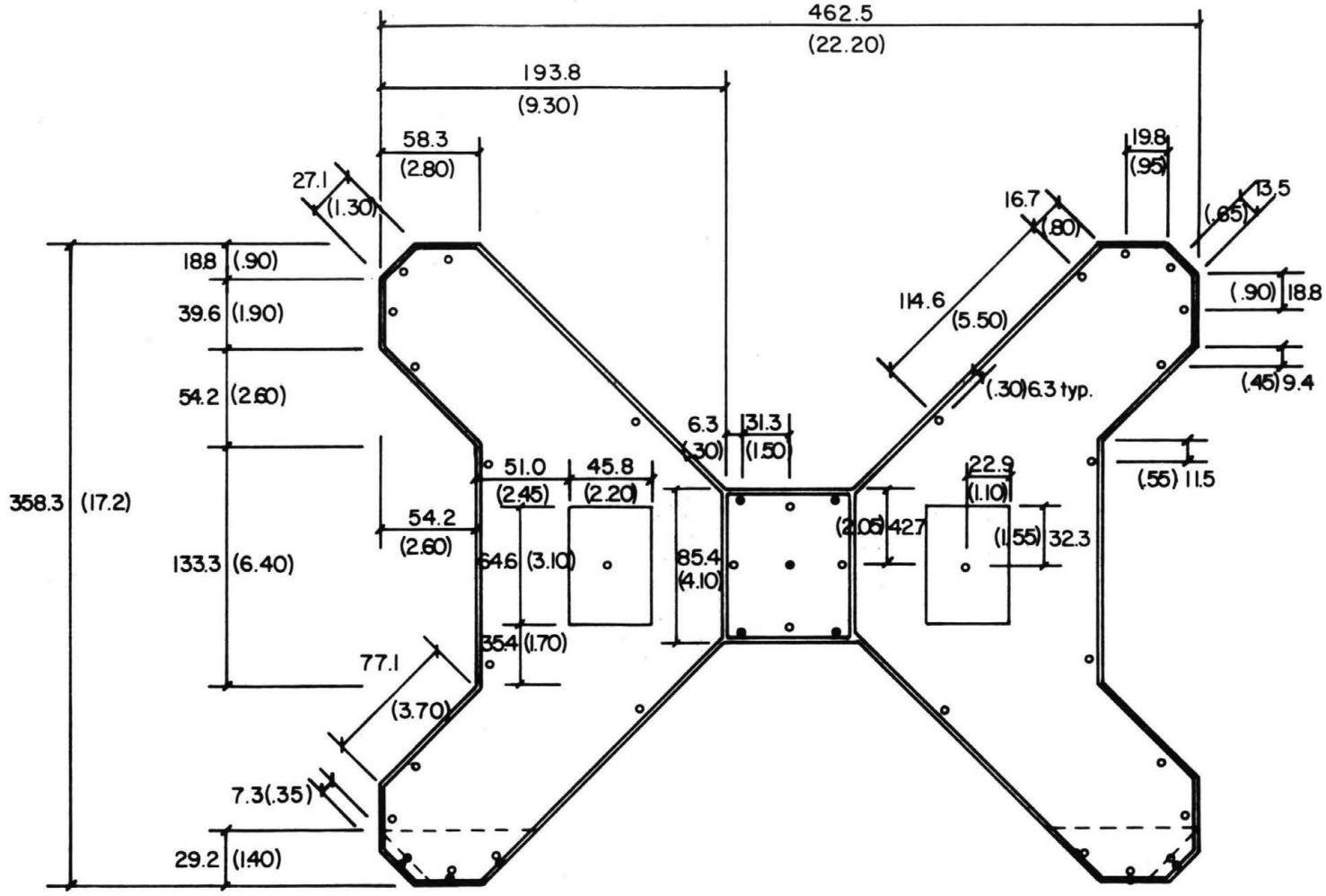

TOWER ROOF (symmetrical)

Tap and Structural Dimensions

Figure 3b. Pressure Tap Locations

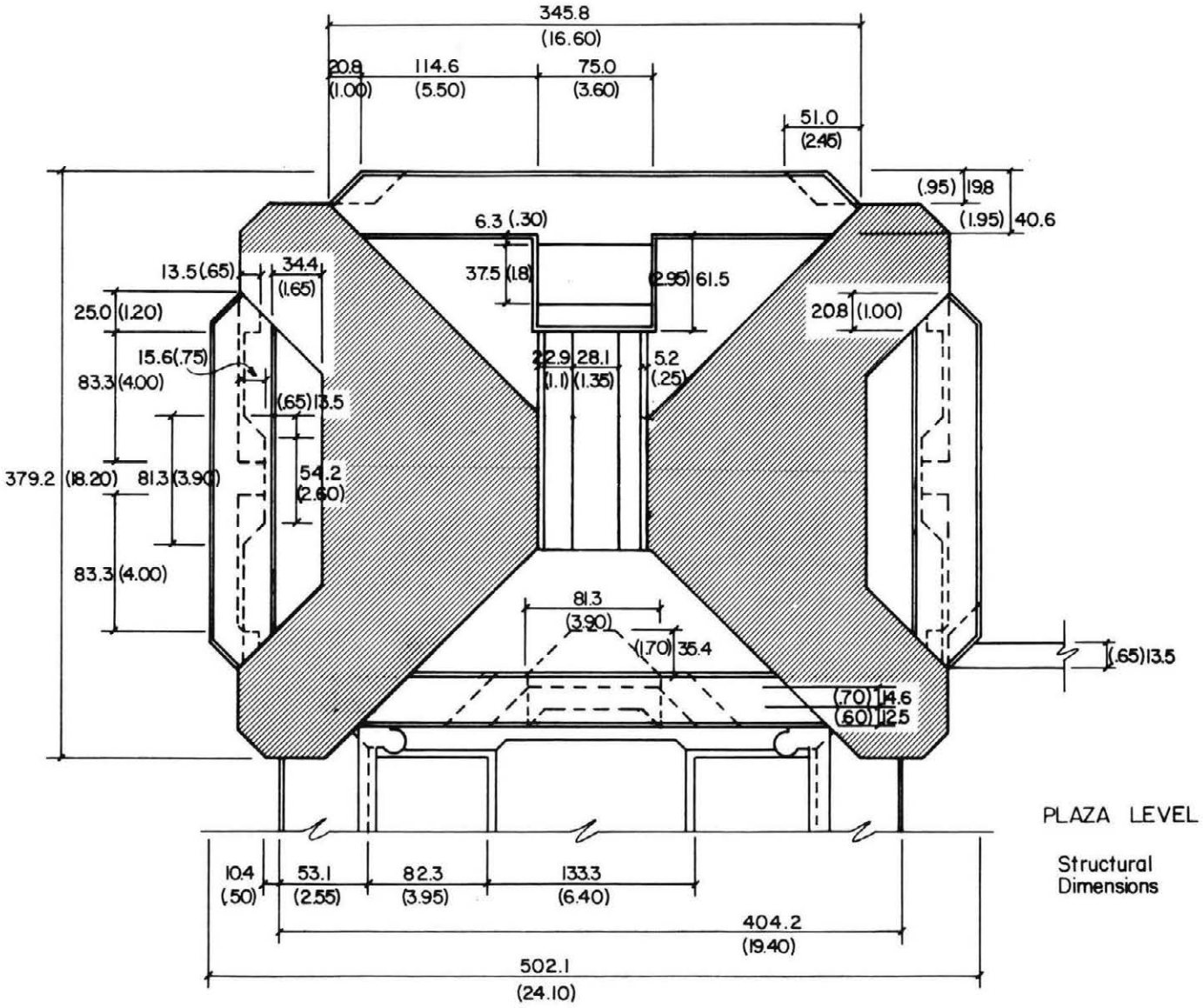

Figure 3c. Pressure Tap Locations

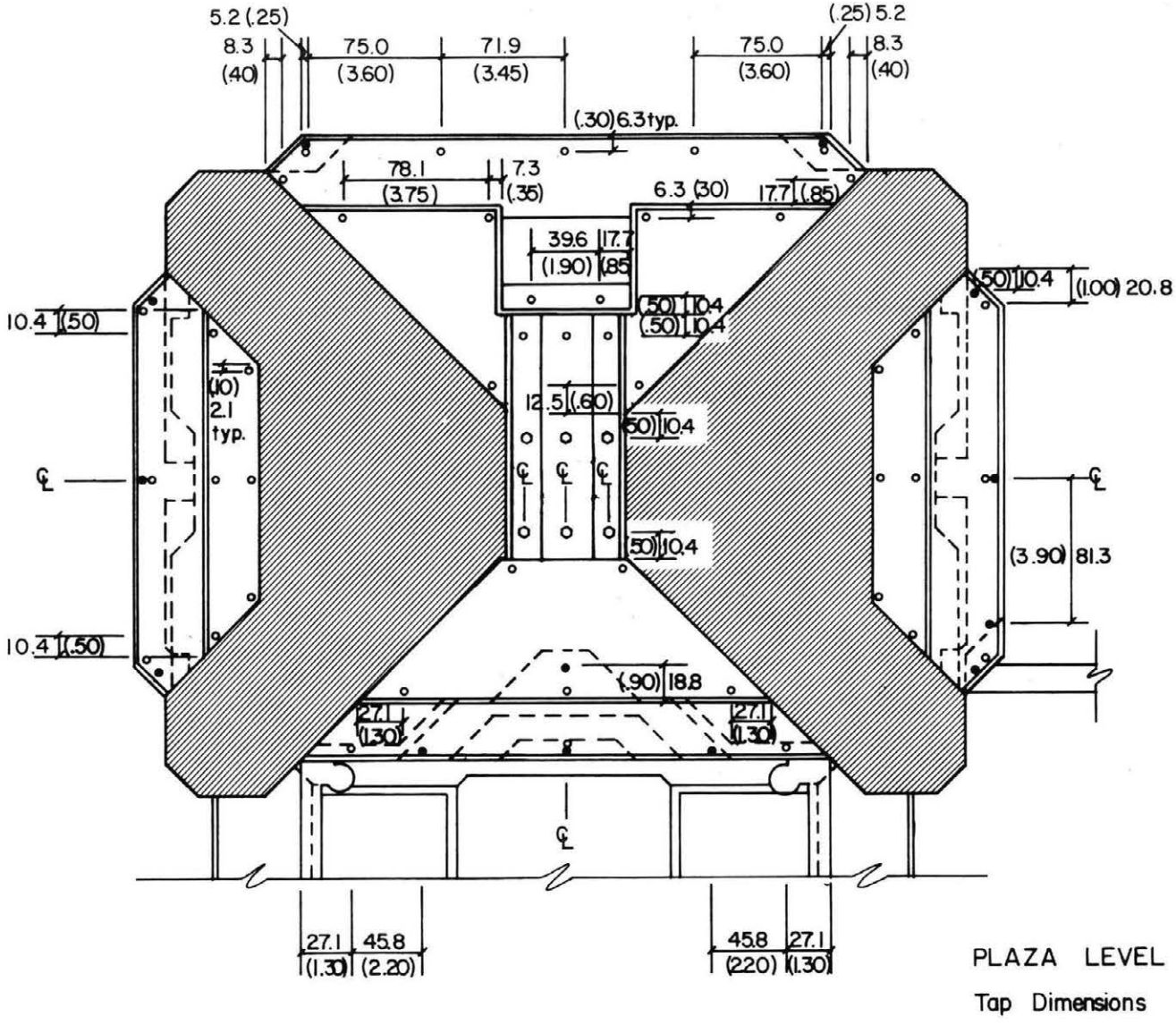

Figure 3d. Pressure Tap Locations

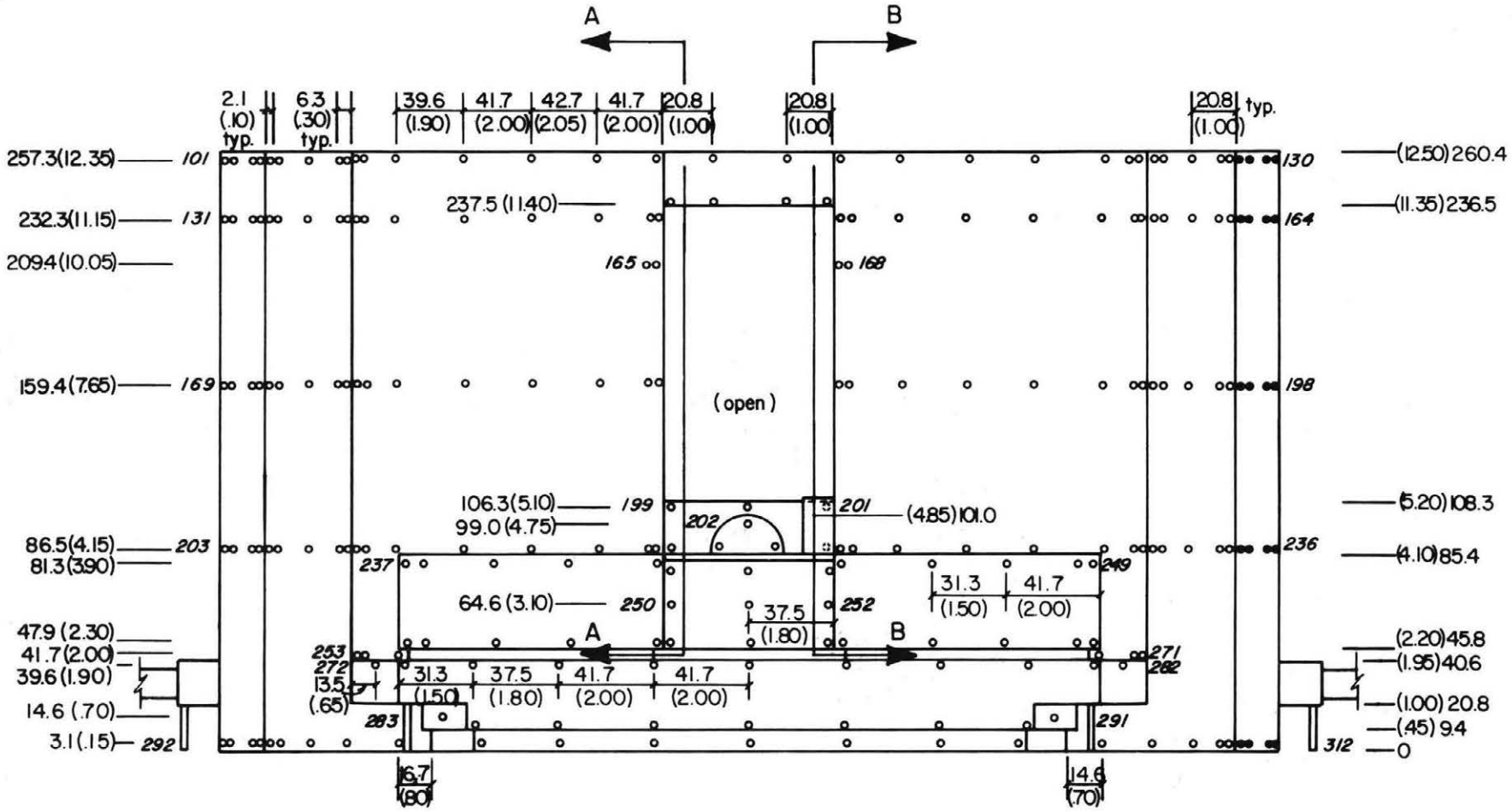

NORTH ELEVATION

All dimensions are actual face dimensions.
Darkened taps represent those taps which are numbered on another elevation.

Figure 3e. Pressure Tap Locations

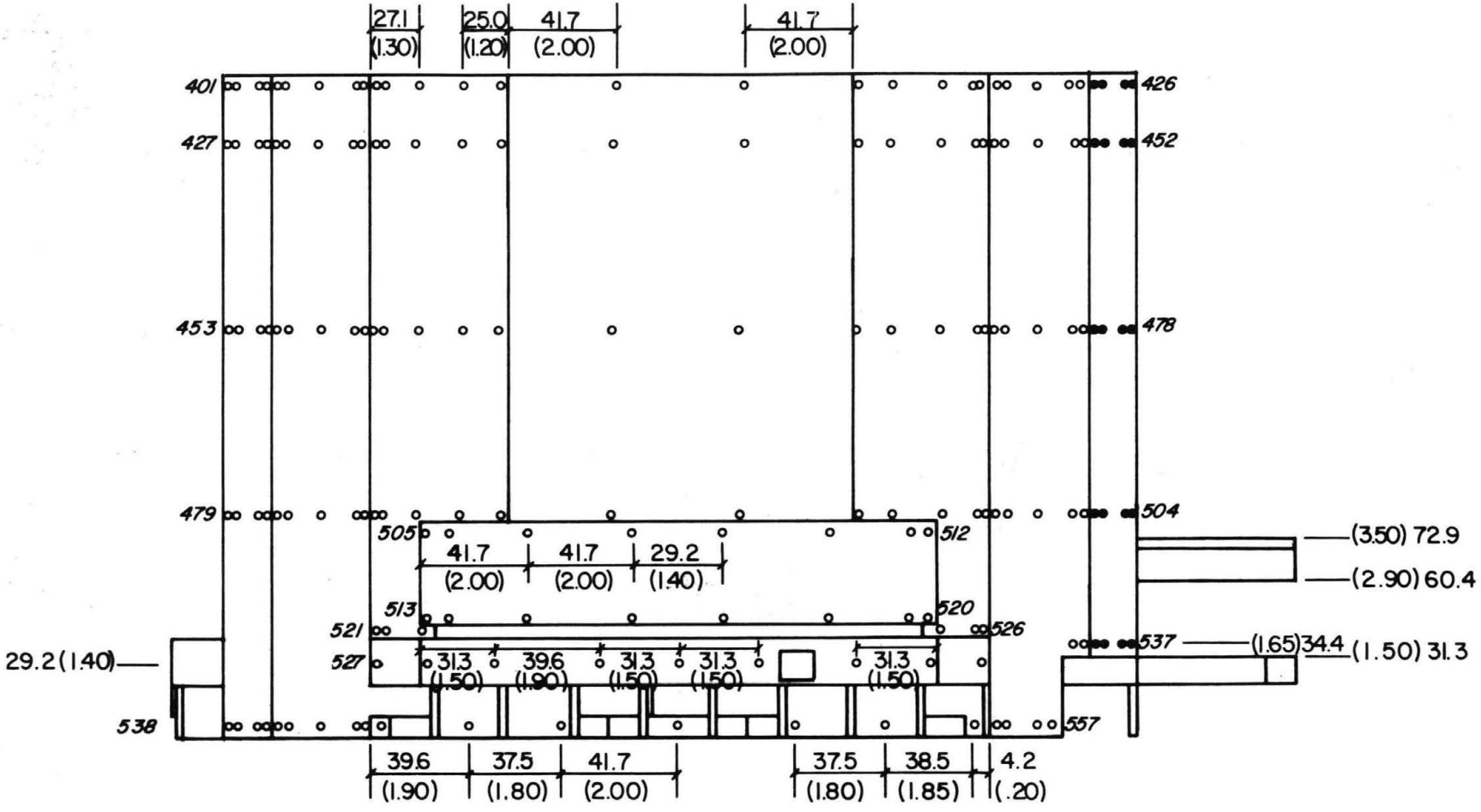

WEST ELEVATION

Figure 3f. Pressure Tap Locations

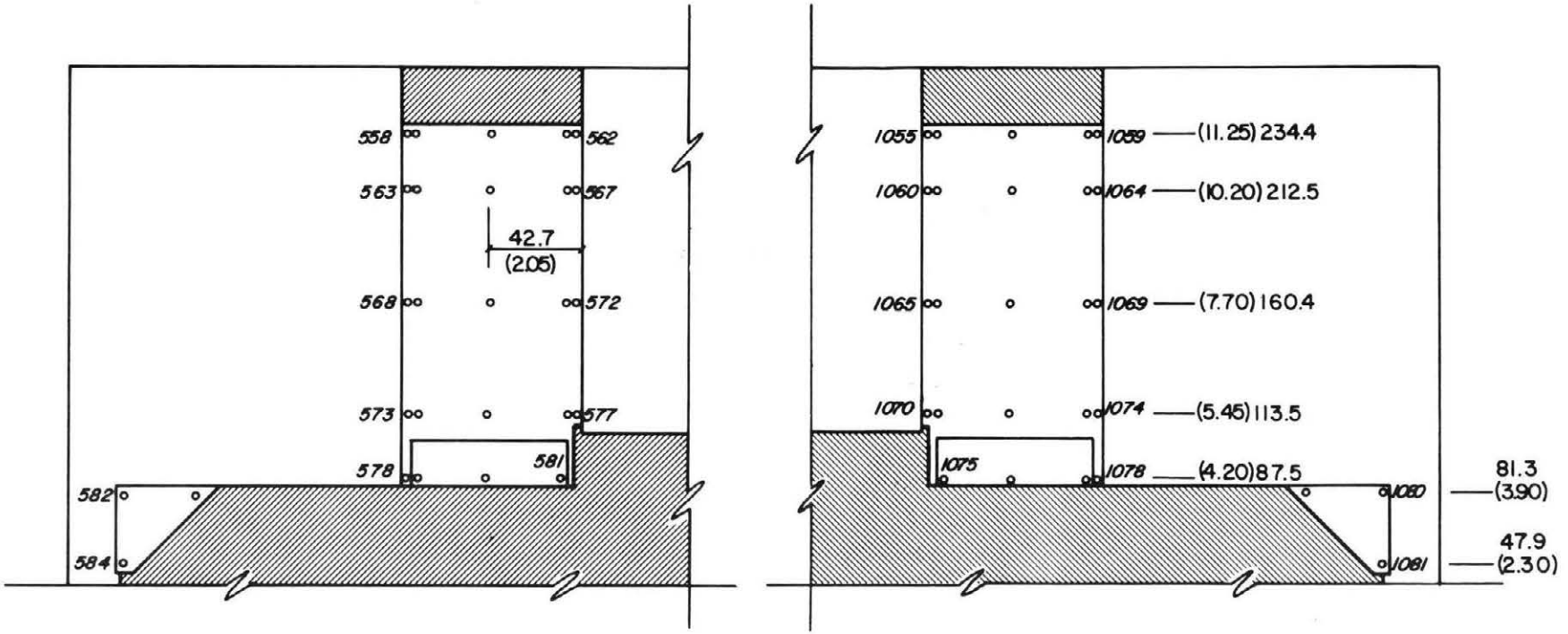

Figure 3g. Pressure Tap Locations

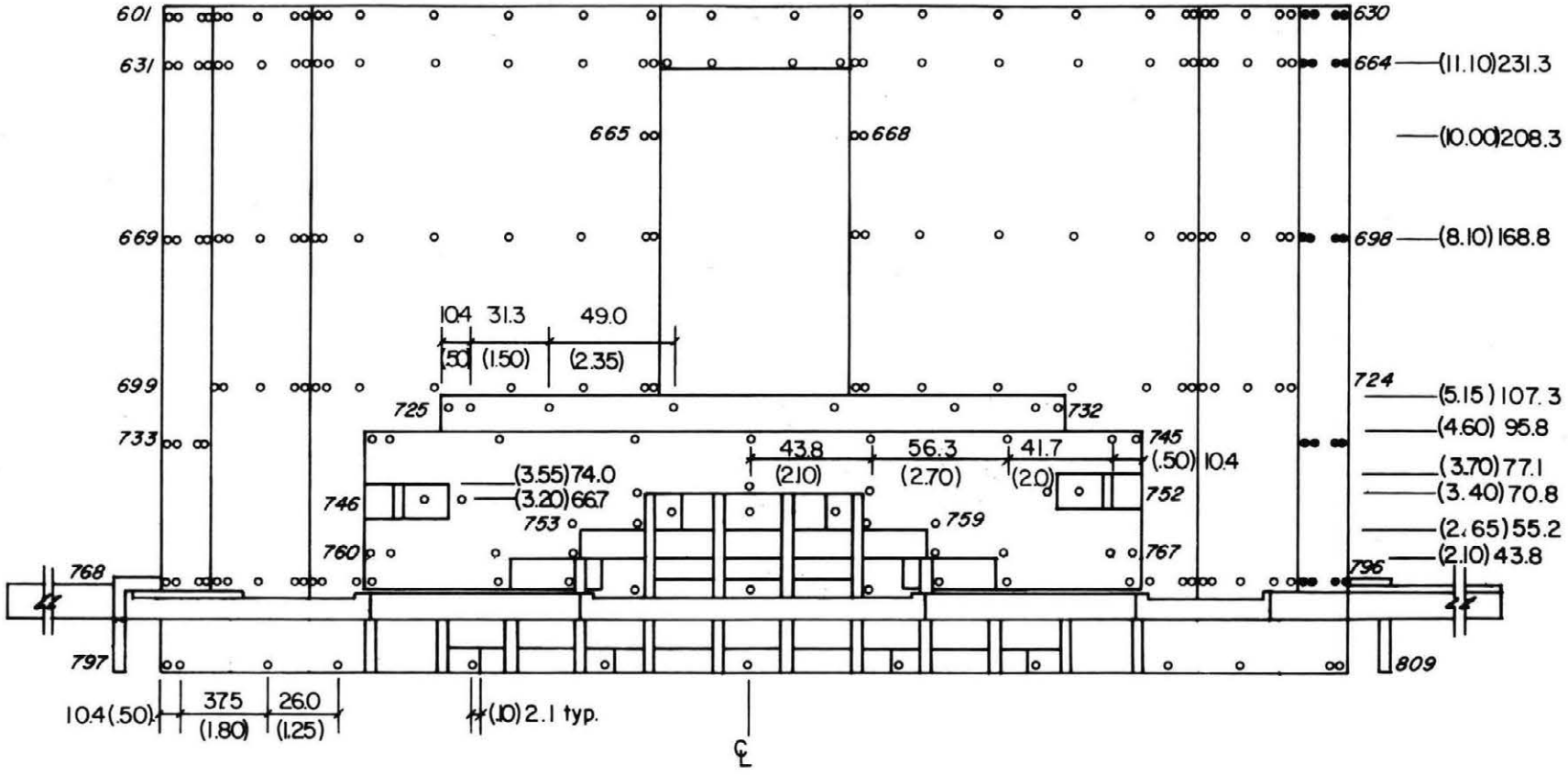

SOUTH ELEVATION

Figure 3h. Pressure Tap Locations

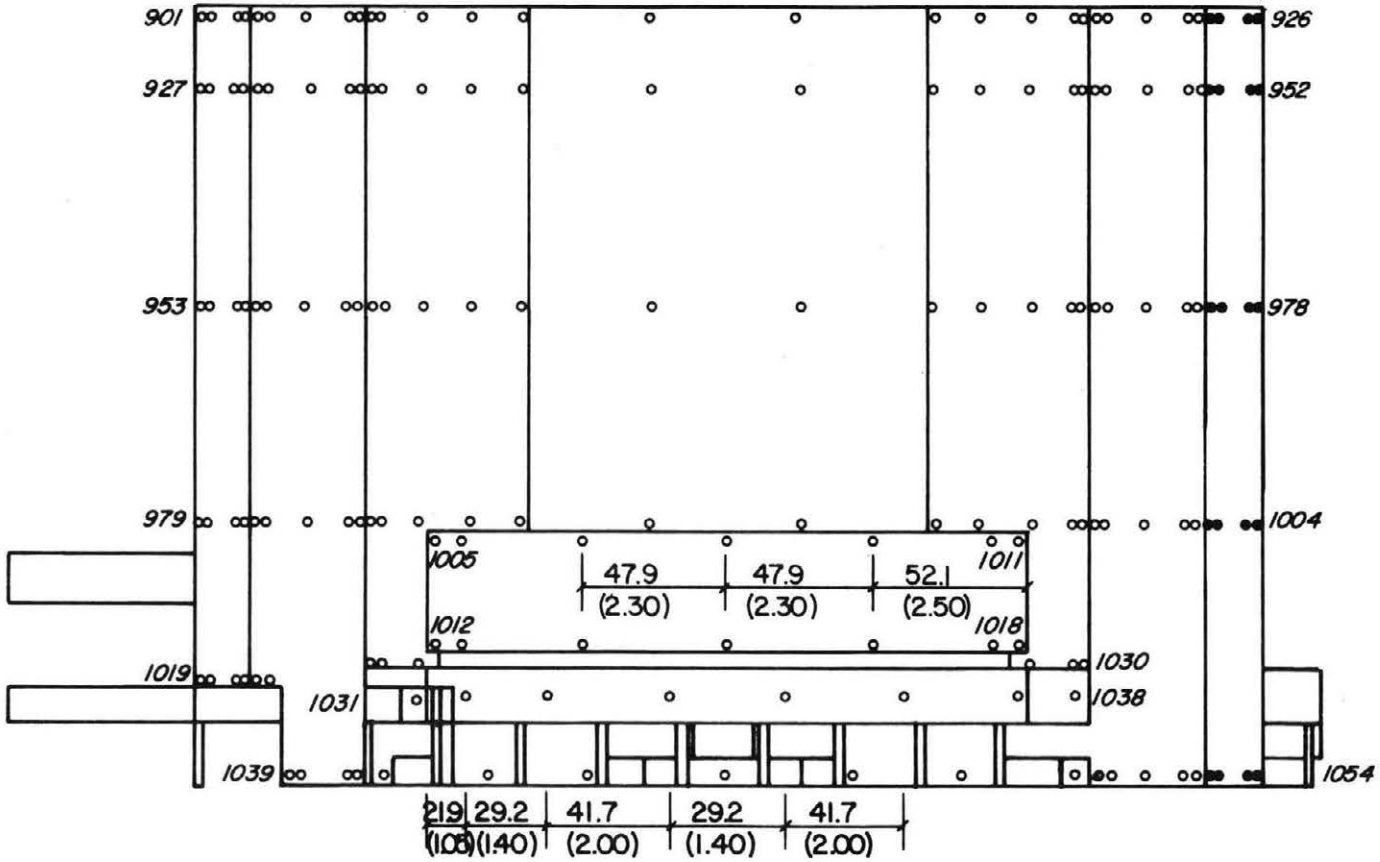

EAST ELEVATION

Figure 3i. Pressure Tap Locations

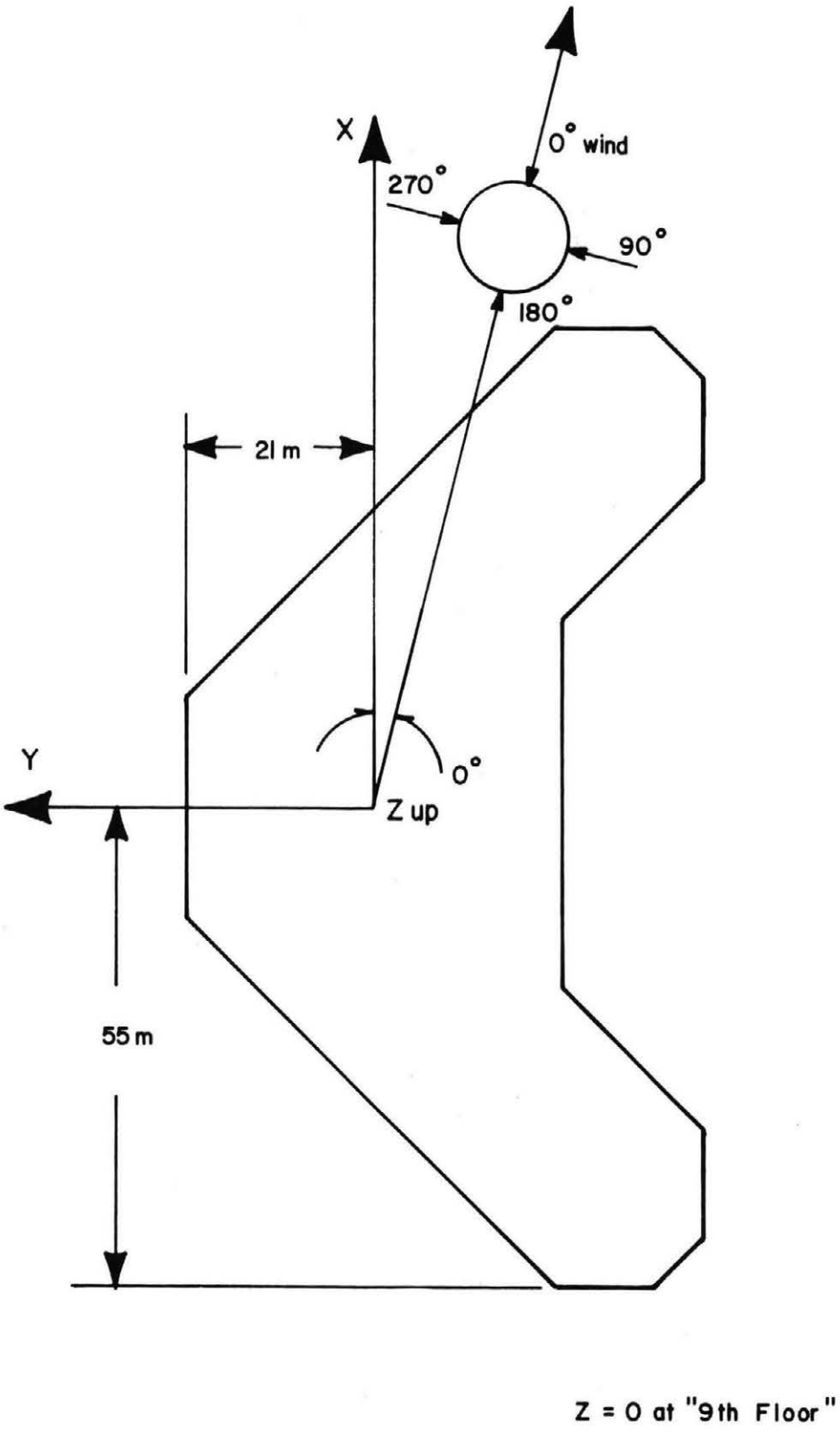

Figure 3j. Pressure Tap Locations

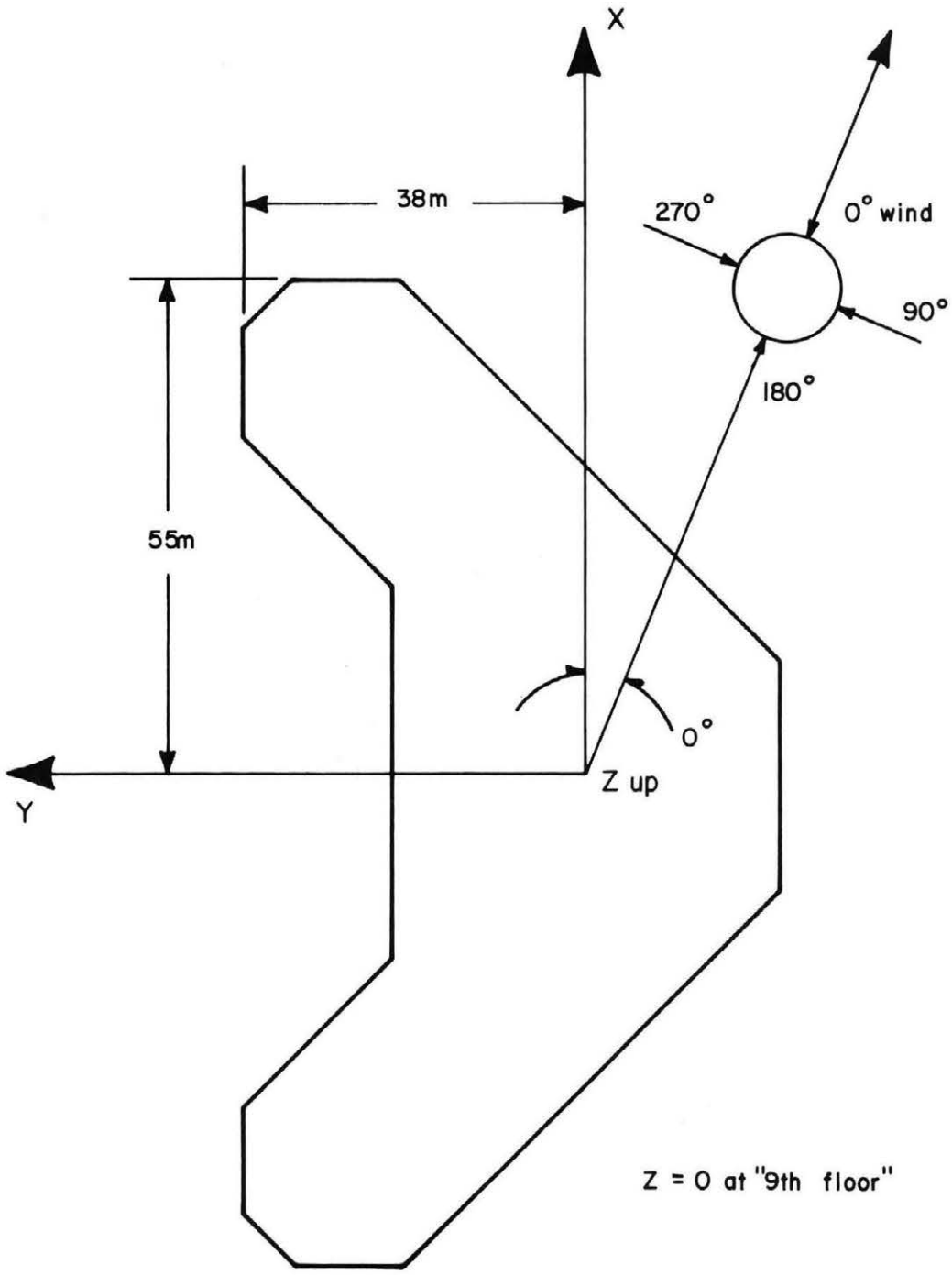

Figure 3k. Pressure Tap Locations

Figure 31. Pressure Tap Locations

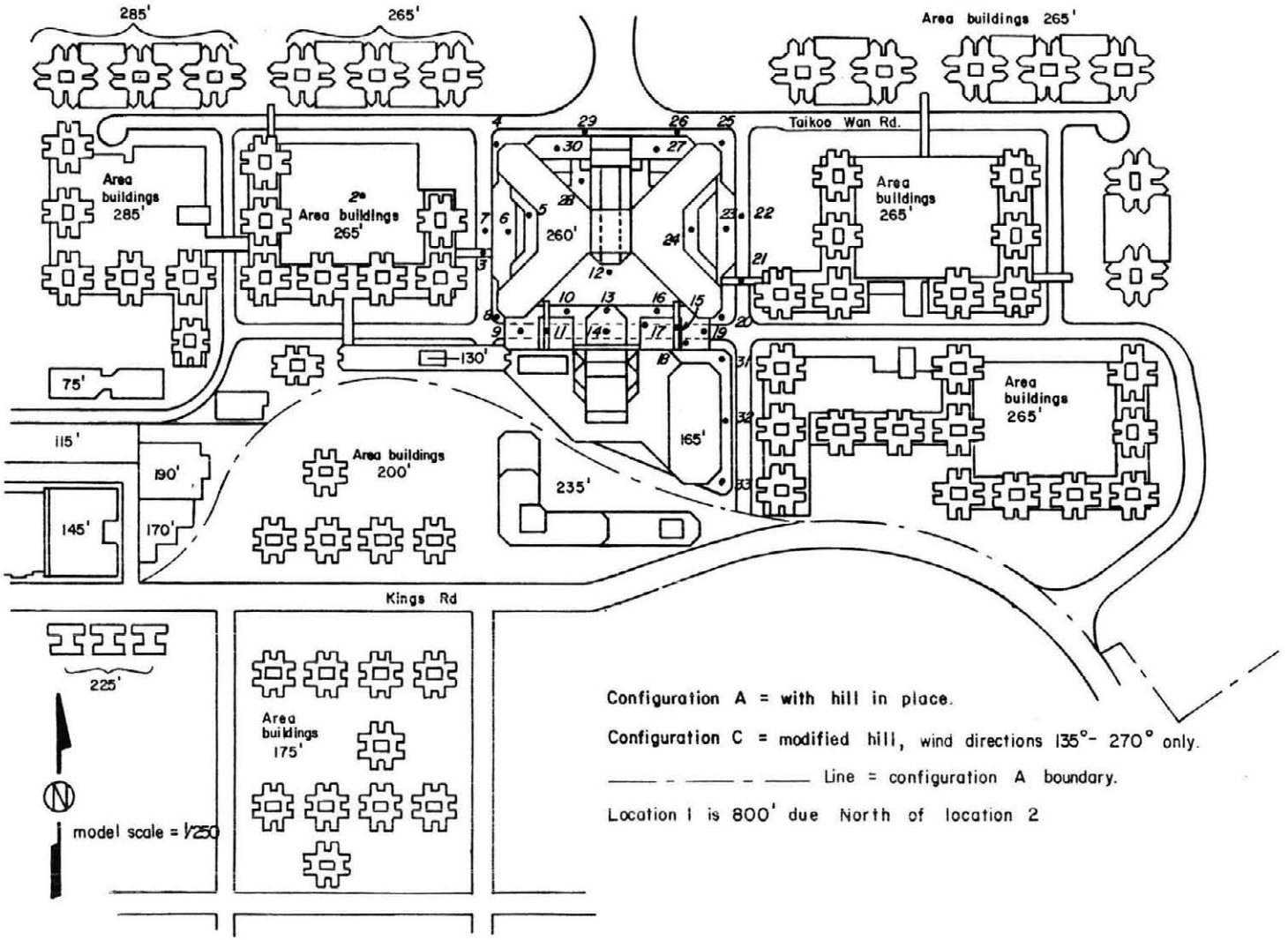

Figure 4. Building Location and Pedestrian Wind Velocity Measuring Positions

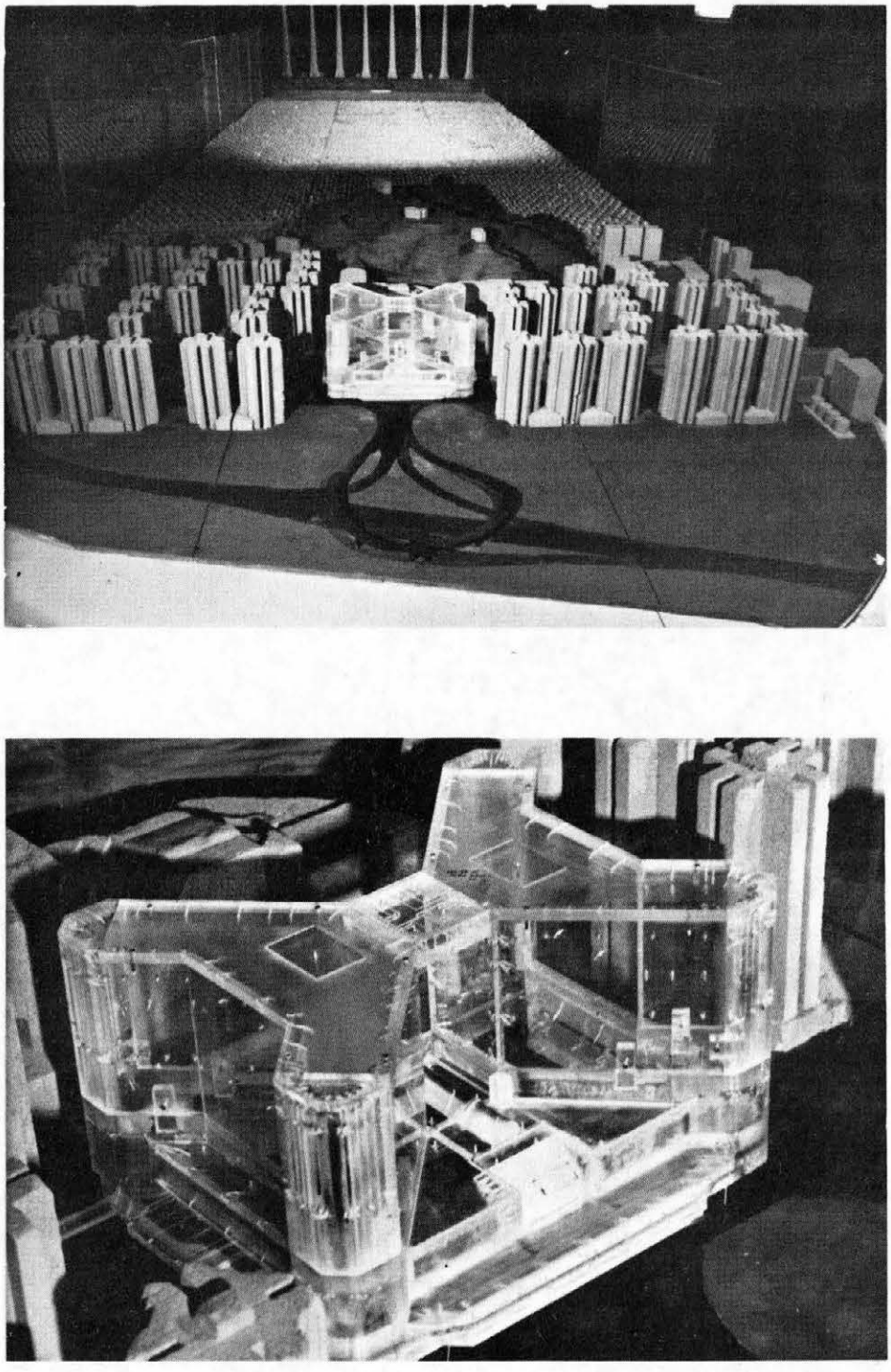

Model to Obtain Pressures

Figure 5. Completed Model in Wind Tunnel

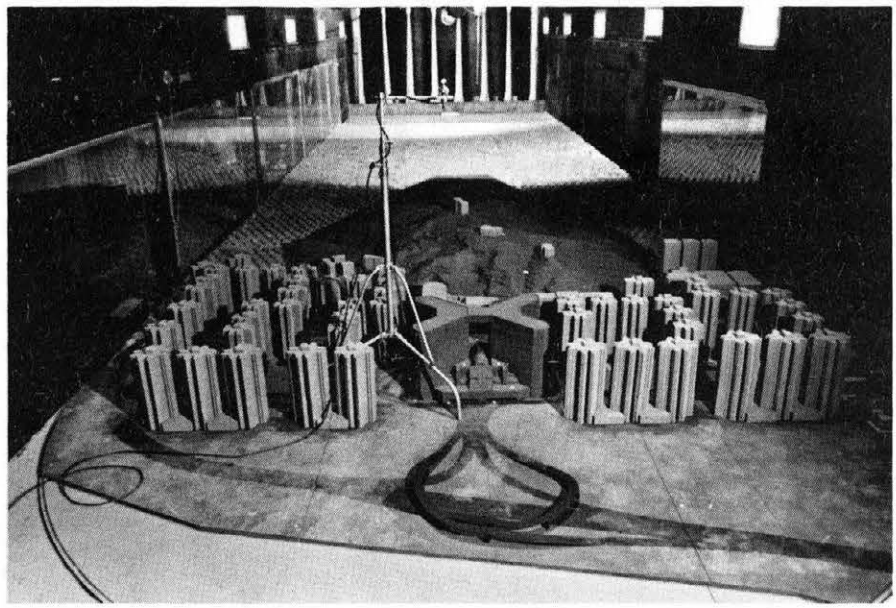

Configuration A - Unmodified Hill

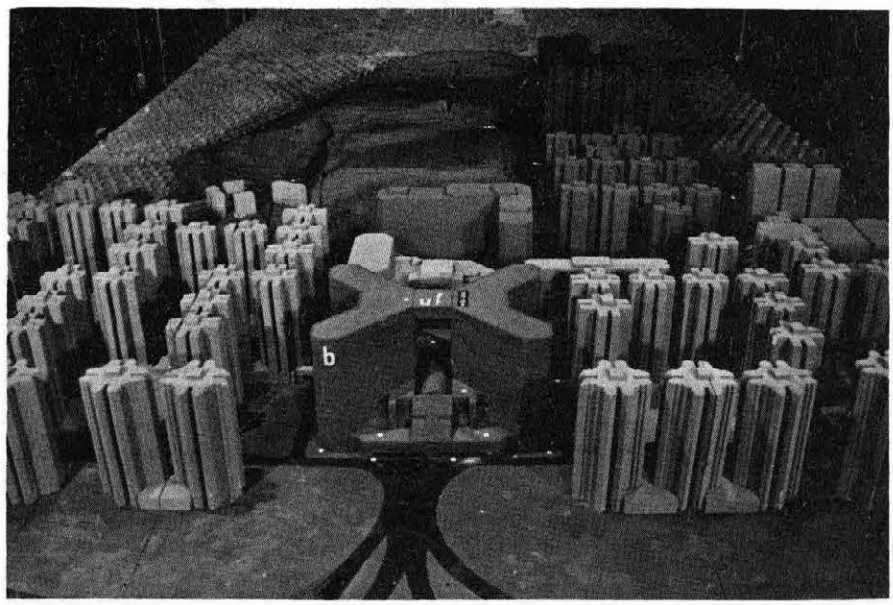

Configuration C - Modified Hill

Flow Visualization Model

Figure 5. Completed Model in Wind Tunnel

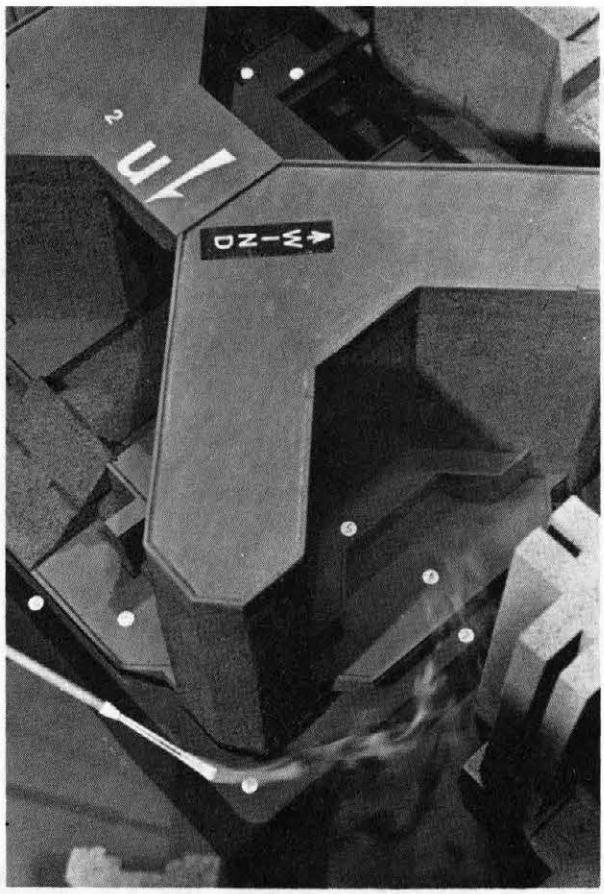

Pedestrian Location 4

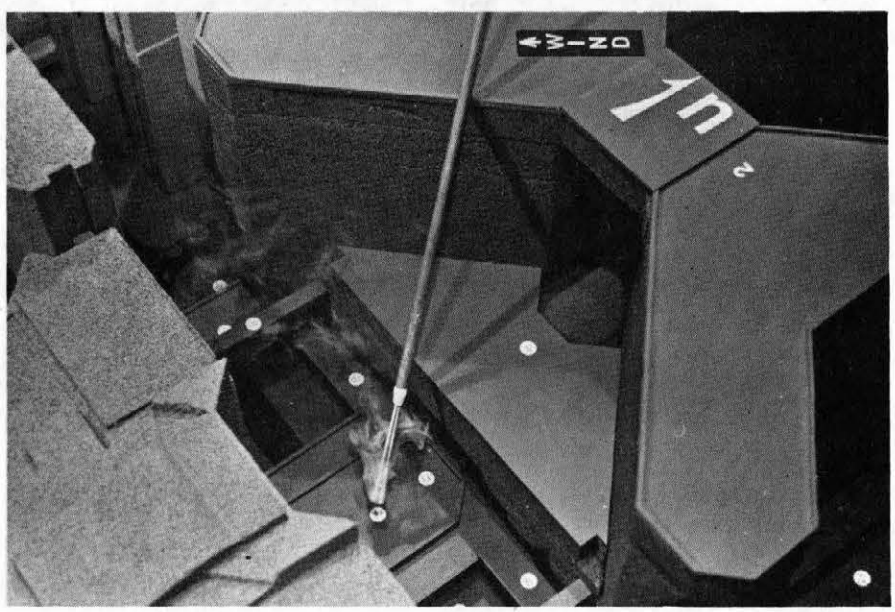

Pedestrian Location 14

Flow Visualization

Figure 5. Completed Model in Wind Tunnel

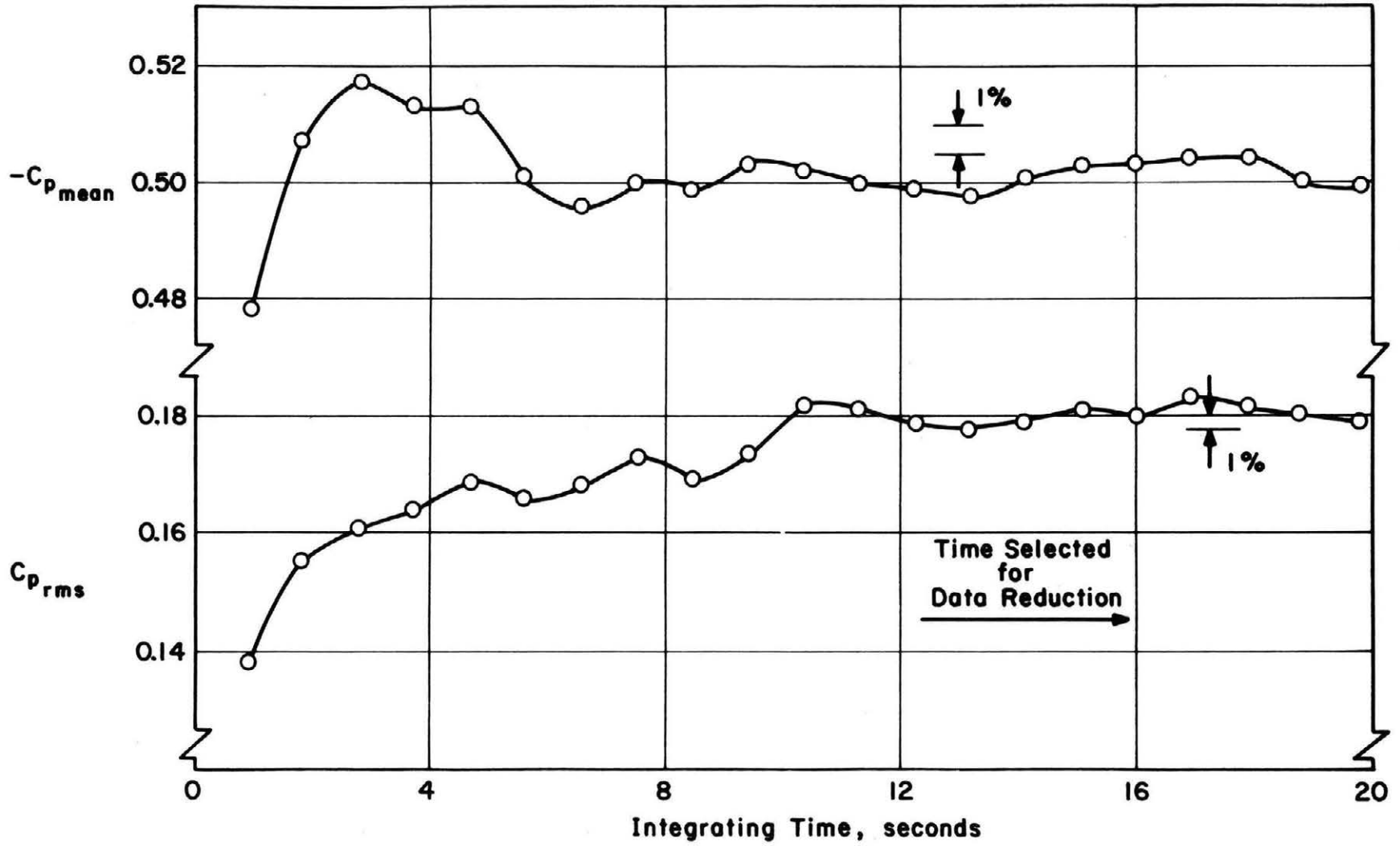

Figure 6. Data Sampling Time Verification

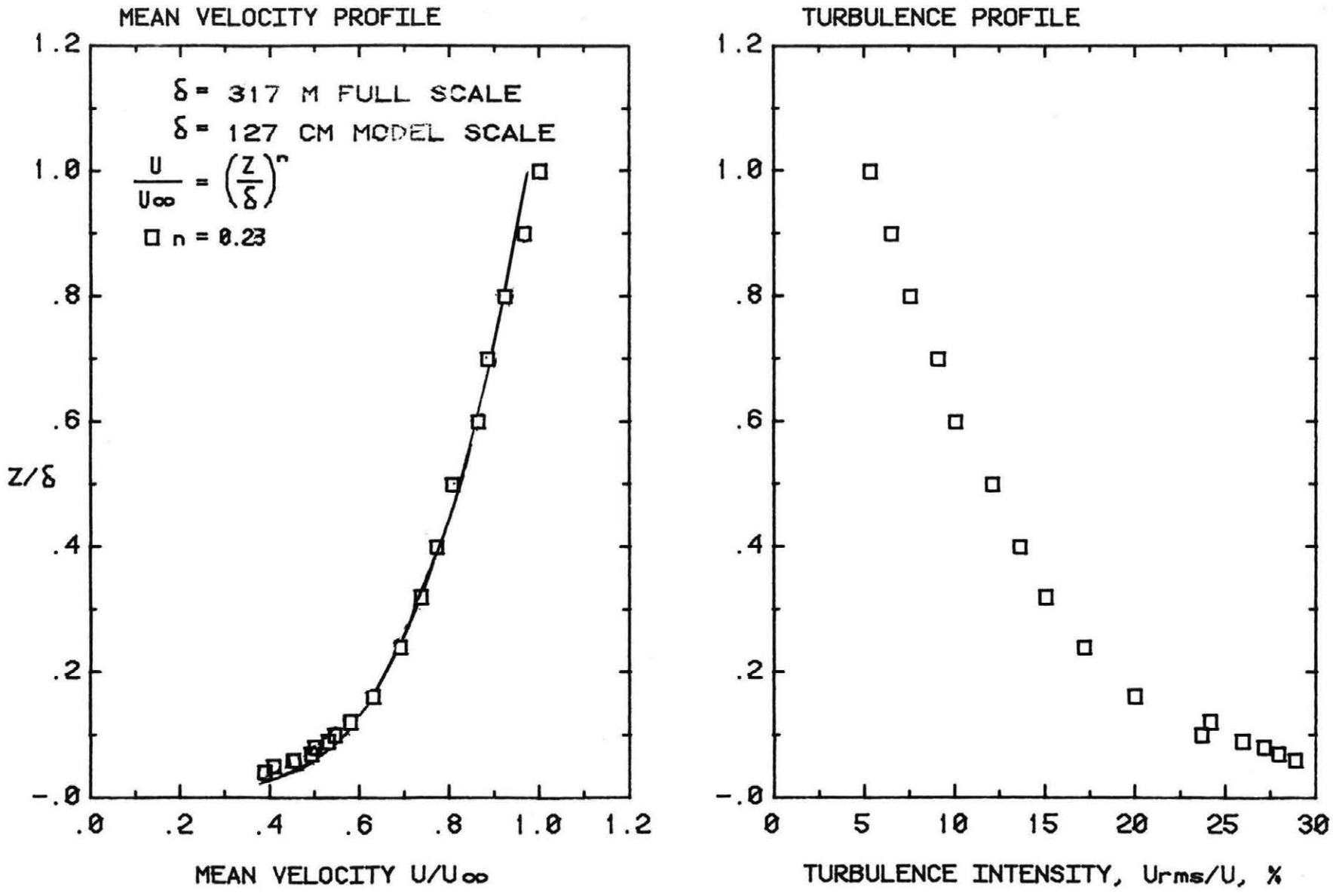

Figure 7. Mean Velocity and Turbulence Profiles Approaching the Model

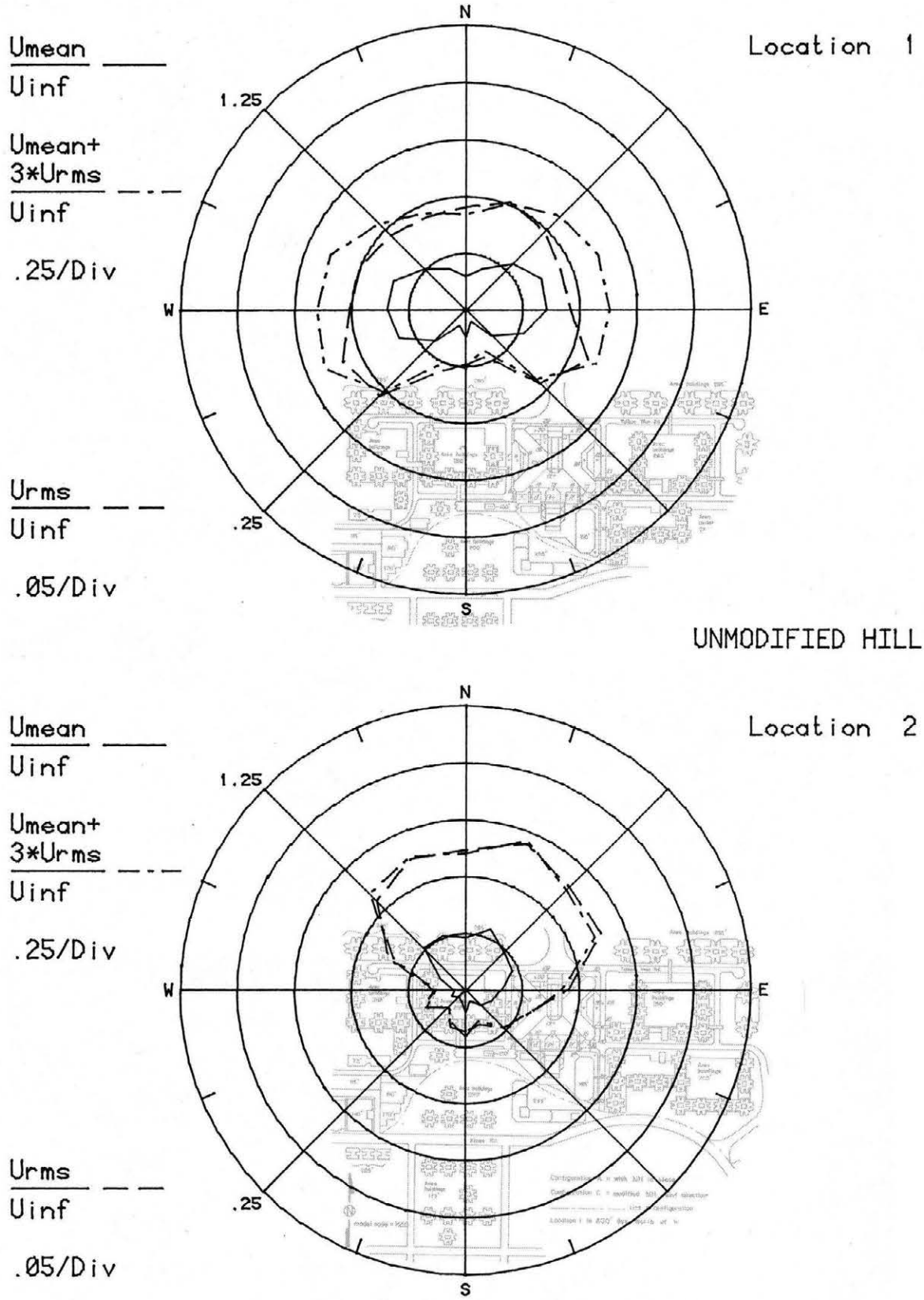

Figure 8a. Mean Velocities and Turbulence Intensities at Pedestrian Locations 1 and 2

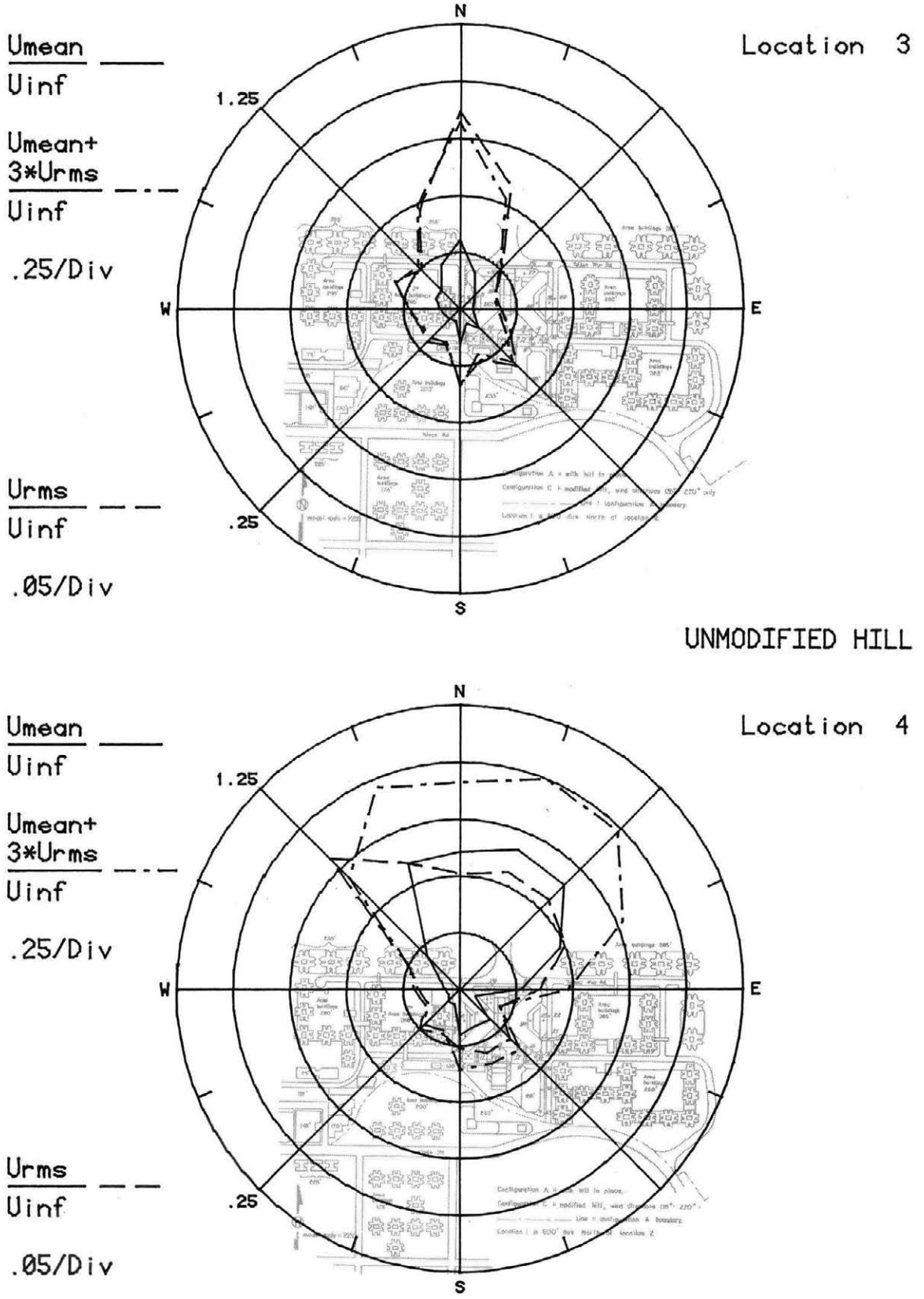

Figure 8b. Mean Velocities and Turbulence Intensities at Pedestrian Locations 3 and 4

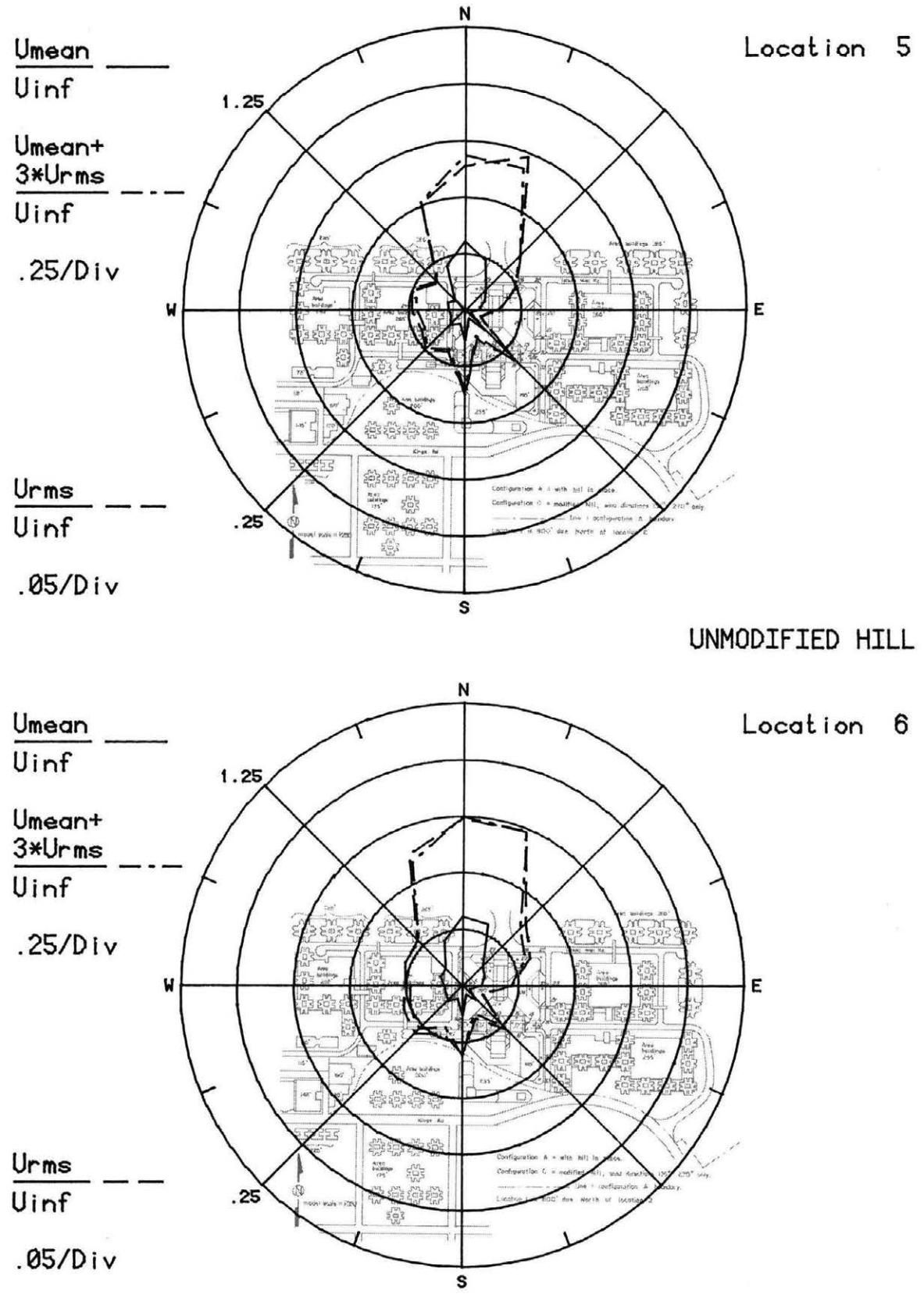

Figure 8c. Mean Velocities and Turbulence Intensities at Pedestrian Locations 5 and 6

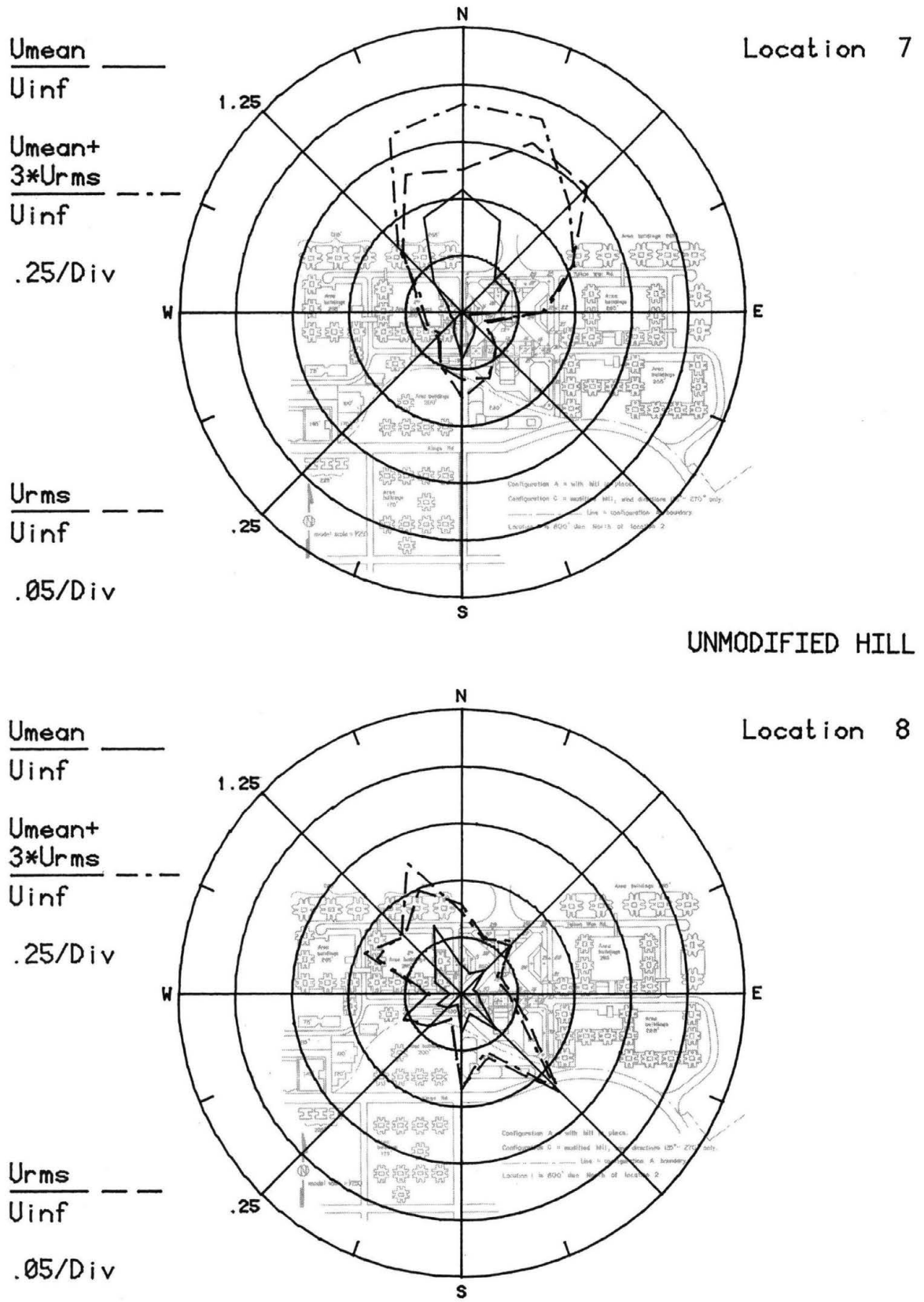

Figure 8d. Mean Velocities and Turbulence Intensities at Pedestrian Locations 7 and 8

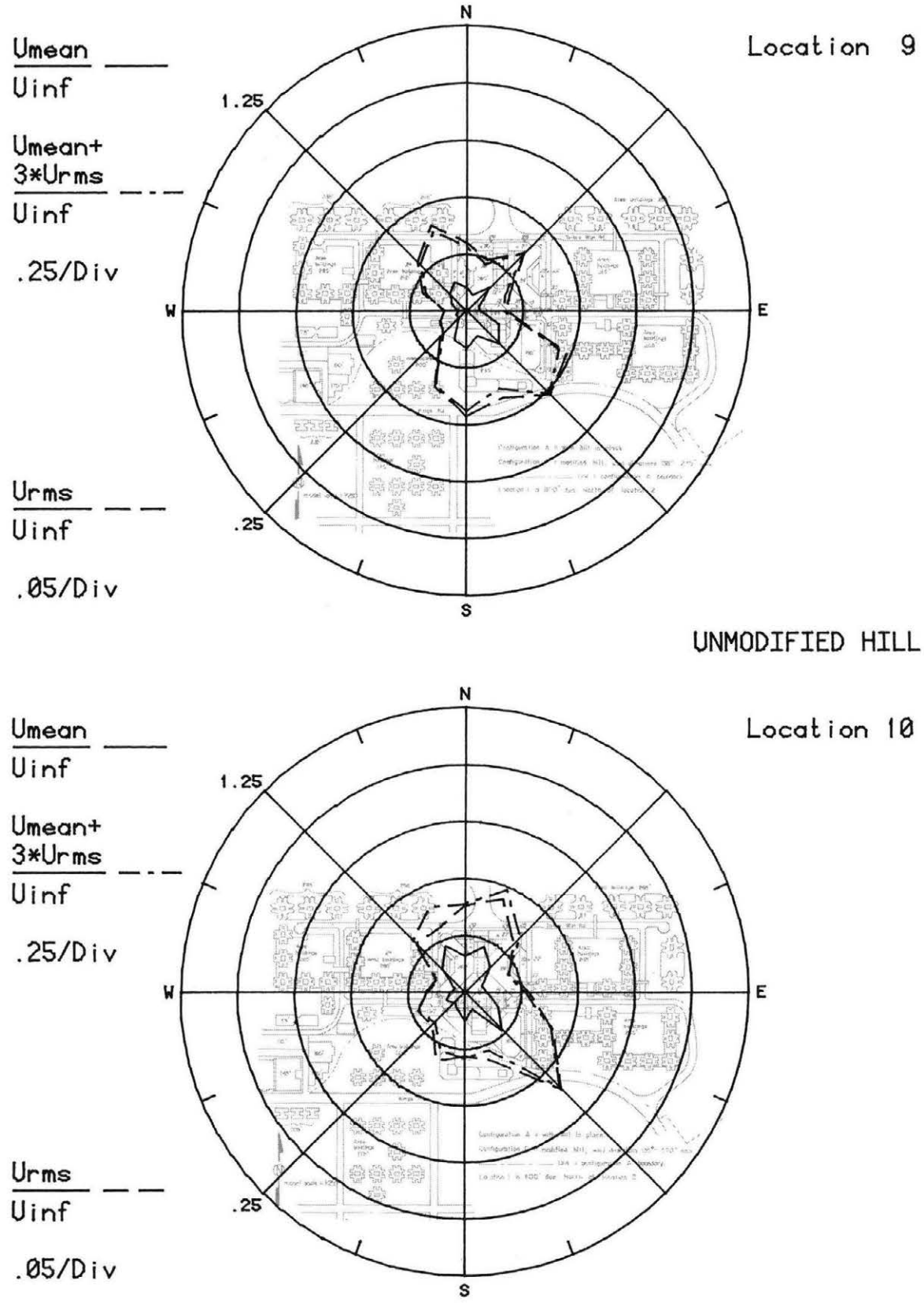

Figure 8e. Mean Velocities and Turbulence Intensities at Pedestrian Locations 9 and 10

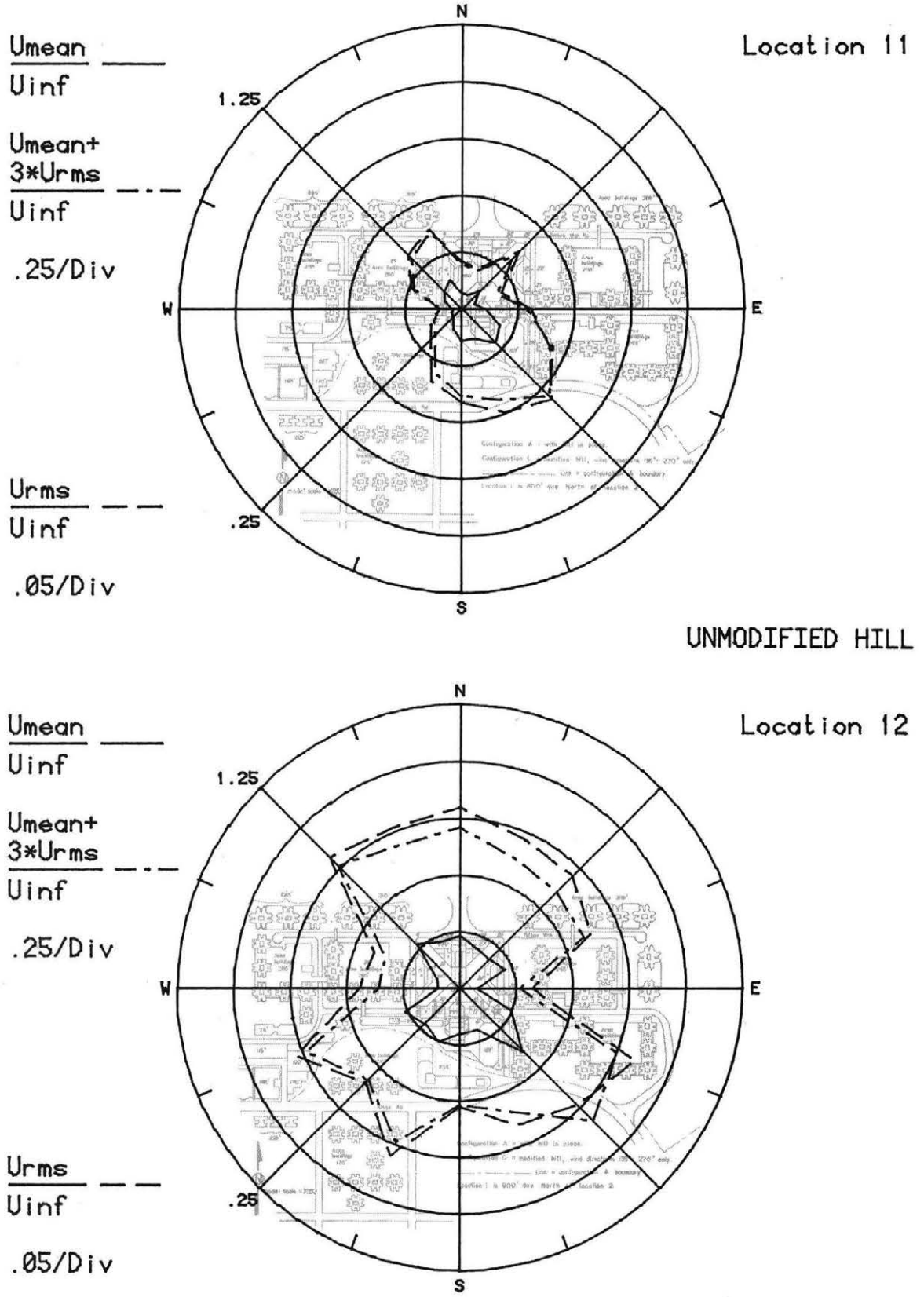

Figure 8f. Mean Velocities and Turbulence Intensities at Pedestrian Locations 11 and 12

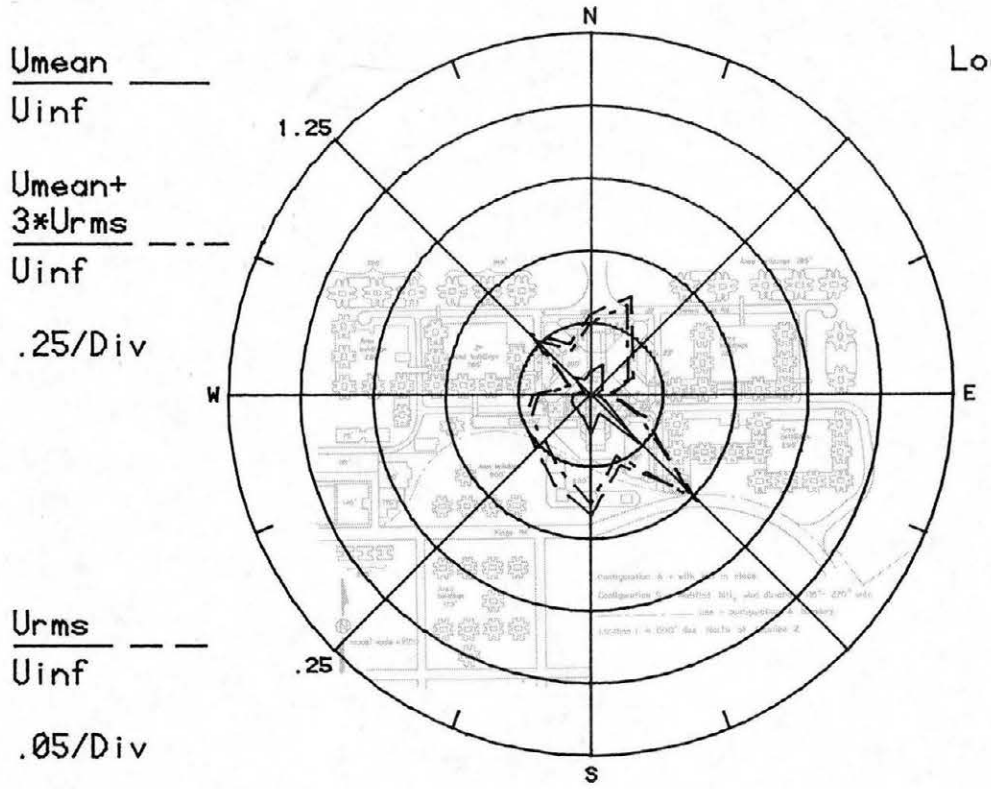

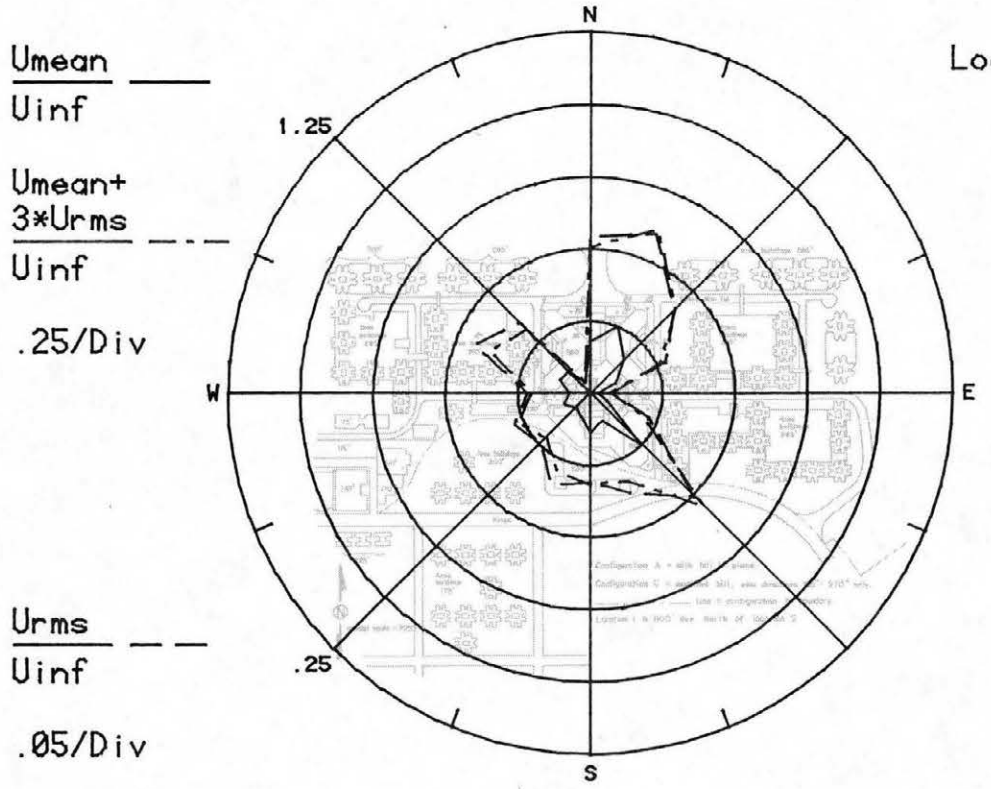

Figure 8g. Mean Velocities and Turbulence Intensities at Pedestrian Locations 13 and 14

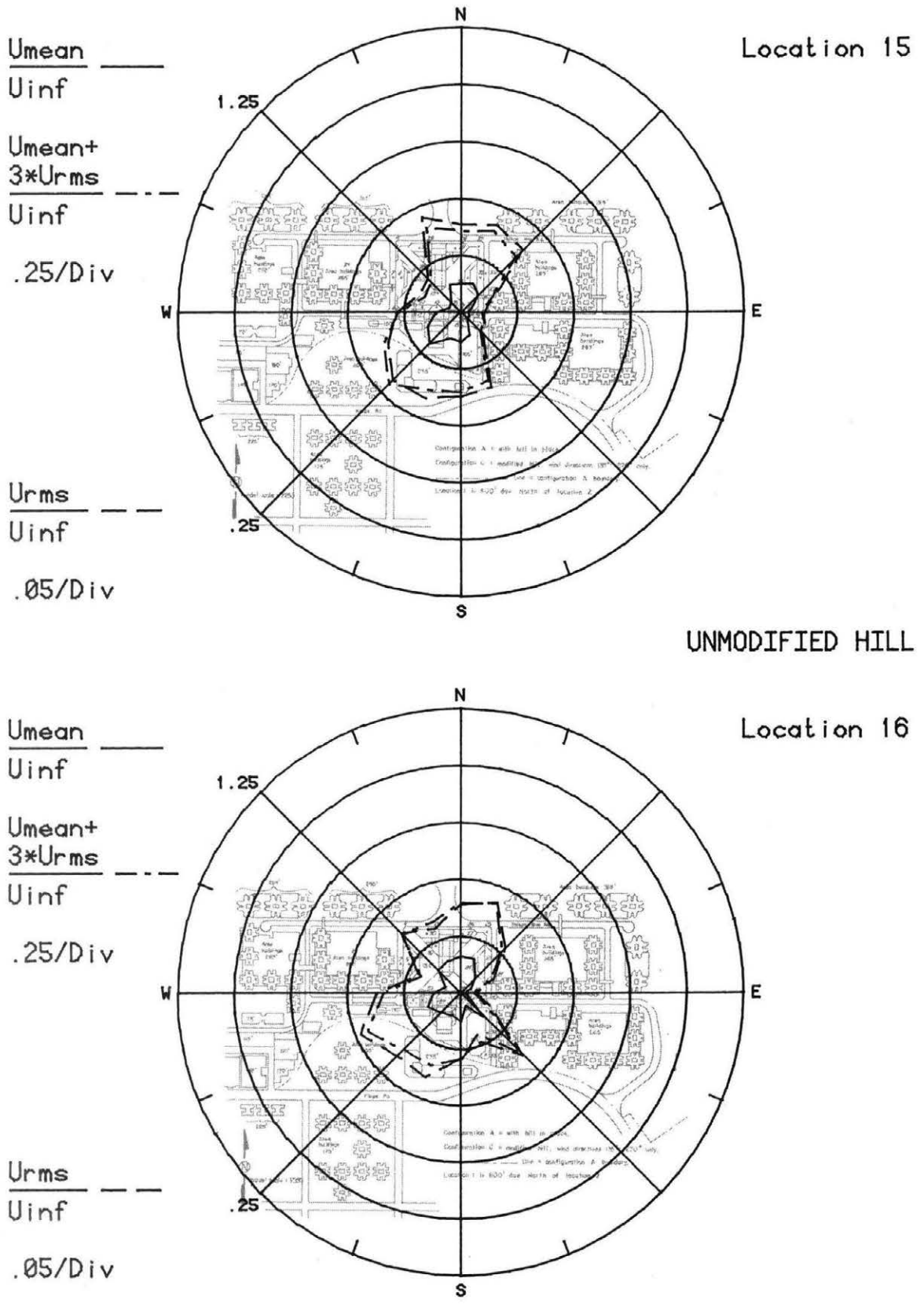

Figure 8h. Mean Velocities and Turbulence Intensities at Pedestrian Locations 15 and 16

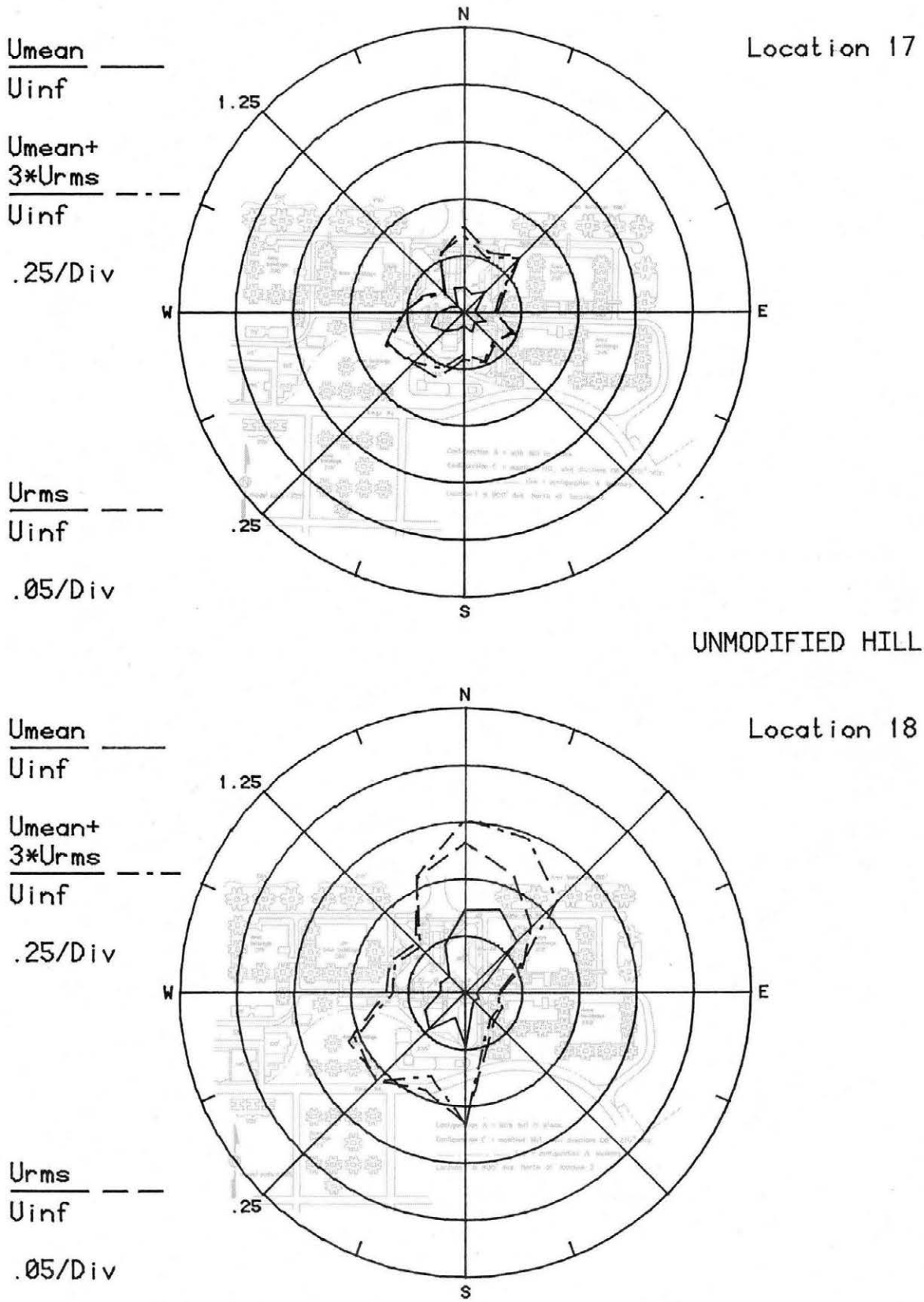

Figure 8i. Mean Velocities and Turbulence Intensities at Pedestrian Locations 17 and 18

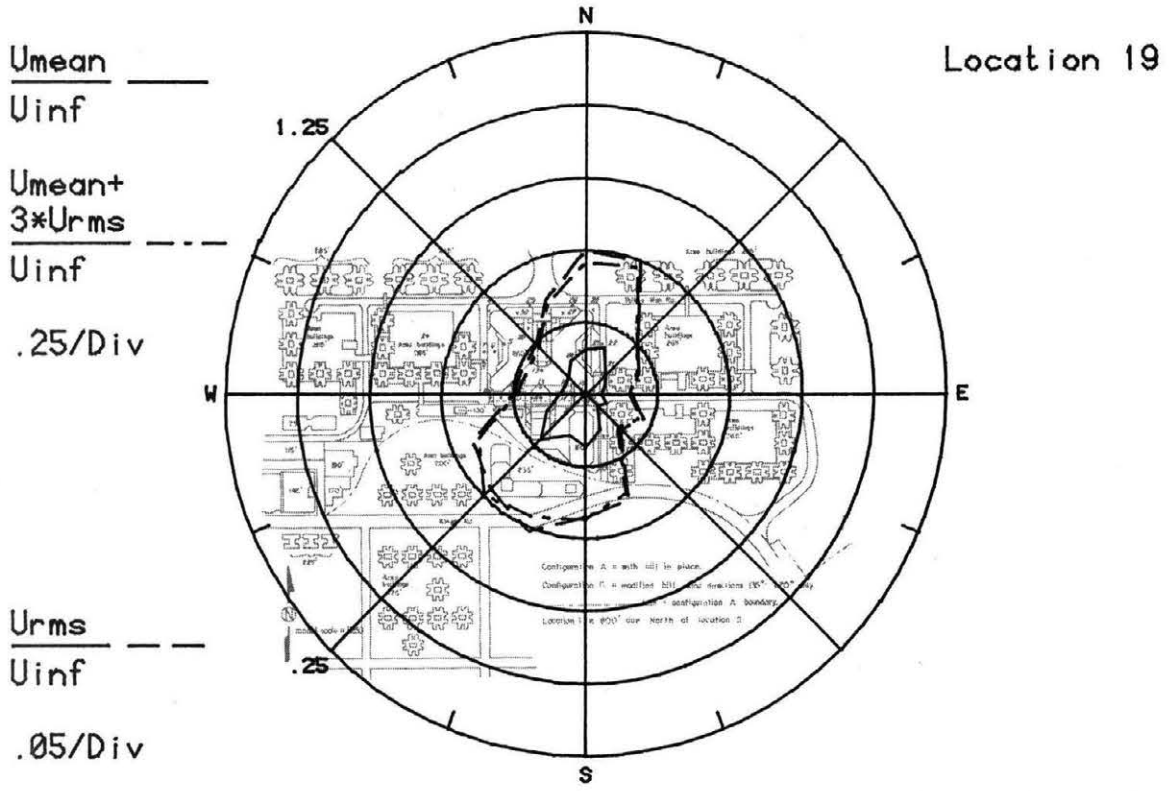

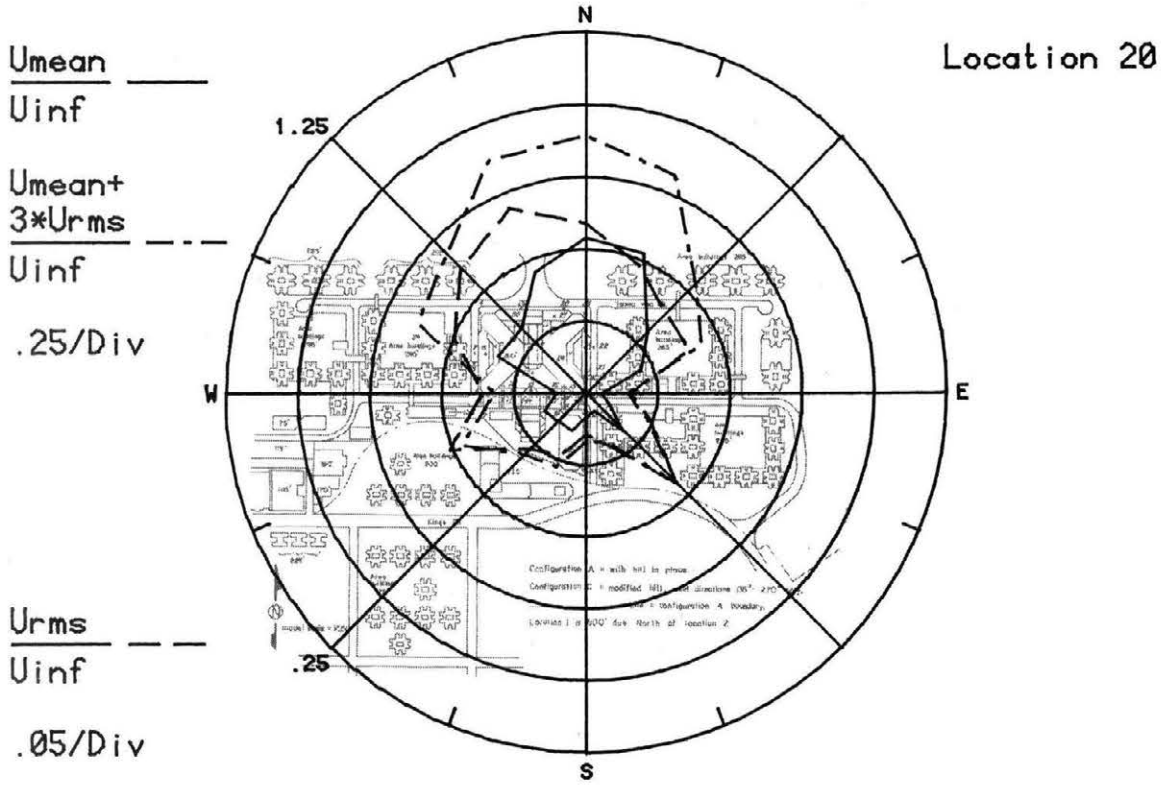

Figure 8j. Mean Velocities and Turbulence Intensities at Pedestrian Locations 19 and 20

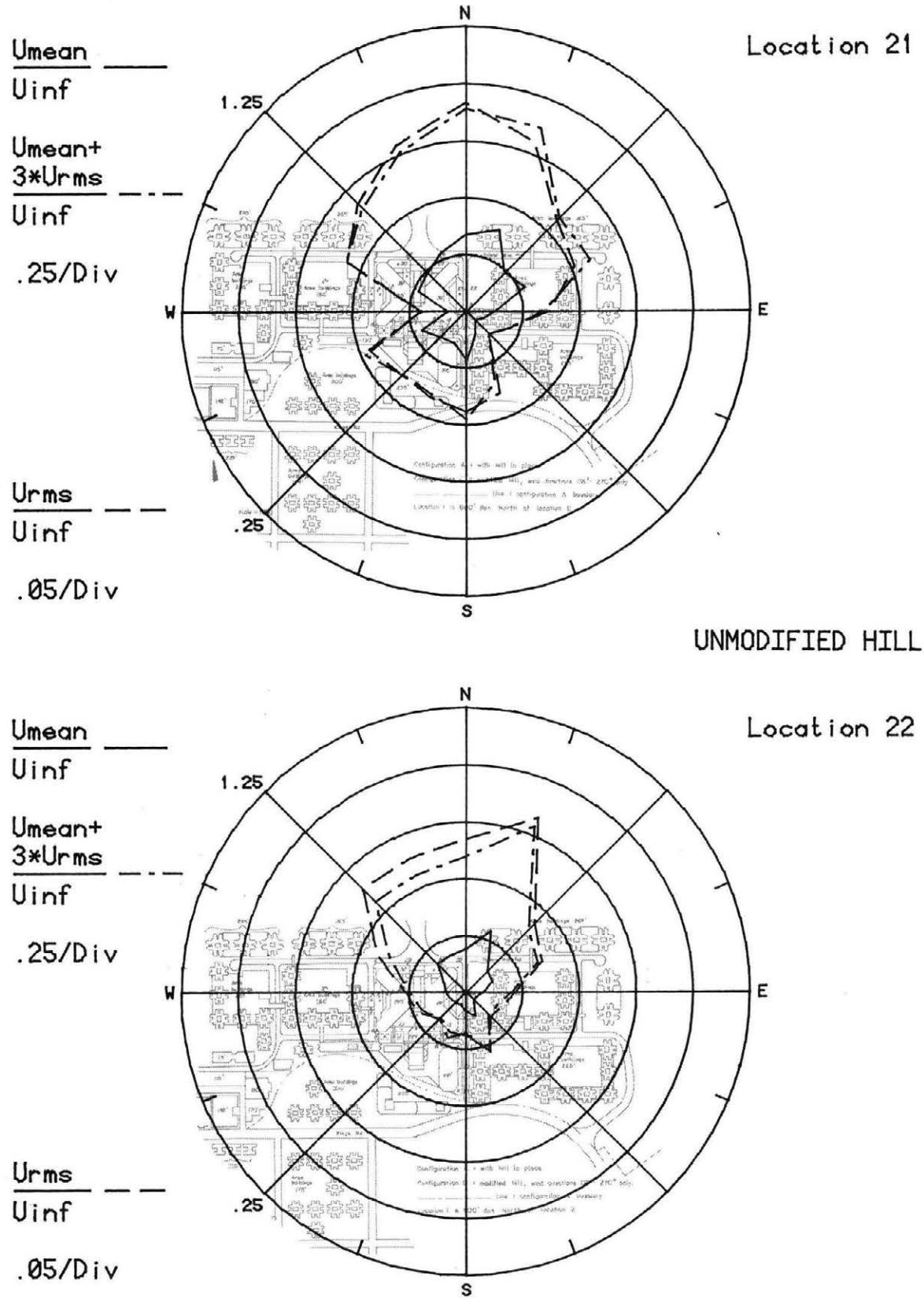

Figure 8k. Mean Velocities and Turbulence Intensities at Pedestrian Locations 21 and 22

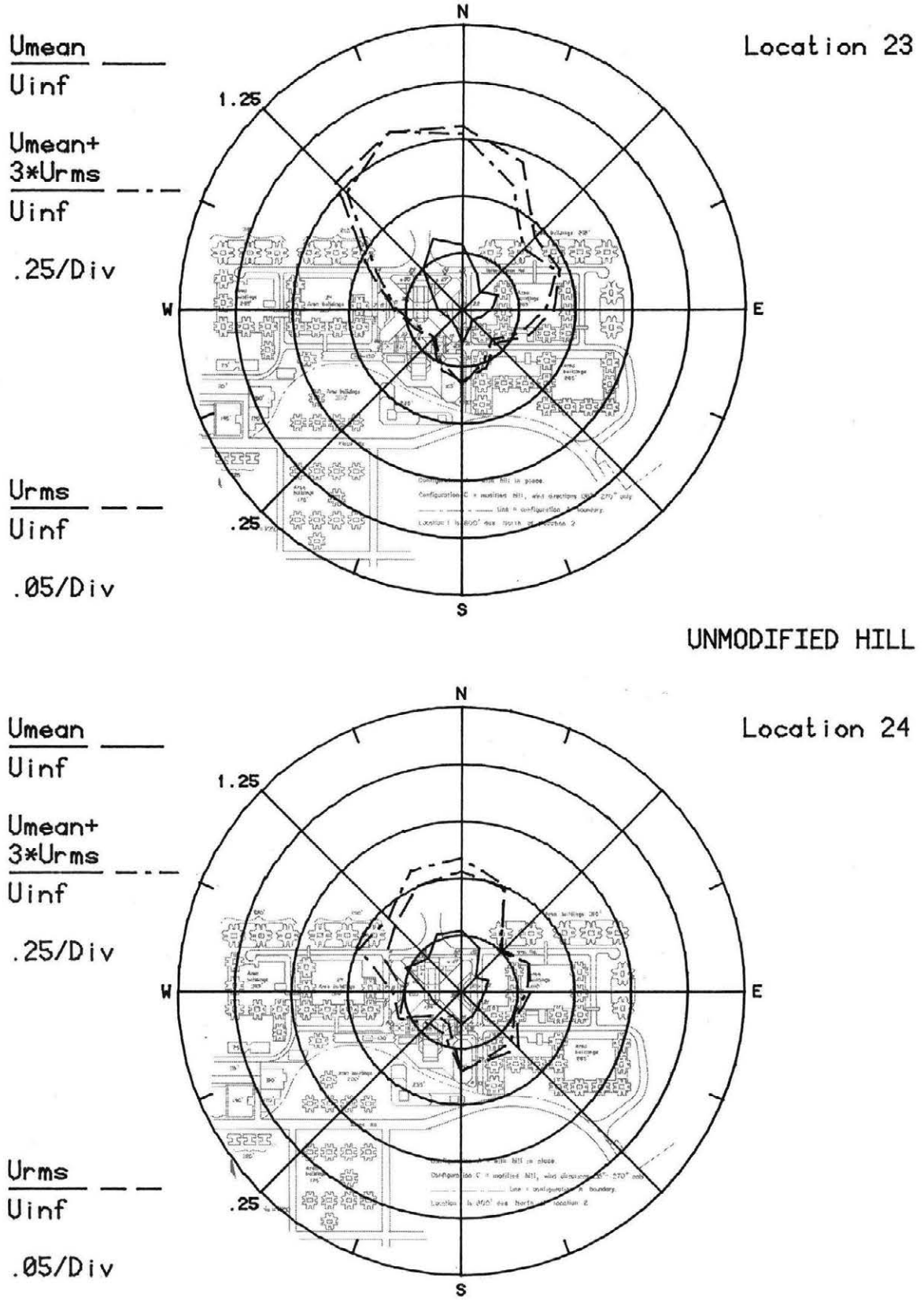

Figure 81. Mean Velocities and Turbulence Intensities at Pedestrian Locations 23 and 24

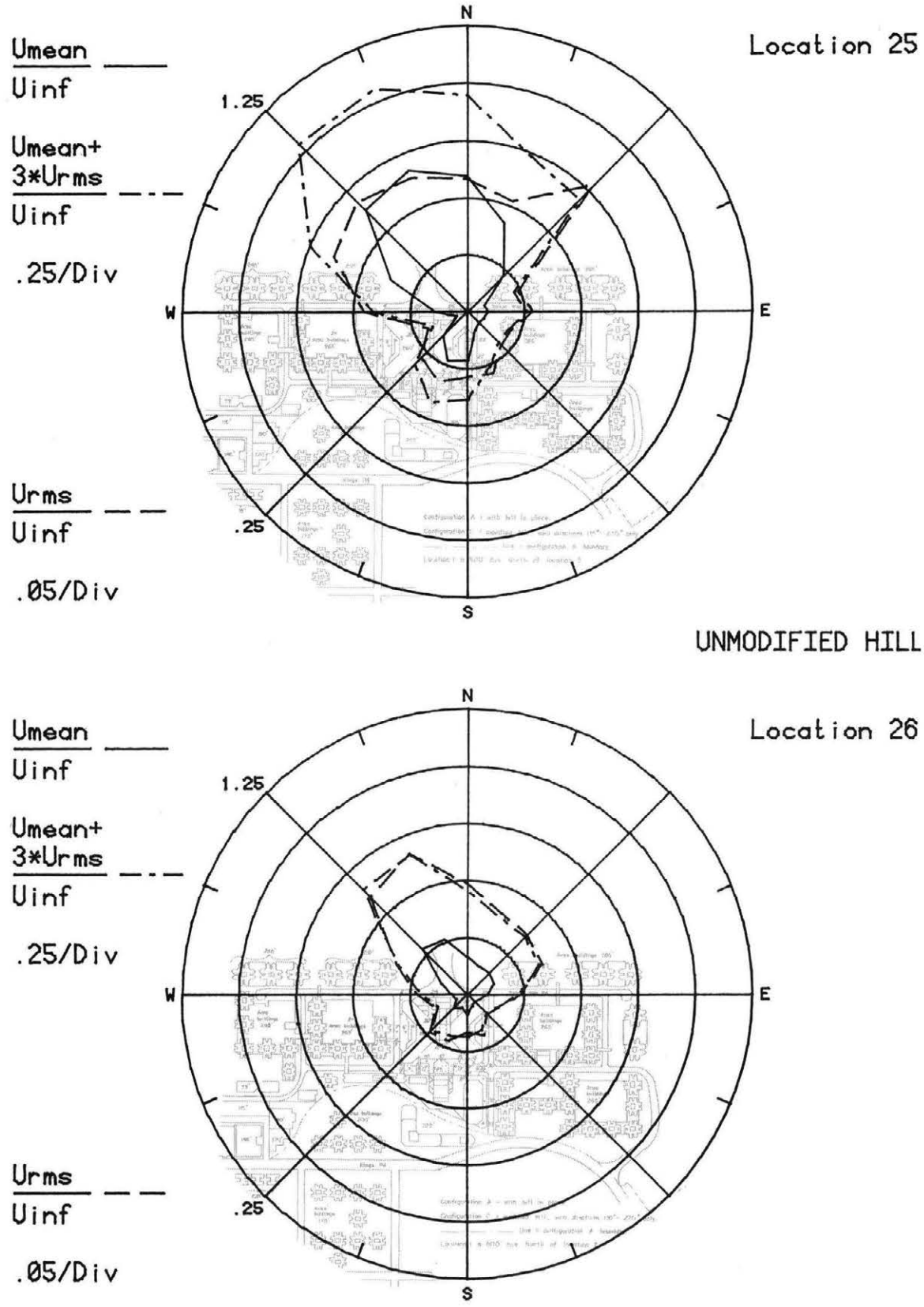

Figure 8m. Mean Velocities and Turbulence Intensities at Pedestrian Locations 25 and 26

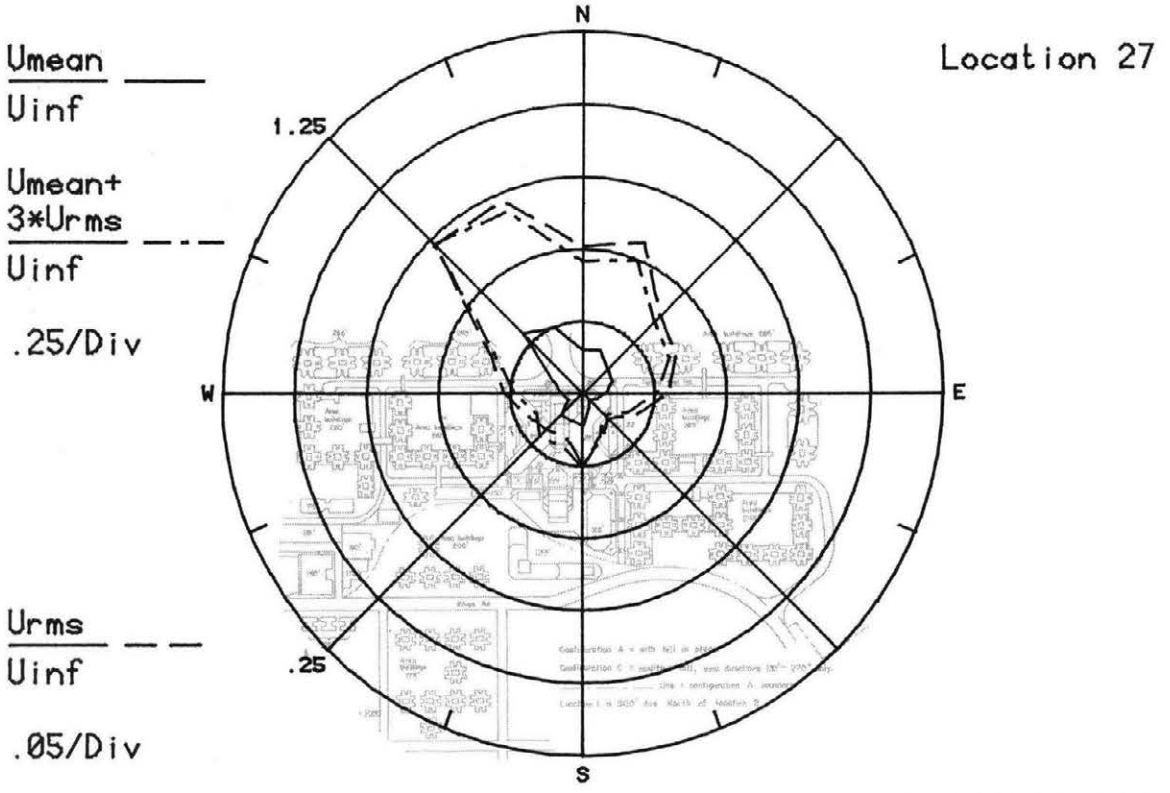

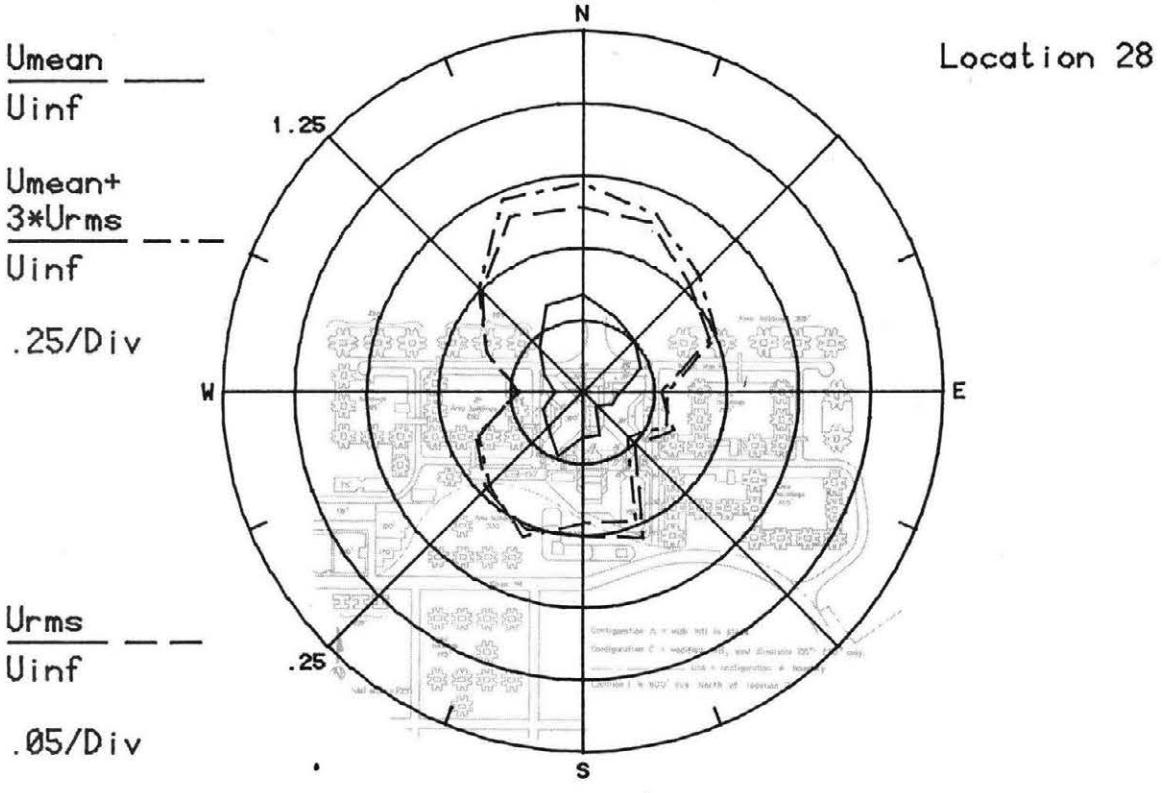

Figure 8n. Mean Velocities and Turbulence Intensities at Pedestrian Locations 27 and 28

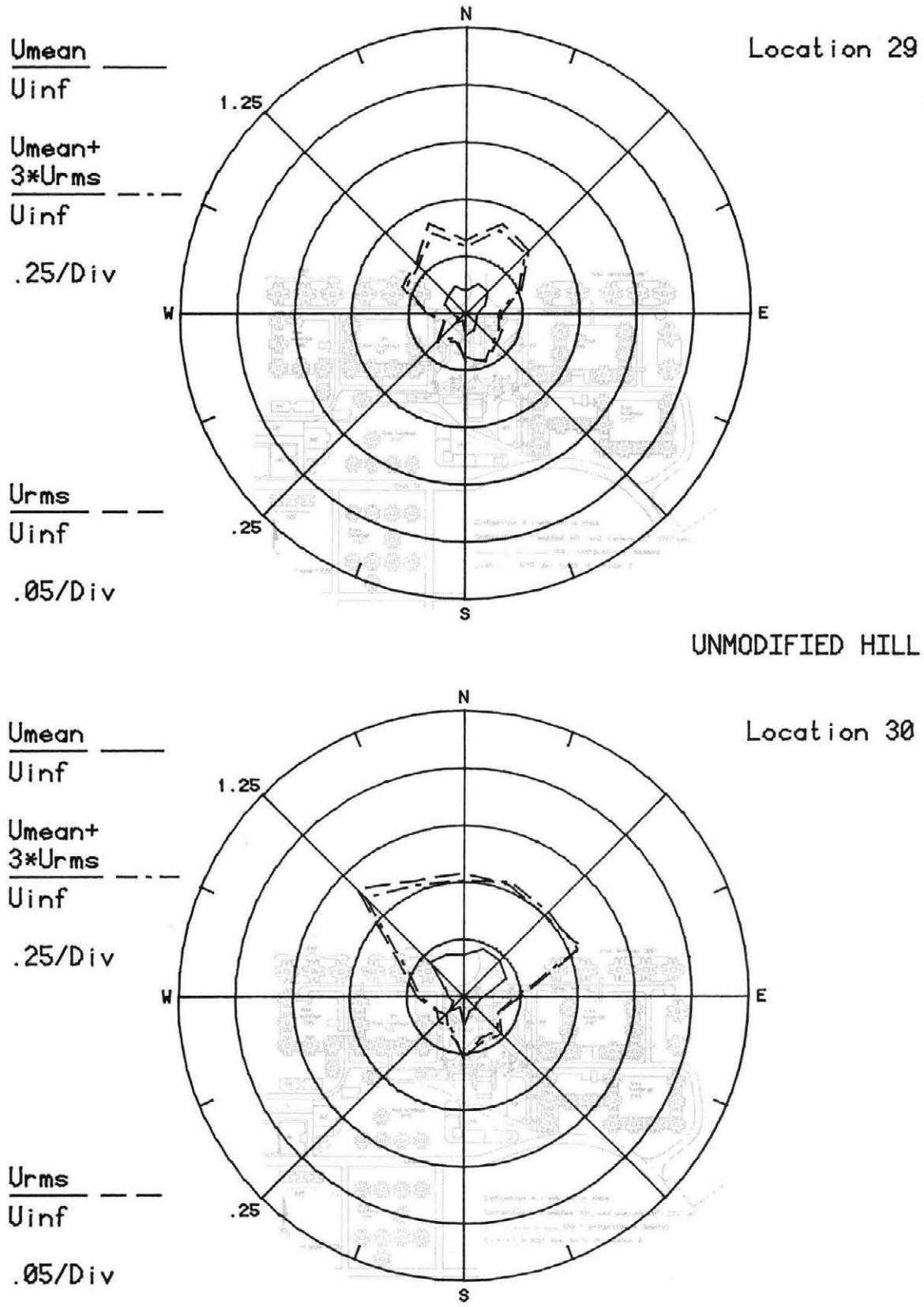

Figure 8o. Mean Velocities and Turbulence Intensities at Pedestrian Locations 29 and 30

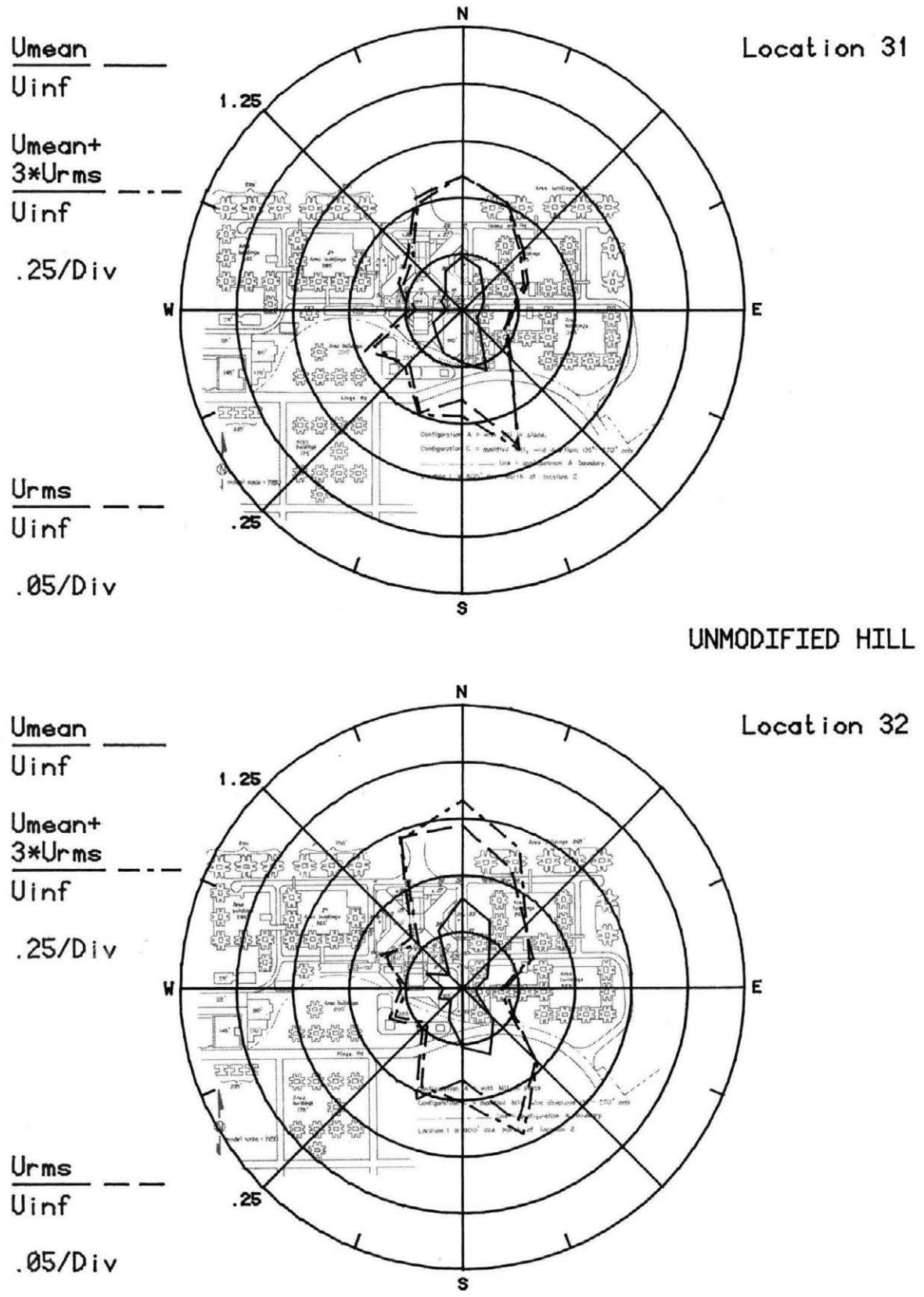

Figure 8p. Mean Velocities and Turbulence Intensities at Pedestrian Locations 31 and 32

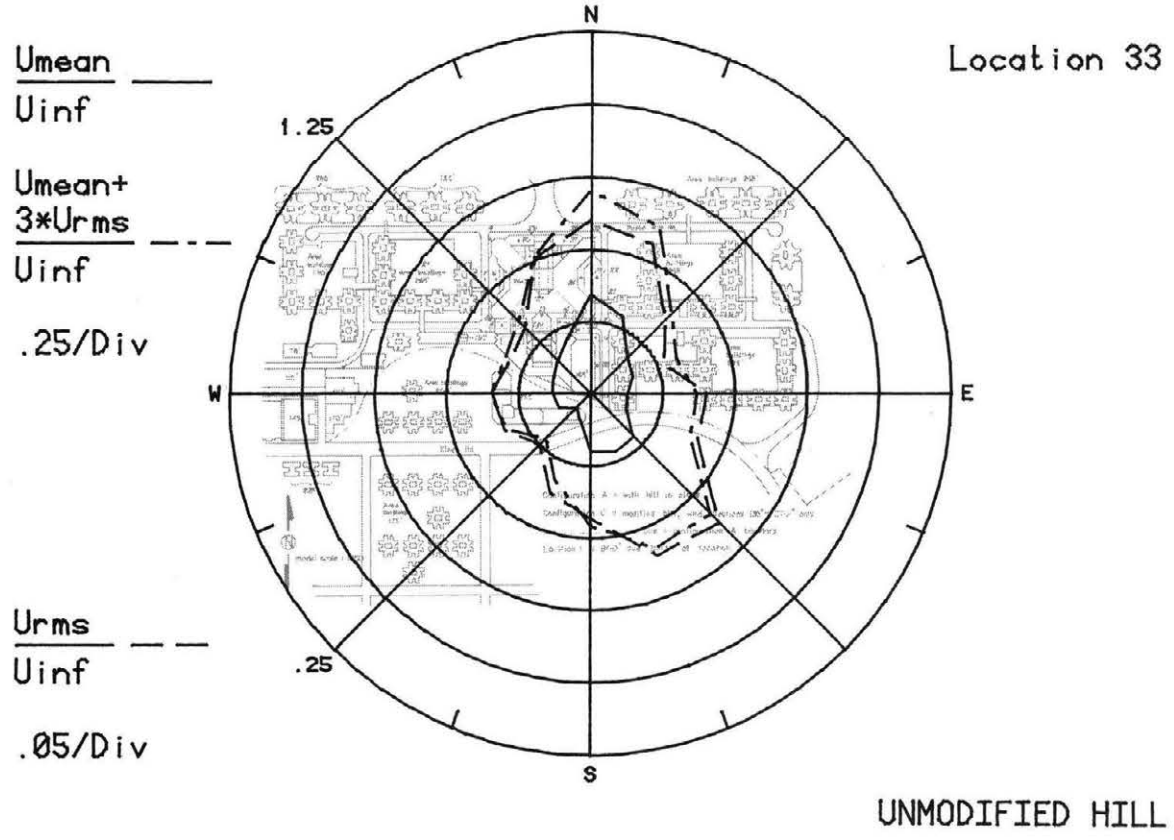

Figure 8q. Mean Velocities and Turbulence Intensities at Pedestrian Location 33

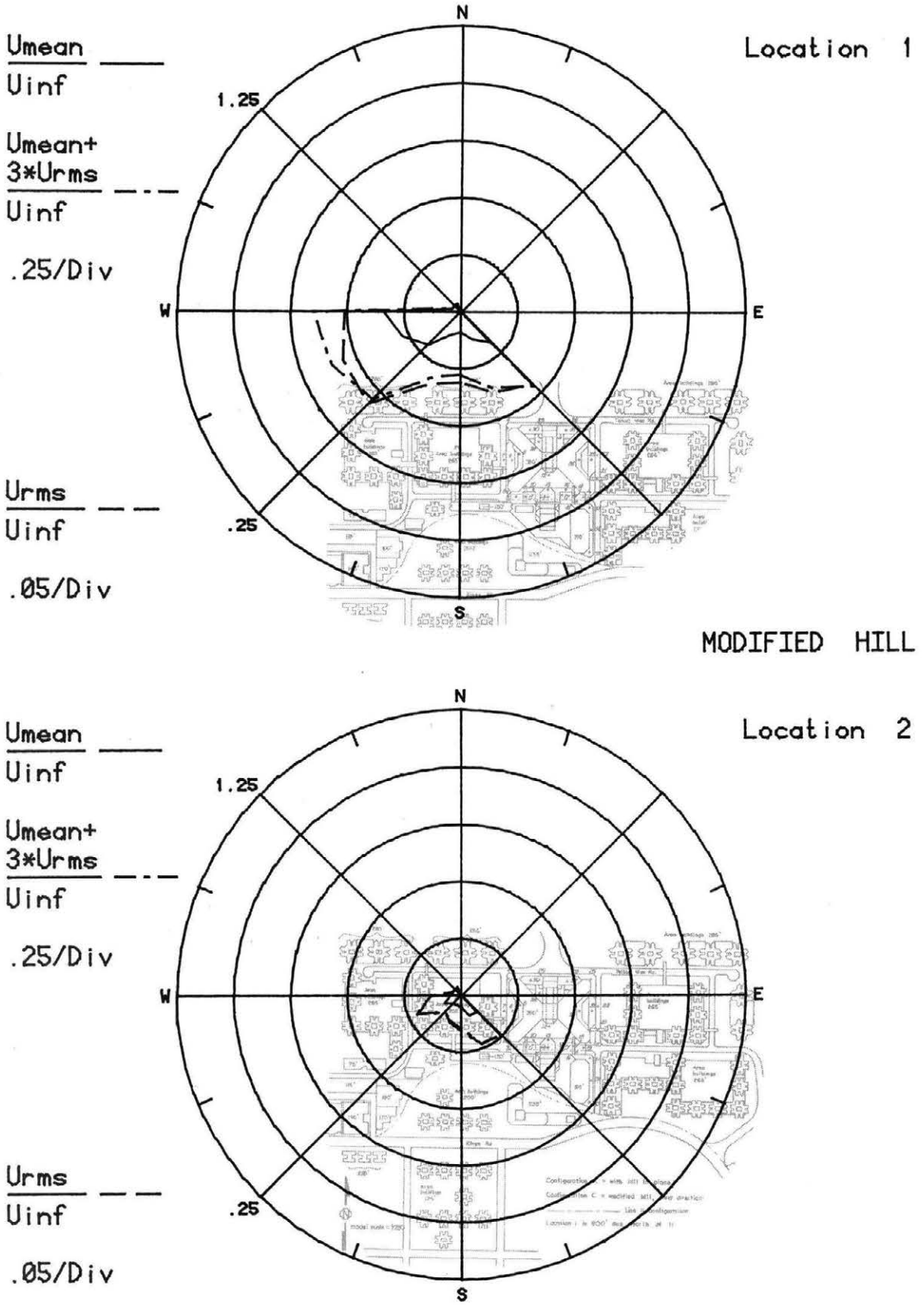

Figure 8A. Mean Velocities and Turbulence Intensities at Pedestrian Locations 1 and 2

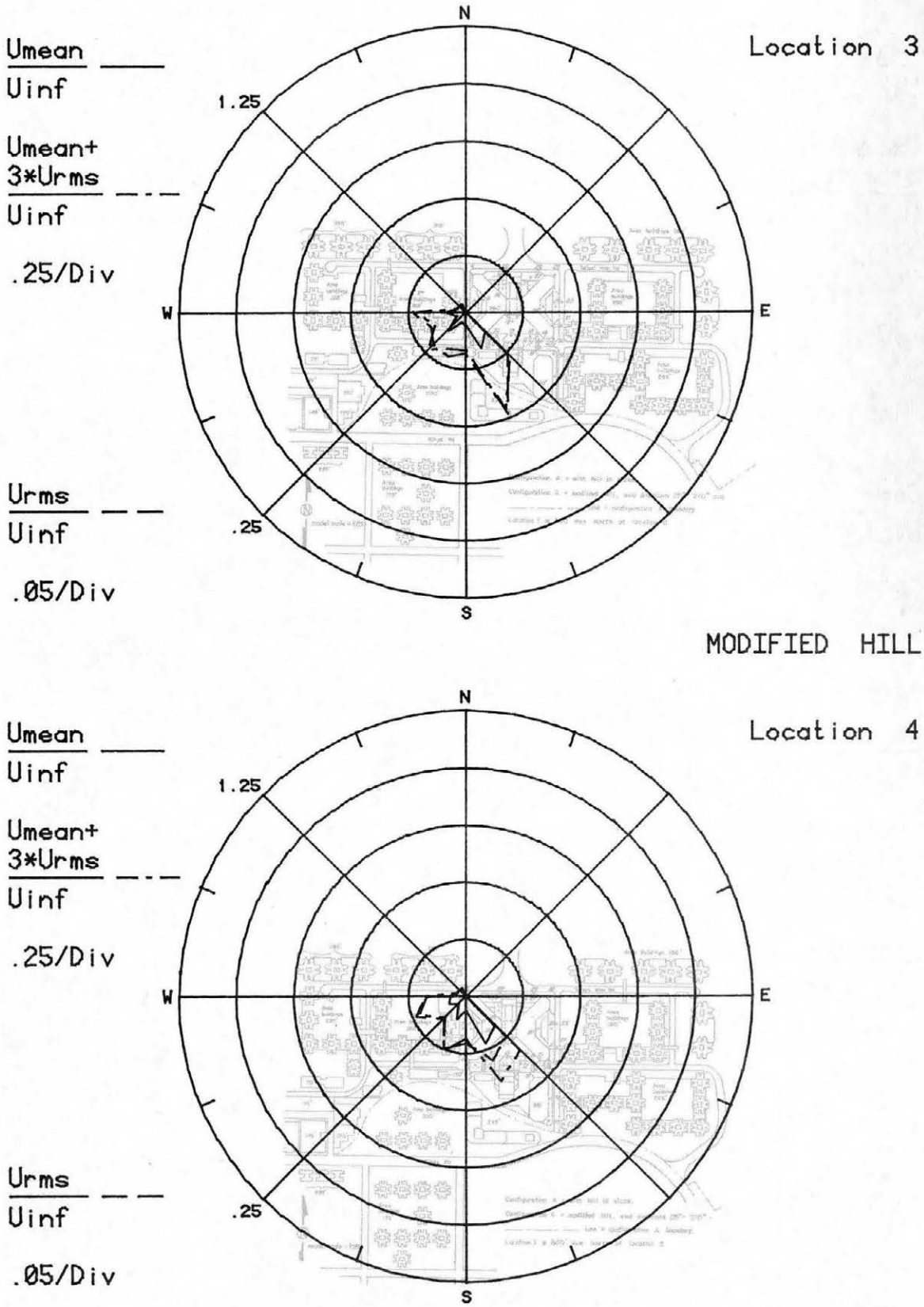

Figure 8B. Mean Velocities and Turbulence Intensities at Pedestrian Locations 3 and 4

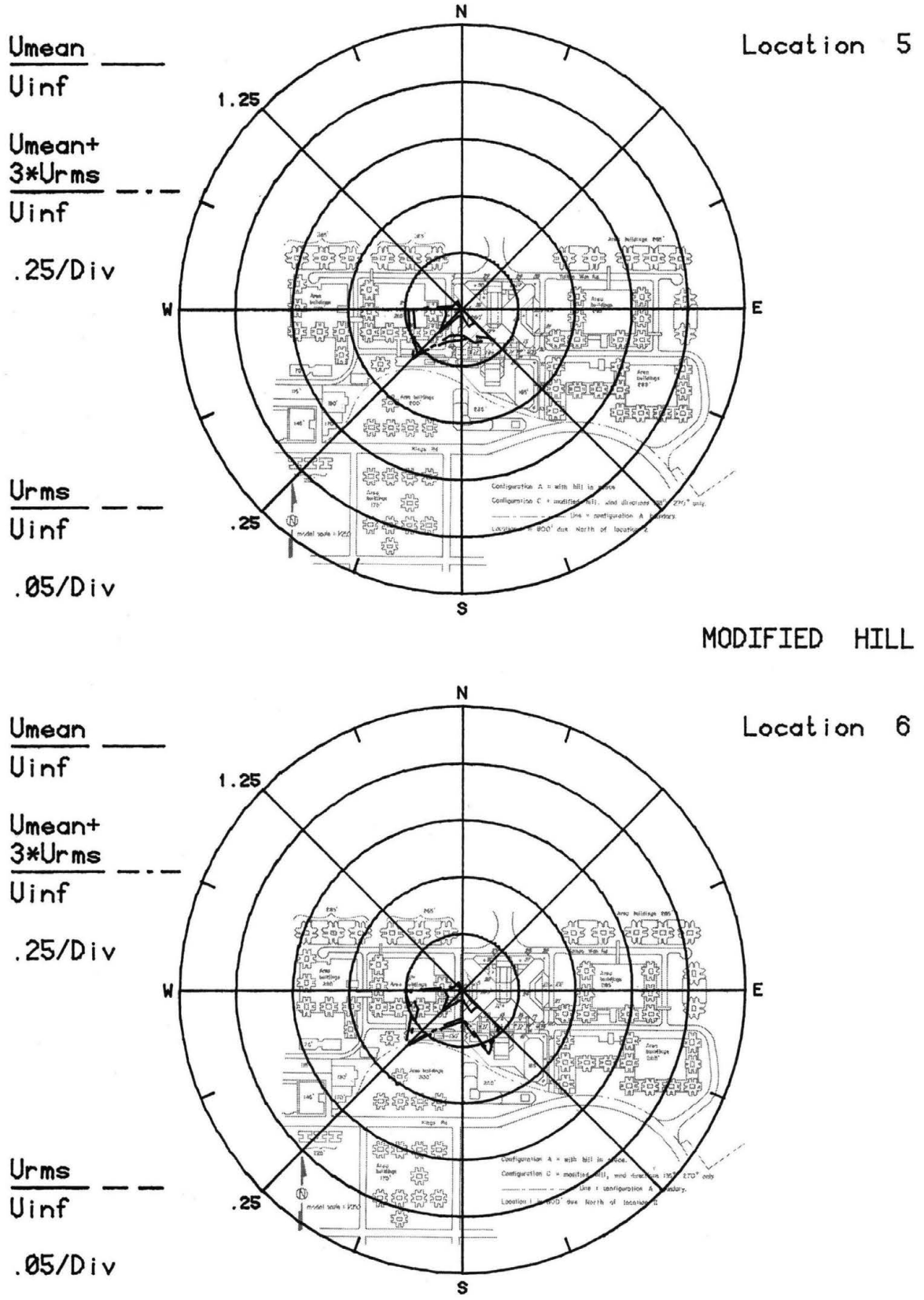

Figure 8C. Mean Velocities and Turbulence Intensities at Pedestrian Locations 5 and 6

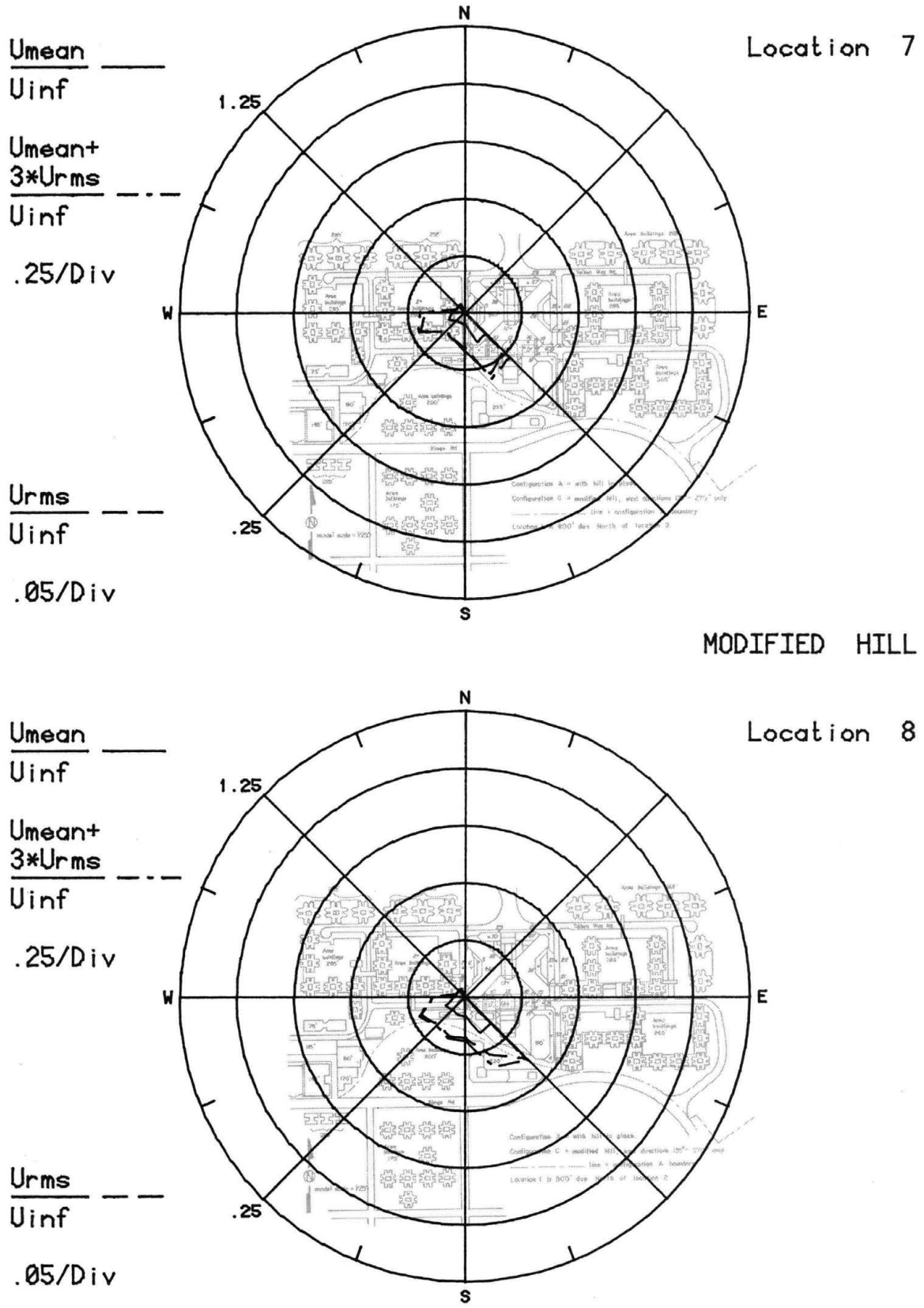

Figure 8D. Mean Velocities and Turbulence Intensities at Pedestrian Locations 7 and 8

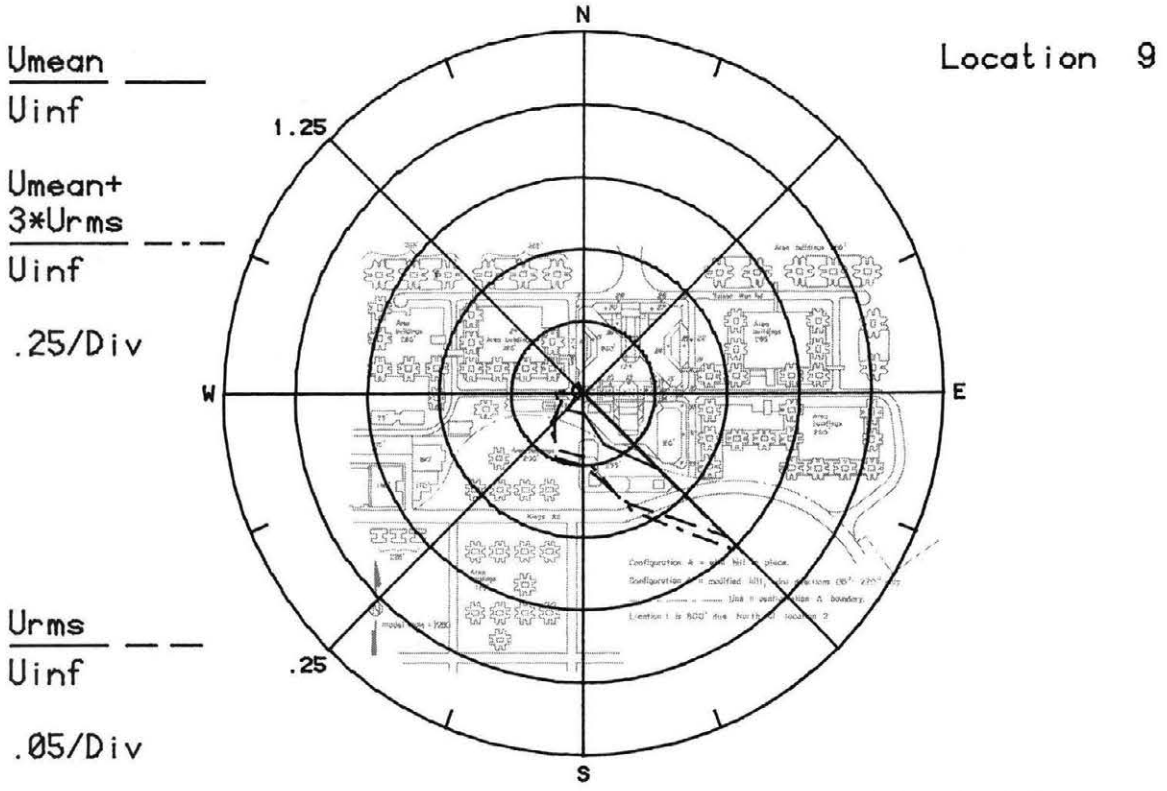

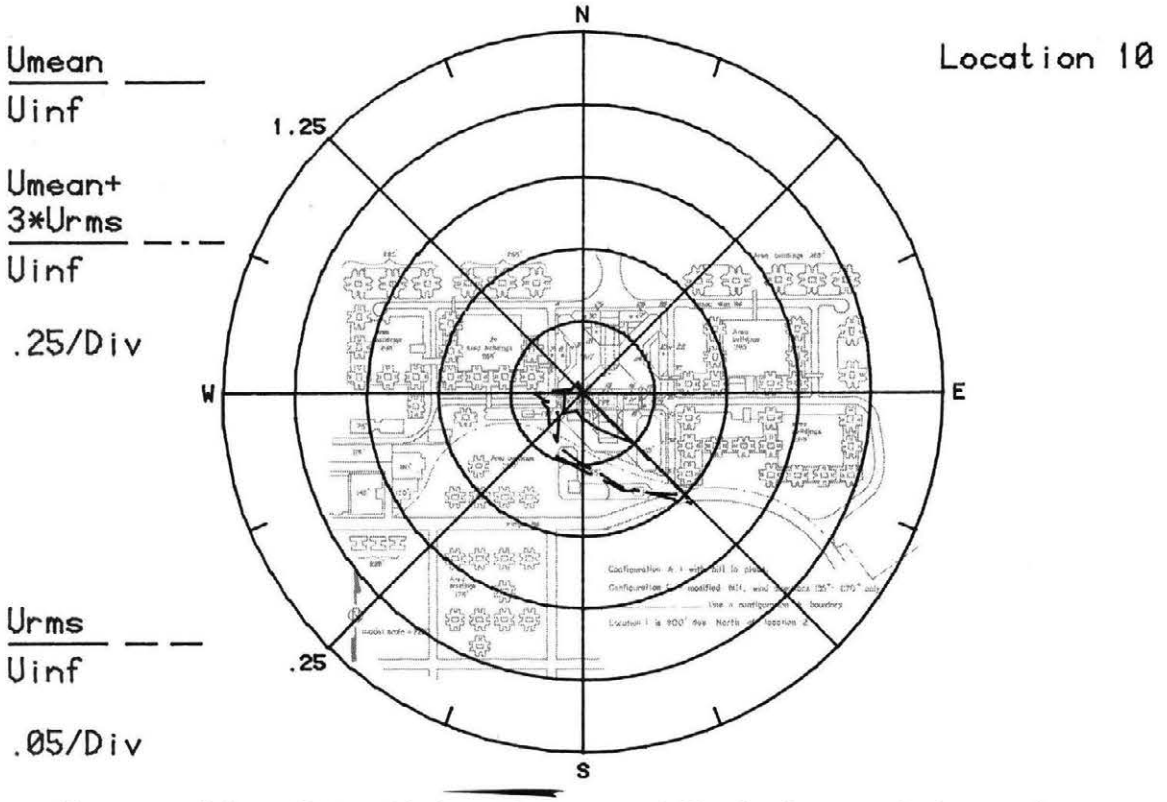

Figure 8E. Mean Velocities and Turbulence Intensities at Pedestrian Locations 9 and 10

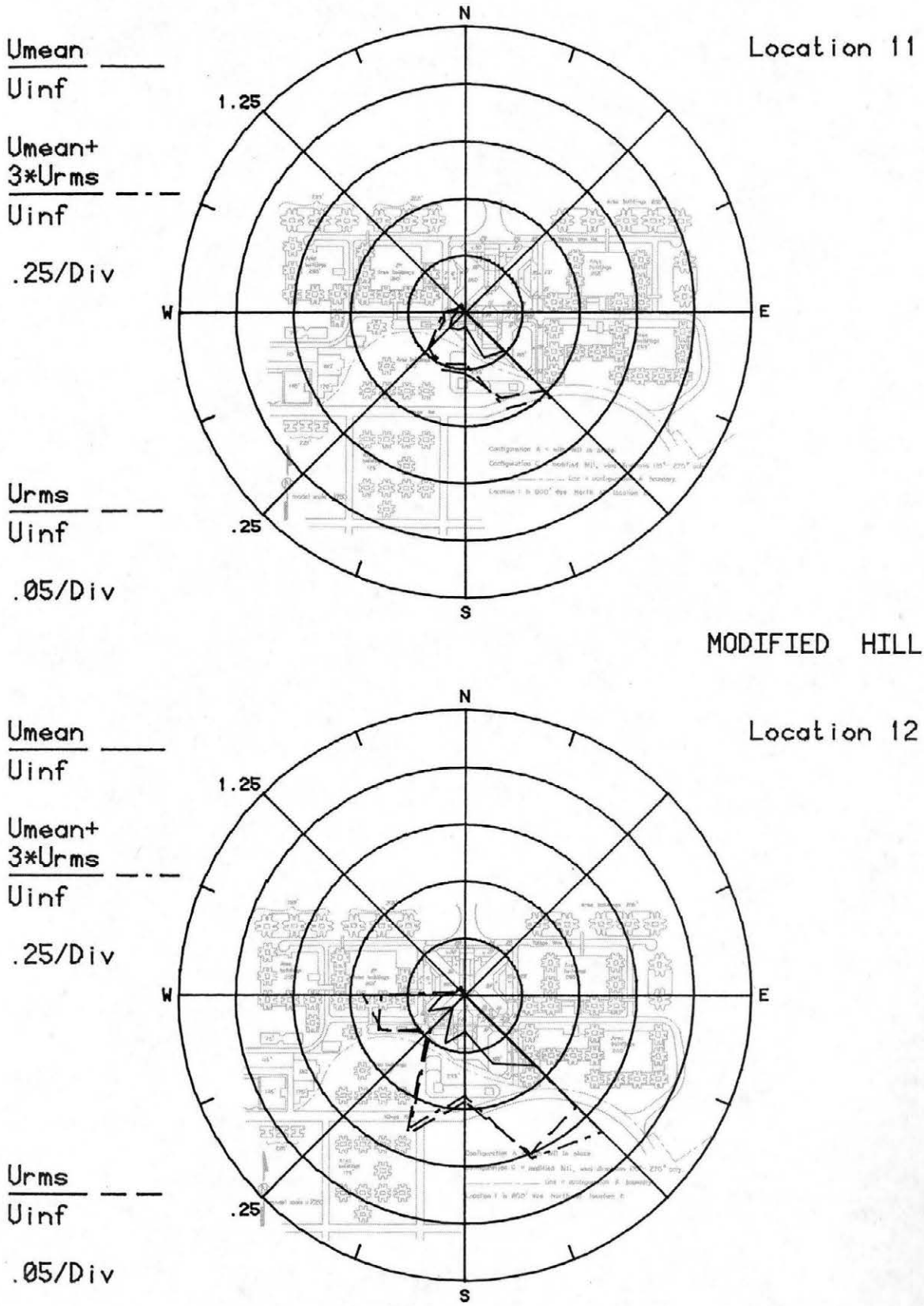

Figure 8F. Mean Velocities and Turbulence Intensities at Pedestrian Locations 11 and 12

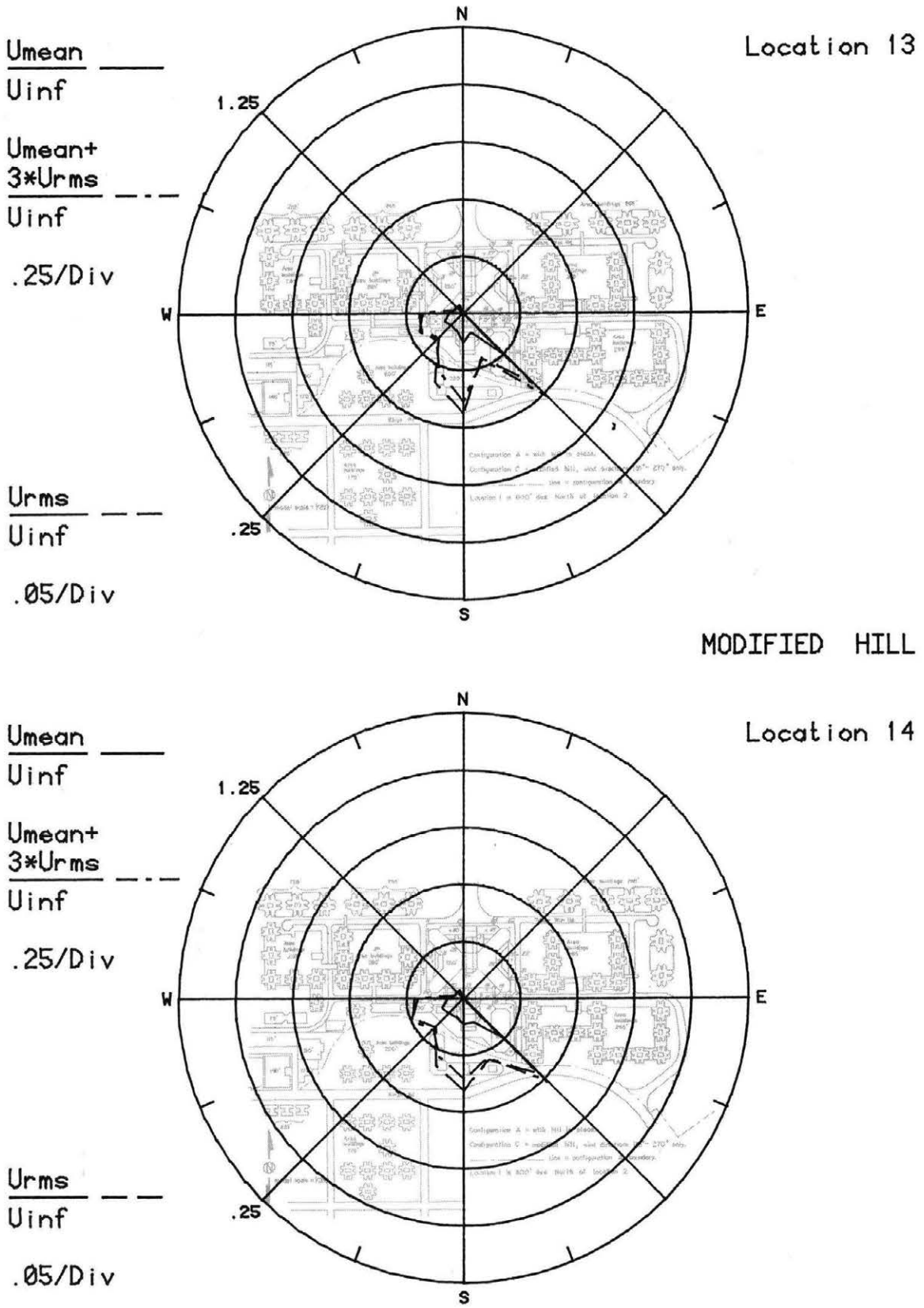

Figure 8G. Mean Velocities and Turbulence Intensities at Pedestrian Locations 13 and 14

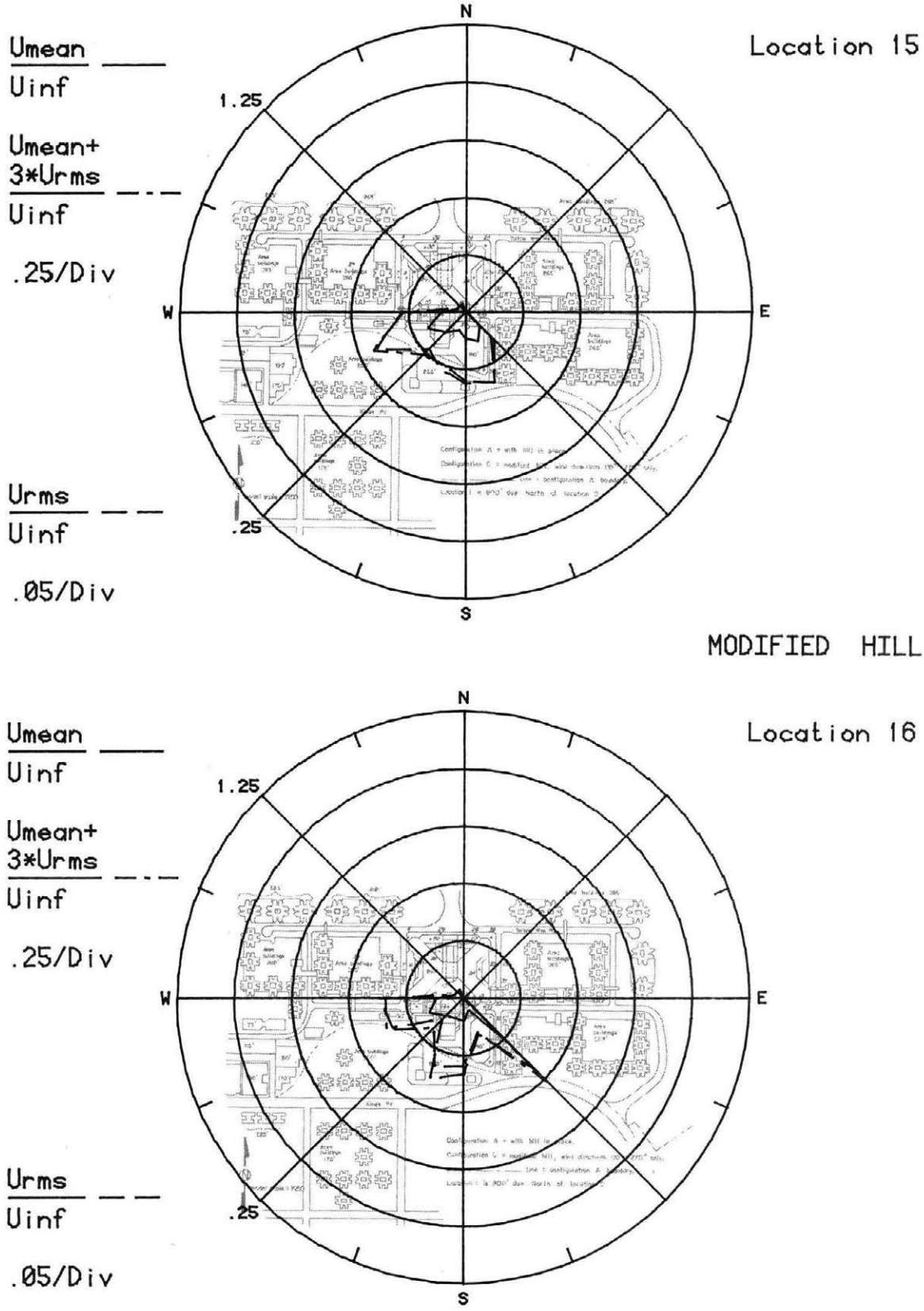

Figure 8H. Mean Velocities and Turbulence Intensities at Pedestrian Locations 15 and 16

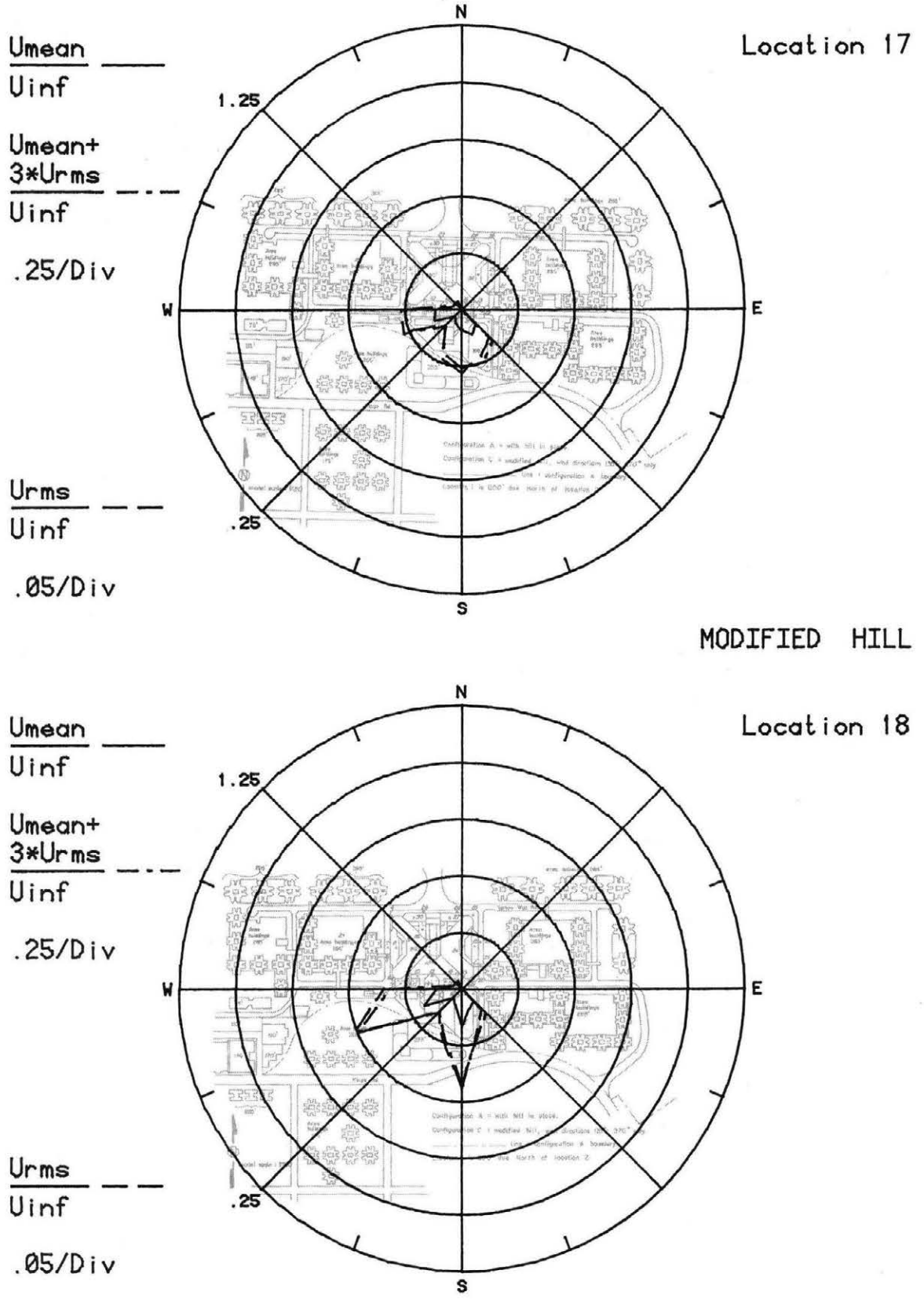

Figure 8I. Mean Velocities and Turbulence Intensities at Pedestrian Locations 17 and 18

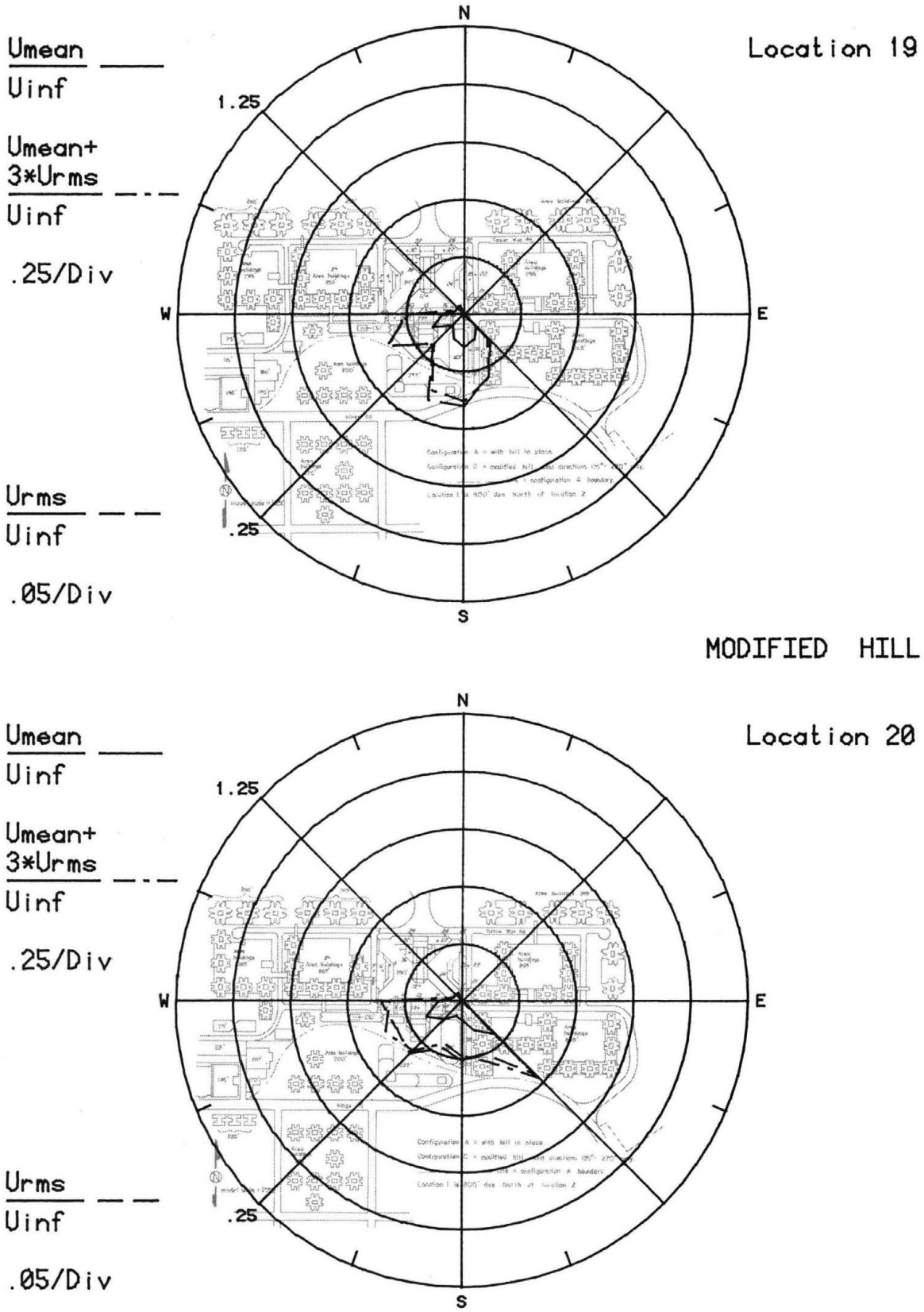

Figure 8J. Mean Velocities and Turbulence Intensities at Pedestrian Locations 19 and 20

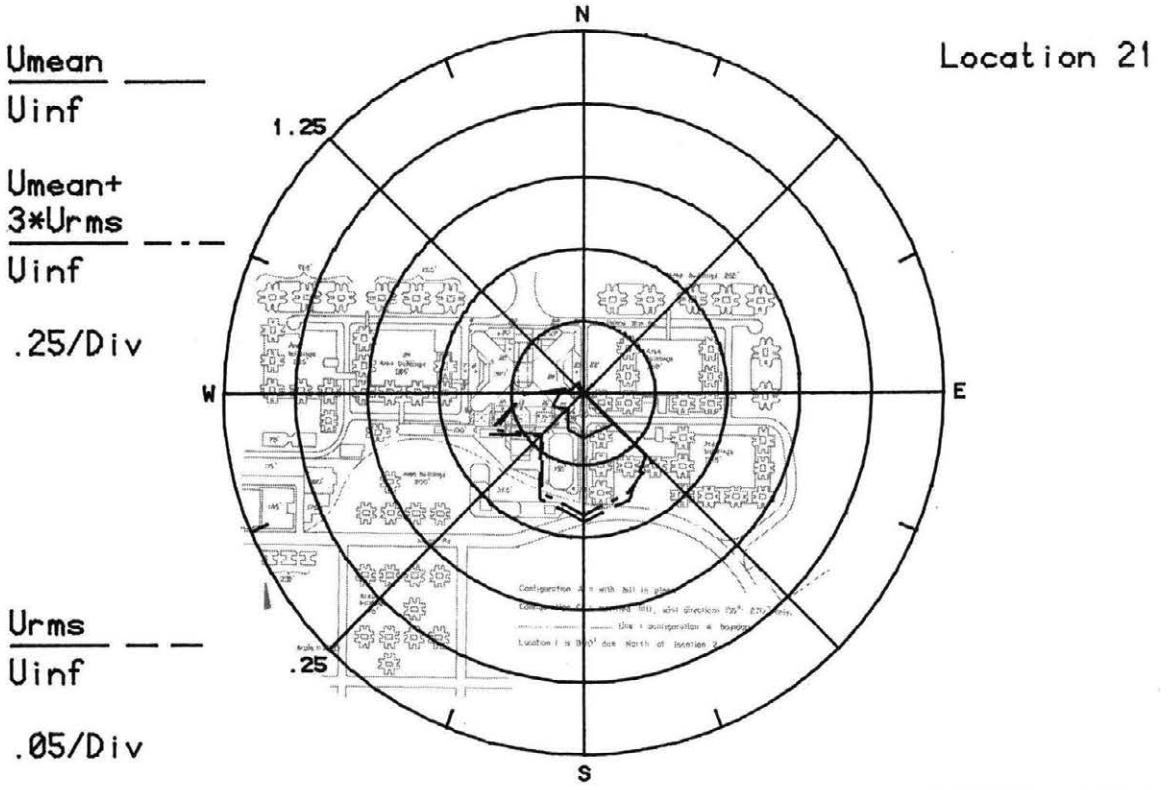

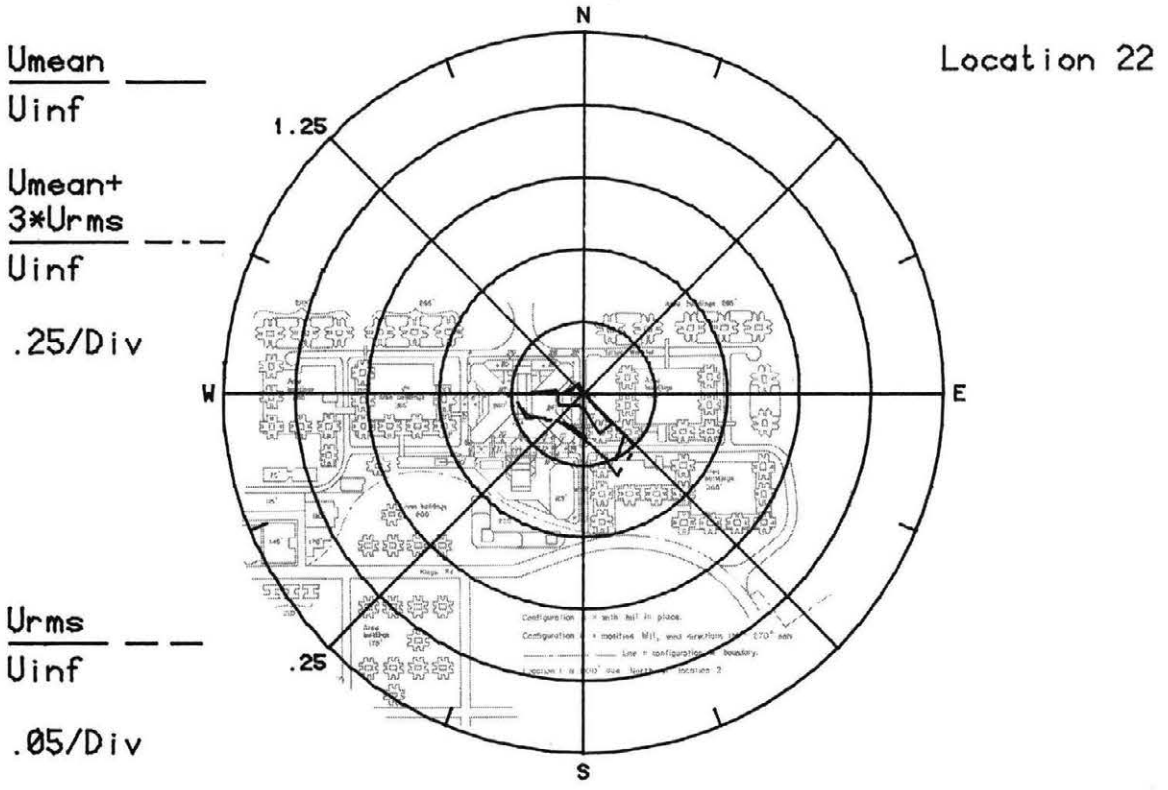

Figure 8K. Mean Velocities and Turbulence Intensities at Pedestrian Locations 21 and 22

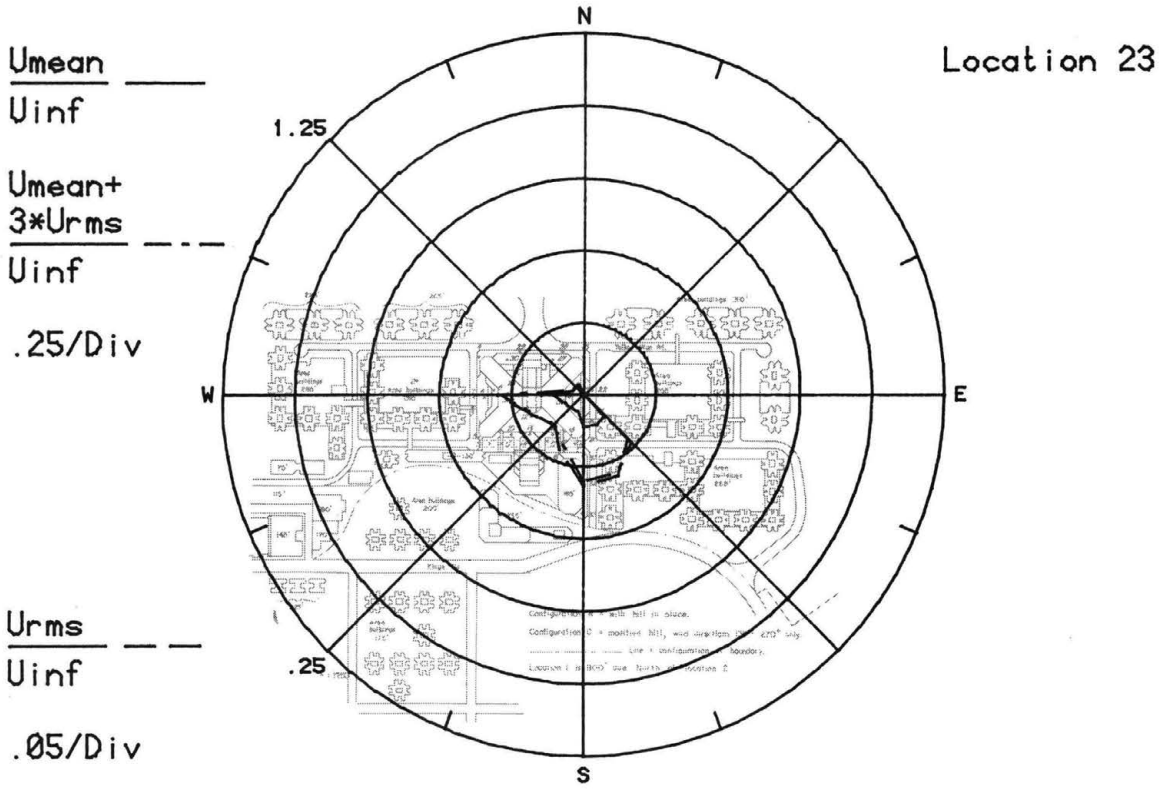

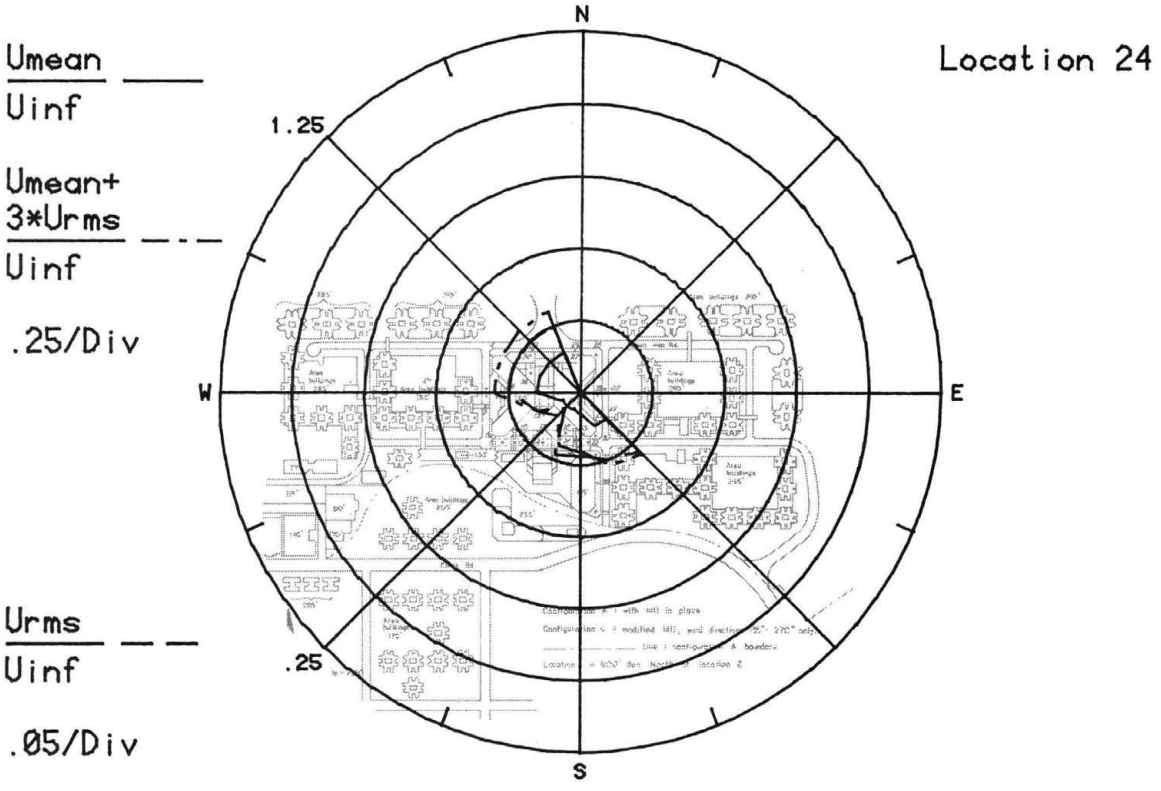

Figure 8L. Mean Velocities and Turbulence Intensities at Pedestrian Locations 23 and 24

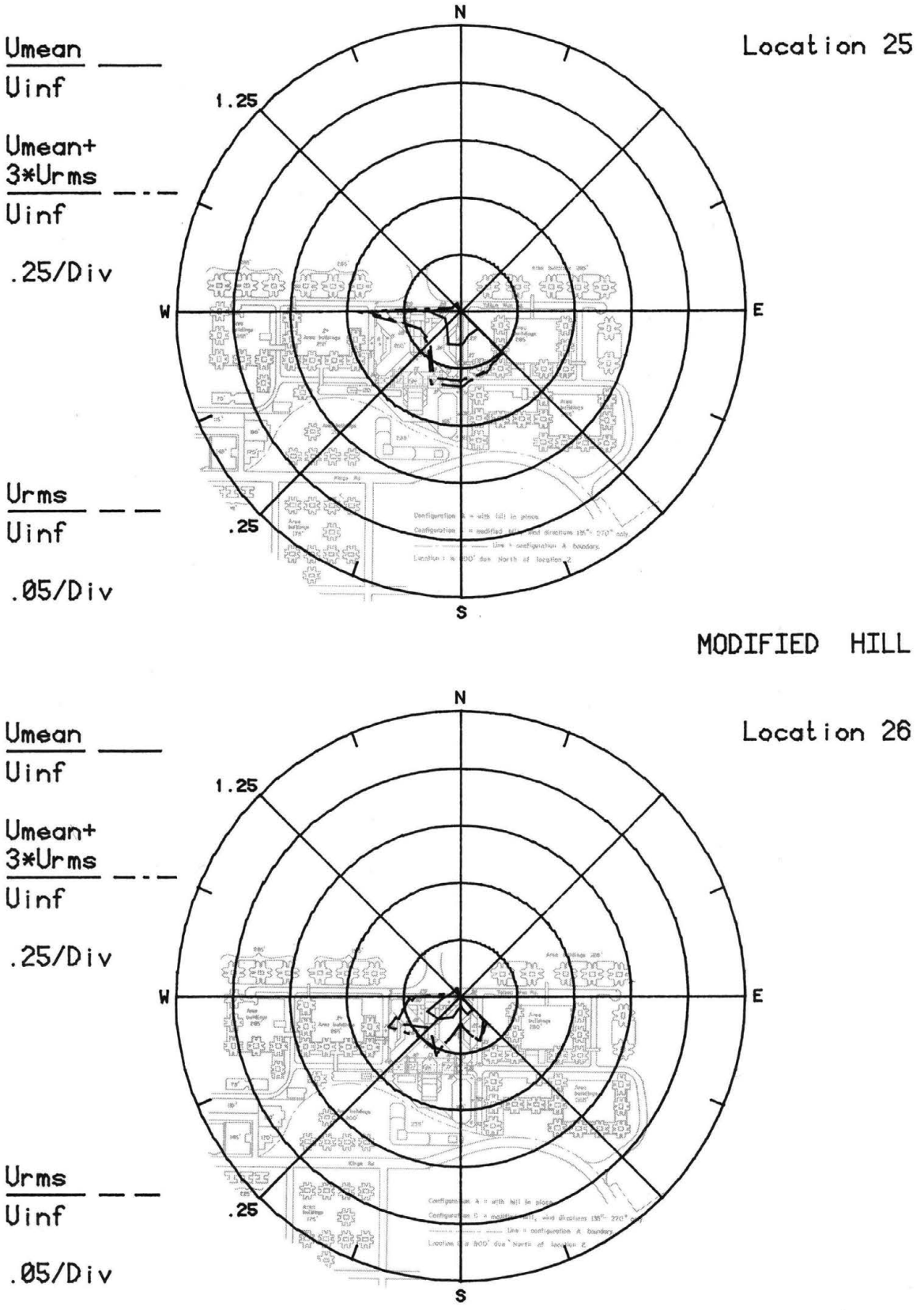

Figure 8M. Mean Velocities and Turbulence Intensities at Pedestrian Locations 25 and 26

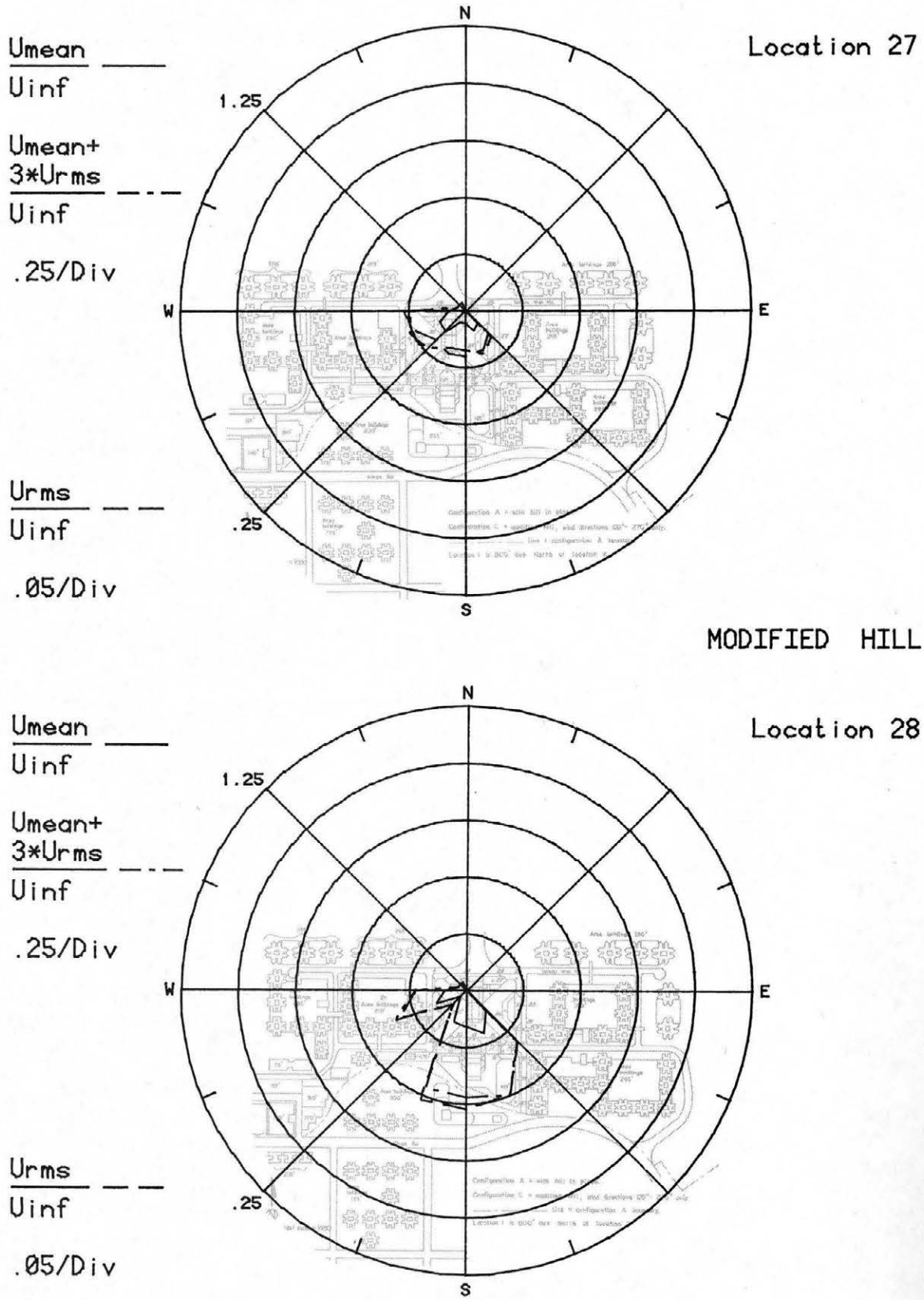

Figure 8N. Mean Velocities and Turbulence Intensities at Pedestrian Locations 27 and 28

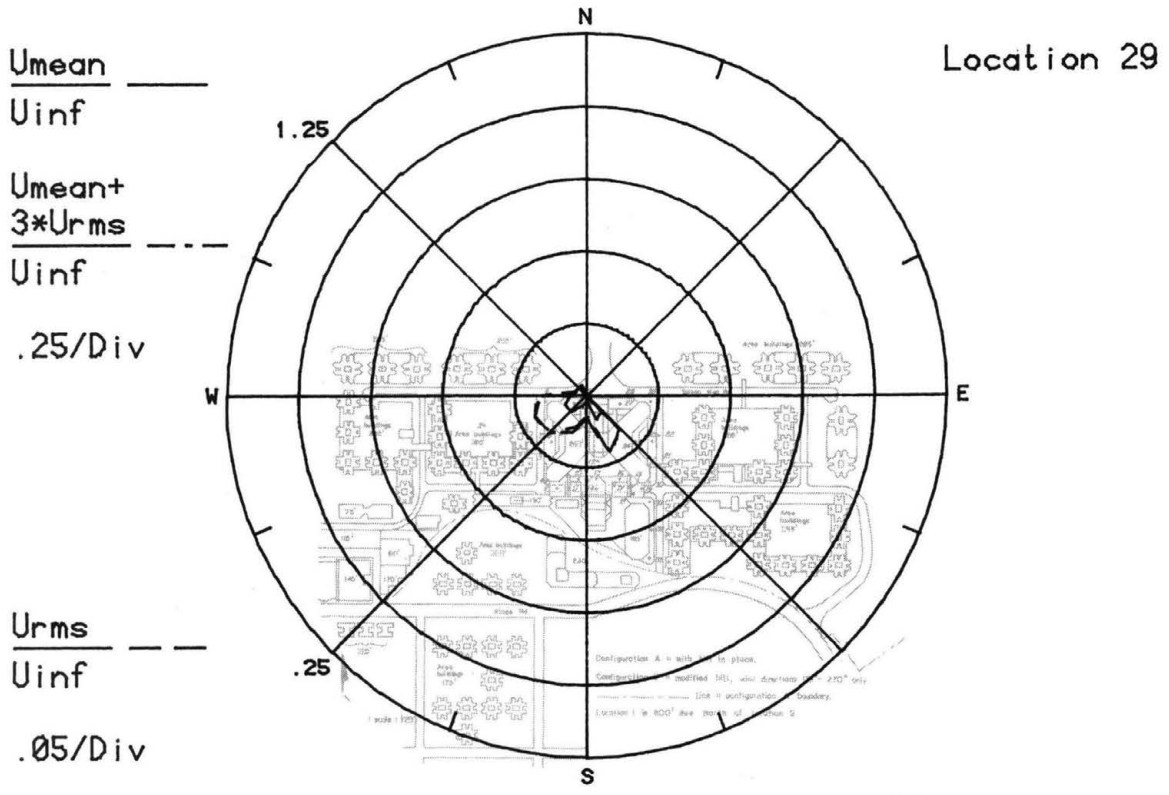

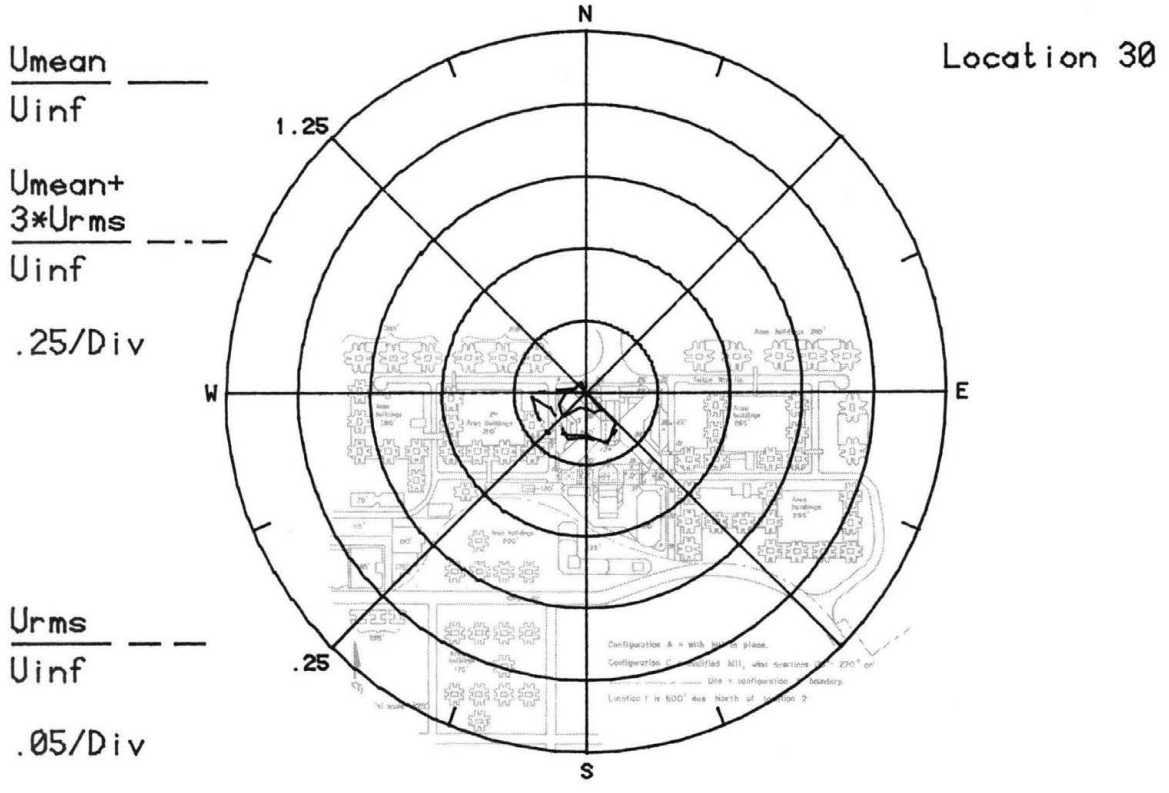

Figure 80. Mean Velocities and Turbulence Intensities at Pedestrian Locations 29 and 30

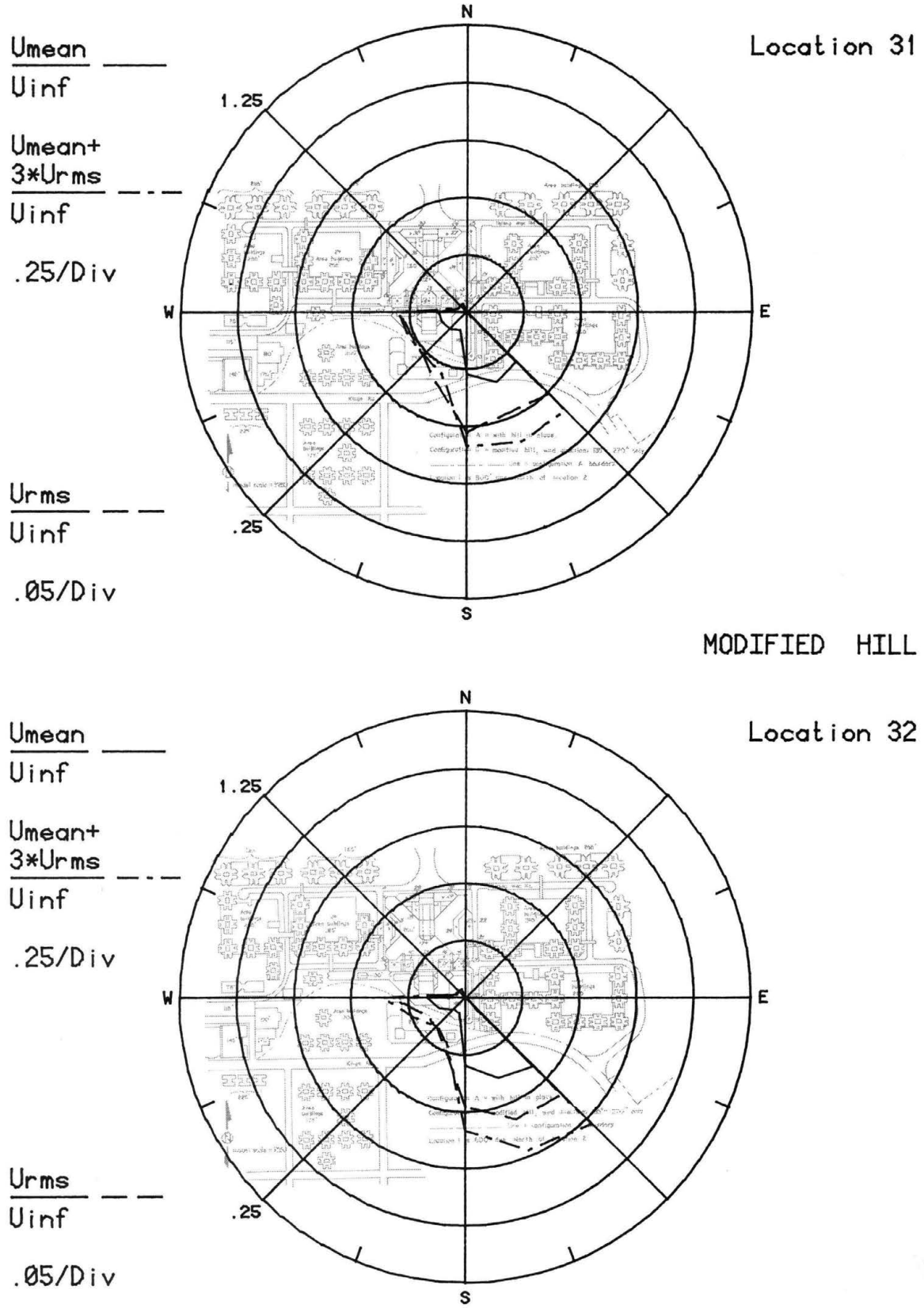

Figure 8P. Mean Velocities and Turbulence Intensities at Pedestrian Locations 31 and 32

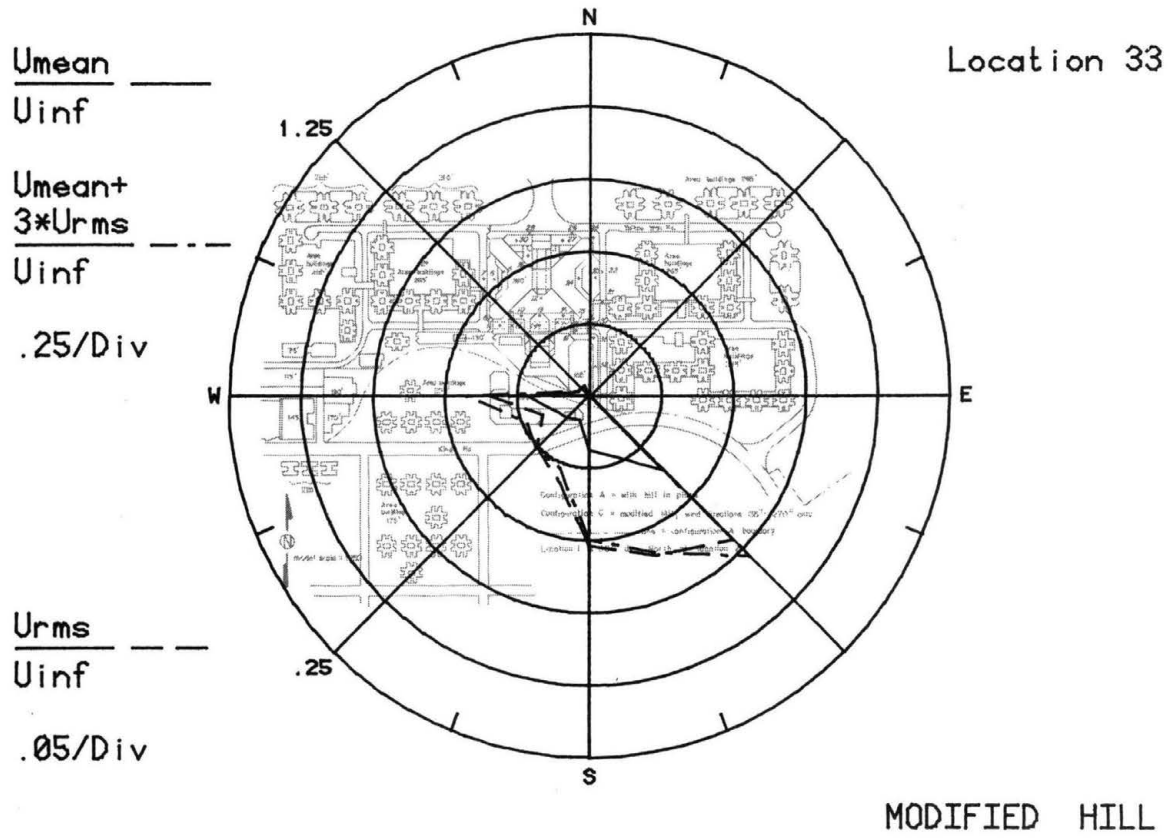

Figure 8Q. Mean Velocities and Turbulence Intensities at Pedestrian Location 33

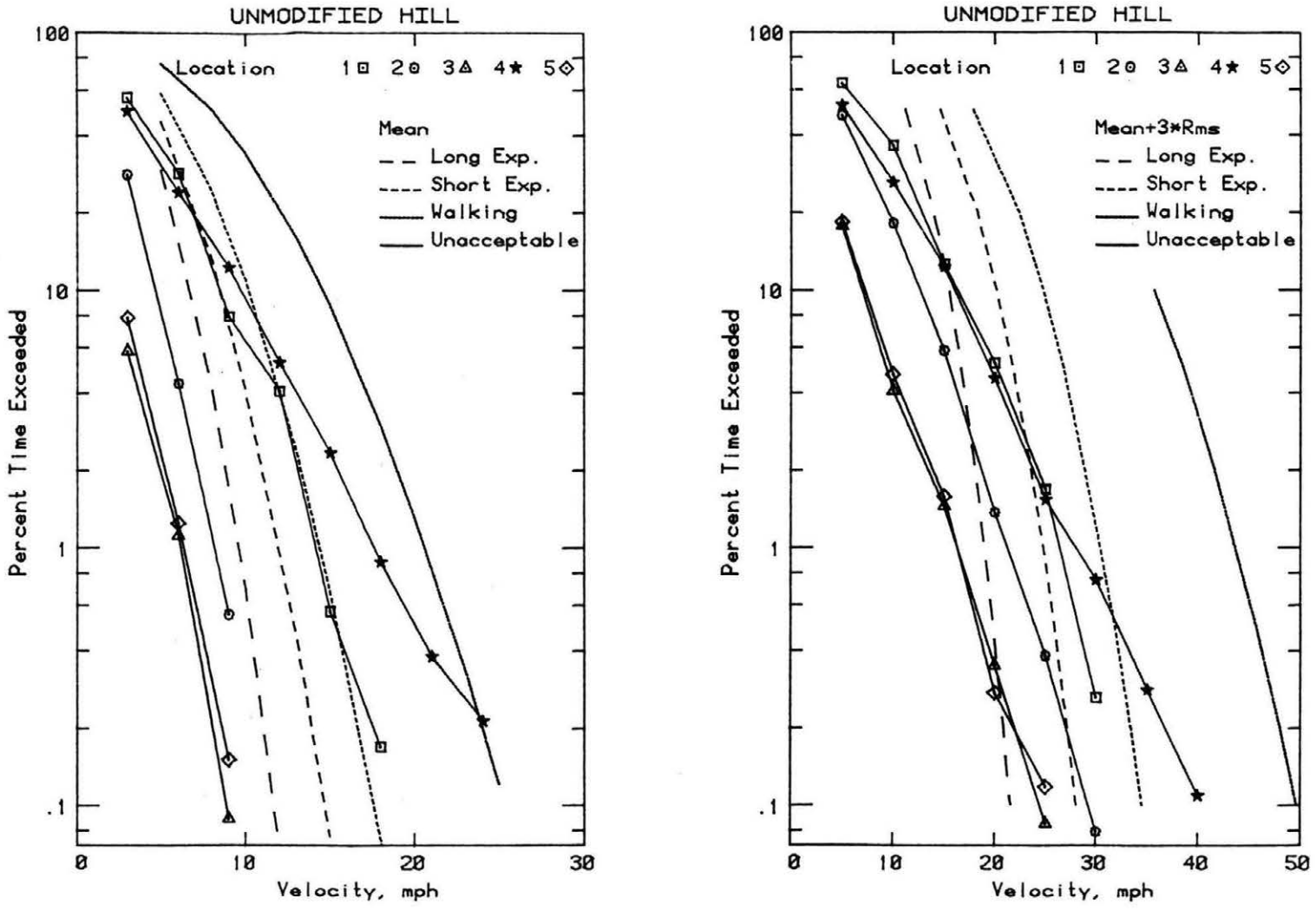

Figure 9a. Wind Velocity Probabilities for Pedestrian Locations

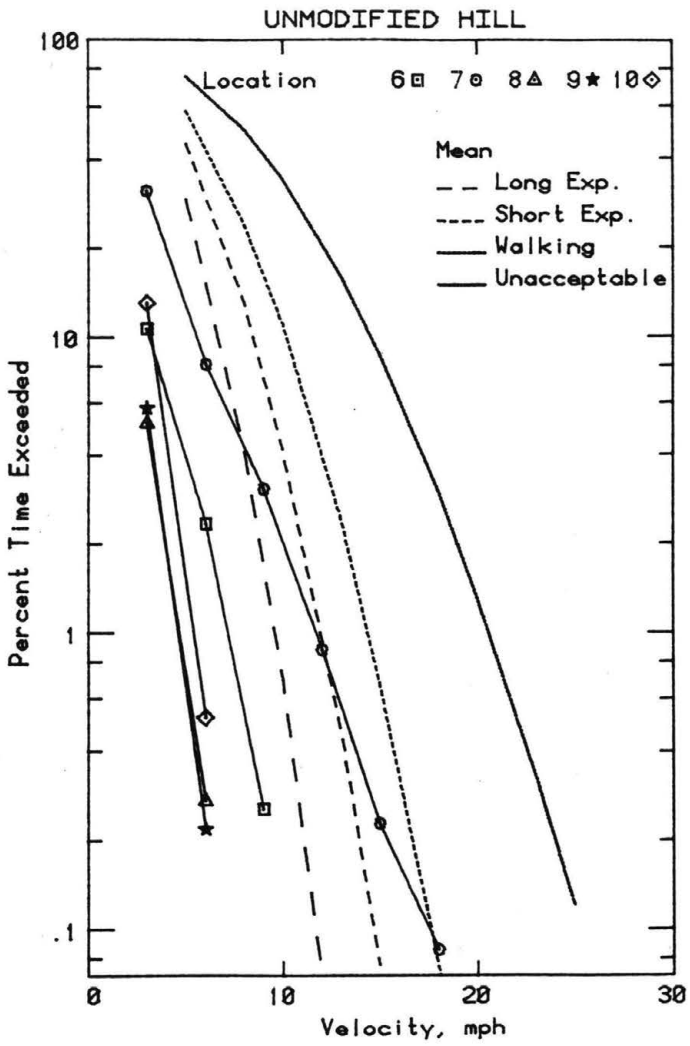

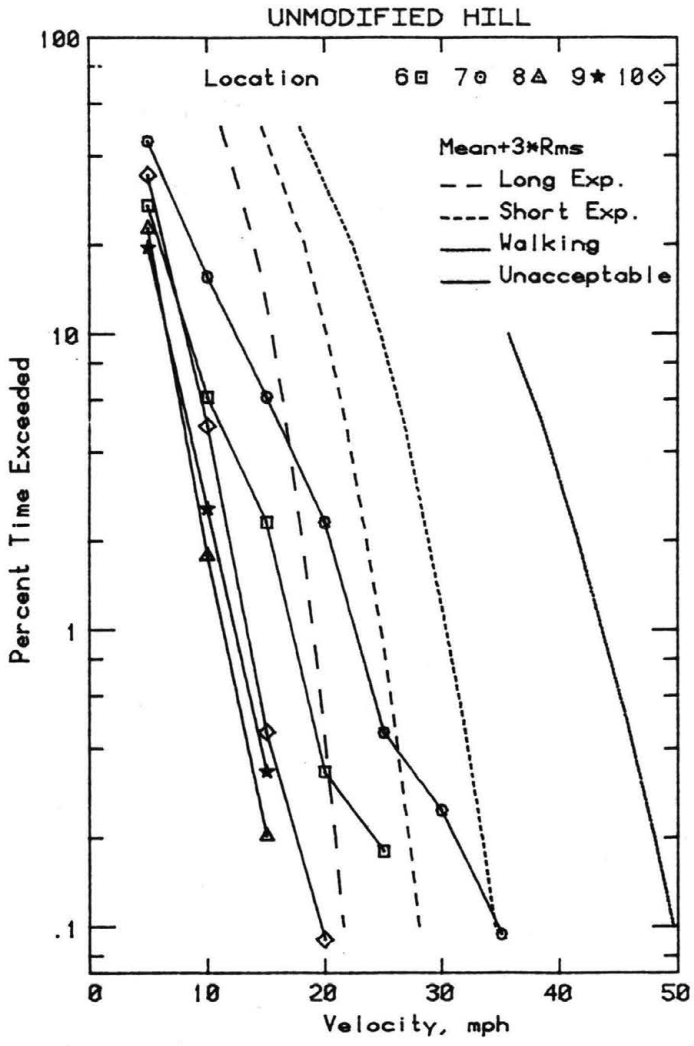

Figure 9b. Wind Velocity Probabilities for Pedestrian Locations

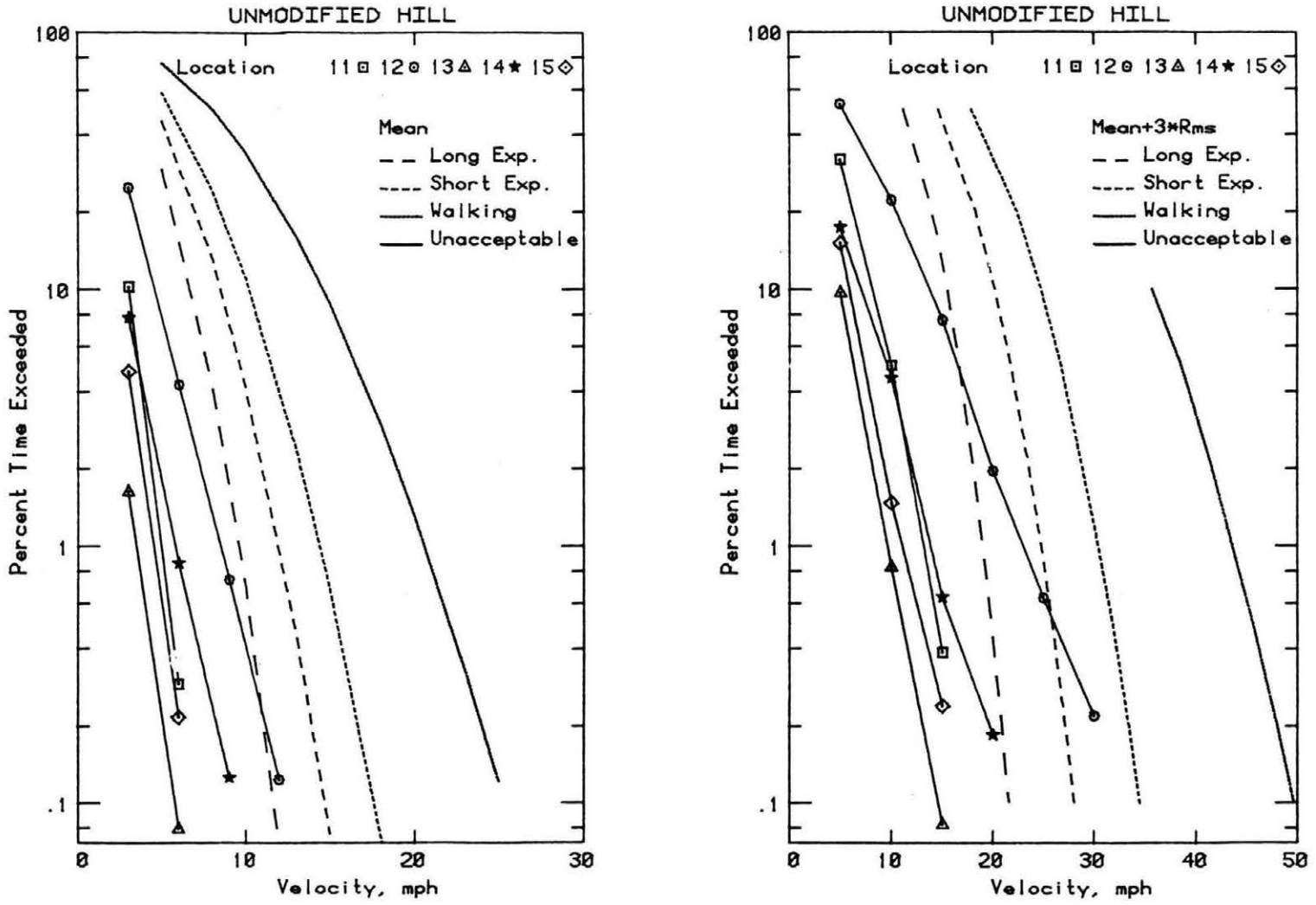

Figure 9c. Wind Velocity Probabilities for Pedestrian Locations

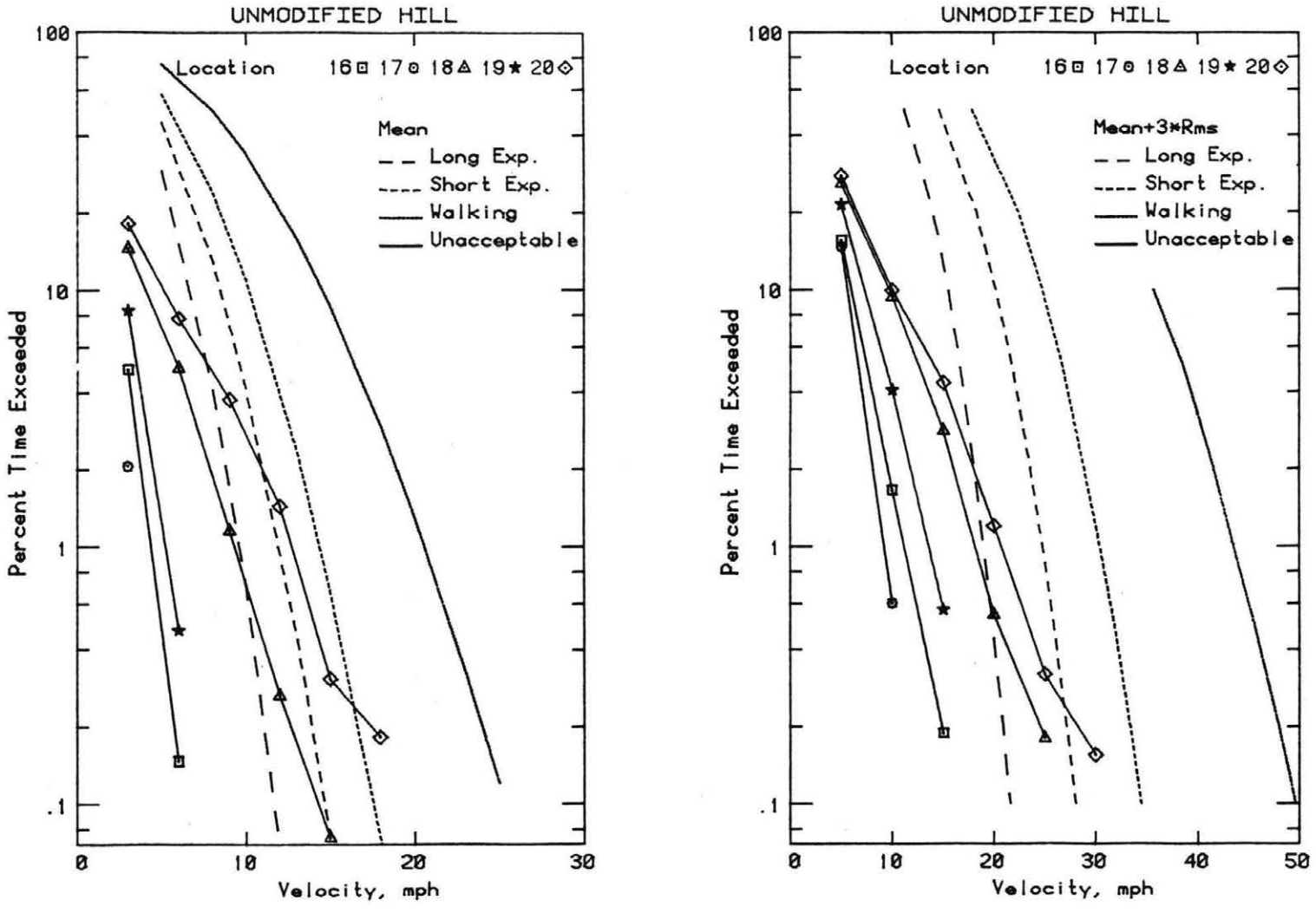

Figure 9d. Wind Velocity Probabilities for Pedestrian Locations

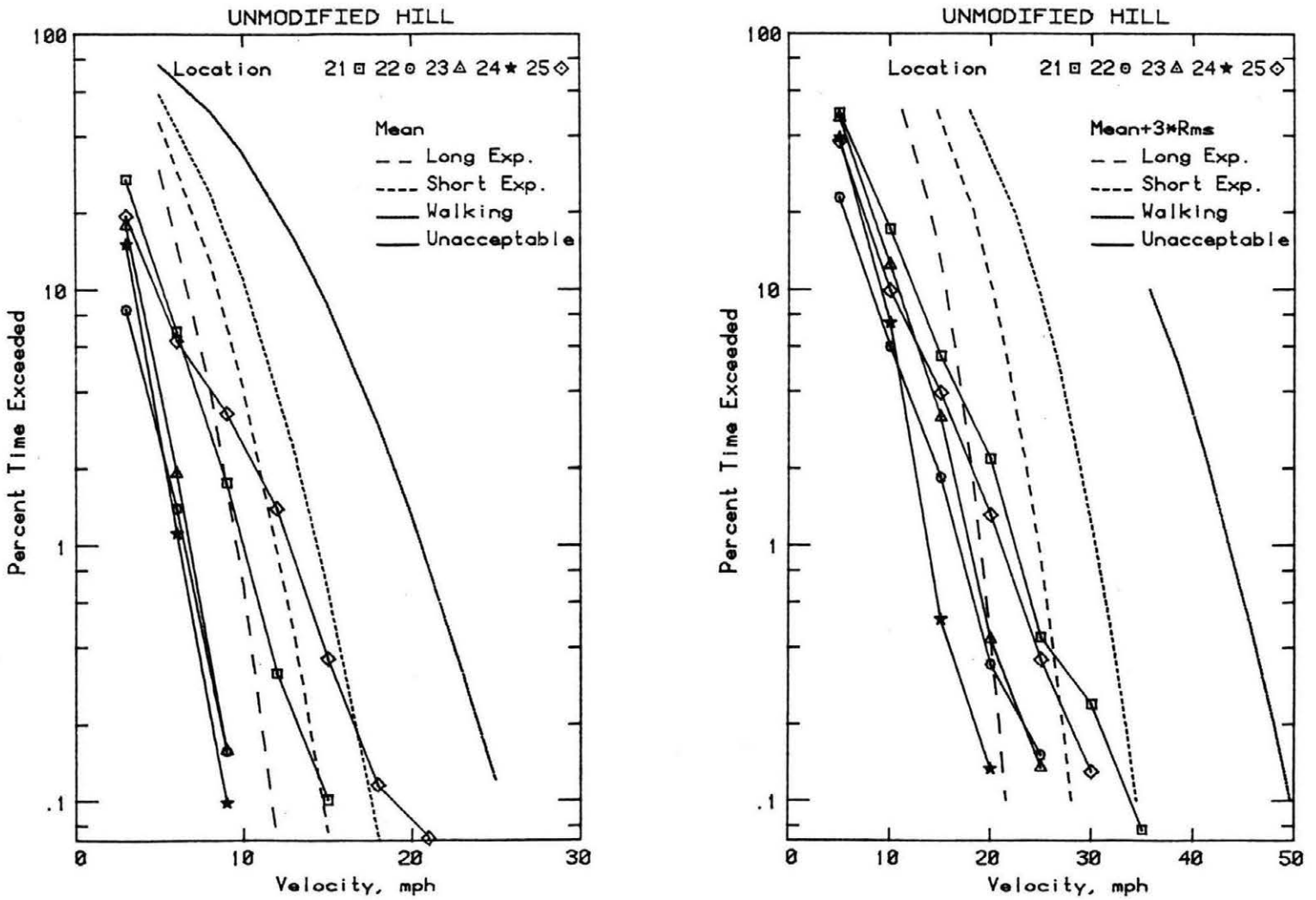

Figure 9e. Wind Velocity Probabilities for Pedestrian Locations

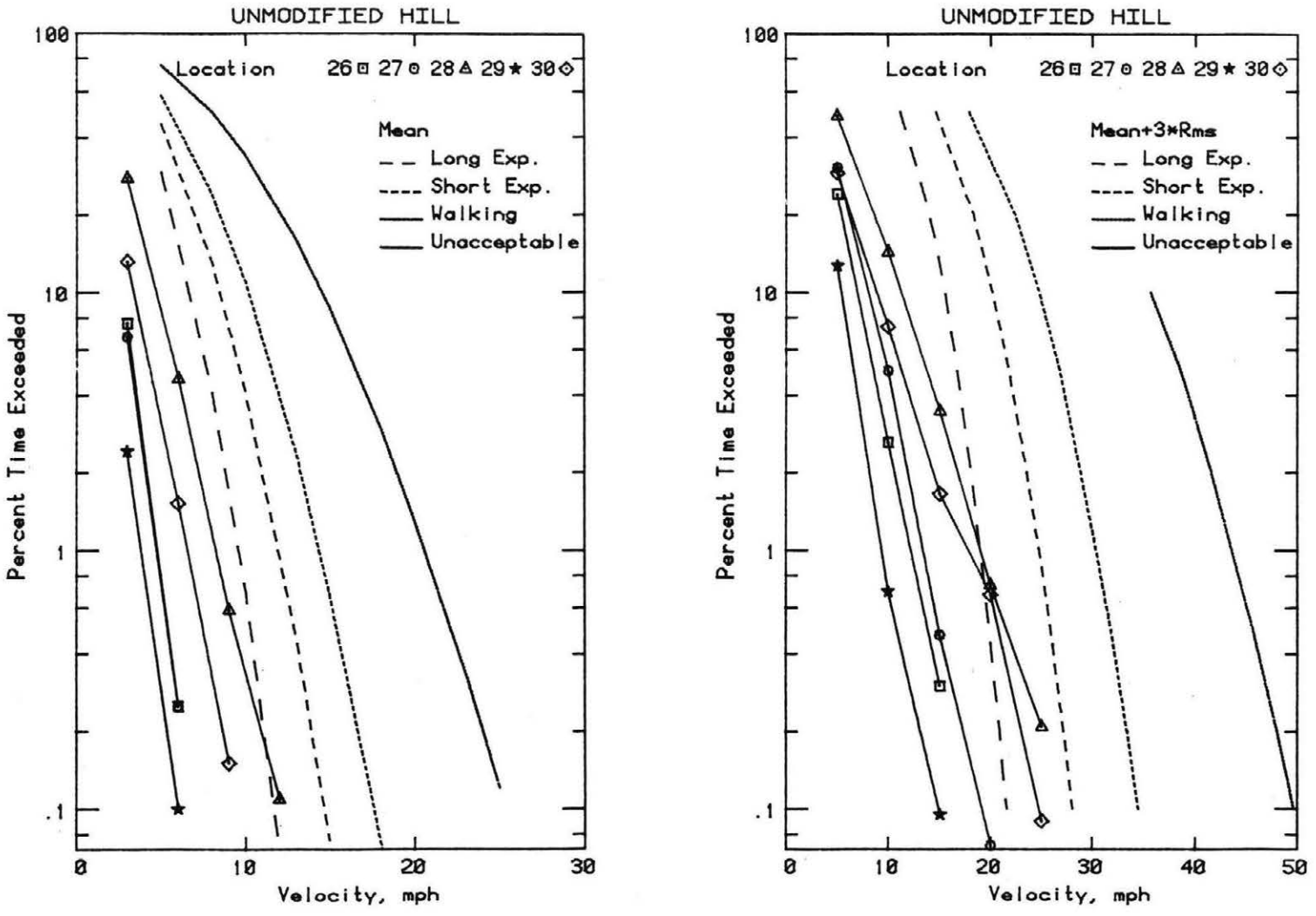

Figure 9f. Wind Velocity Probabilities for Pedestrian Locations

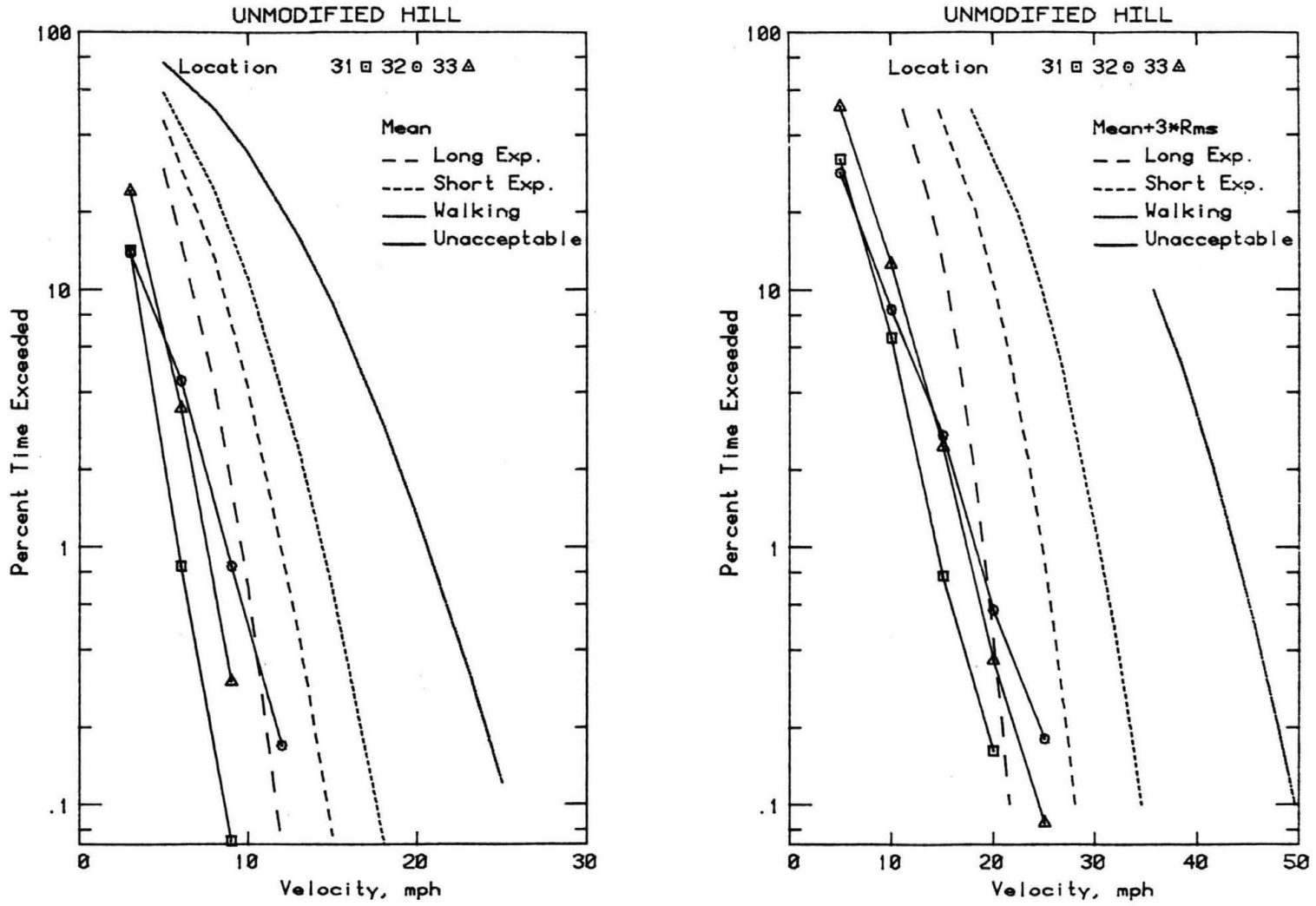

Figure 9g. Wind Velocity Probabilities for Pedestrian Locations

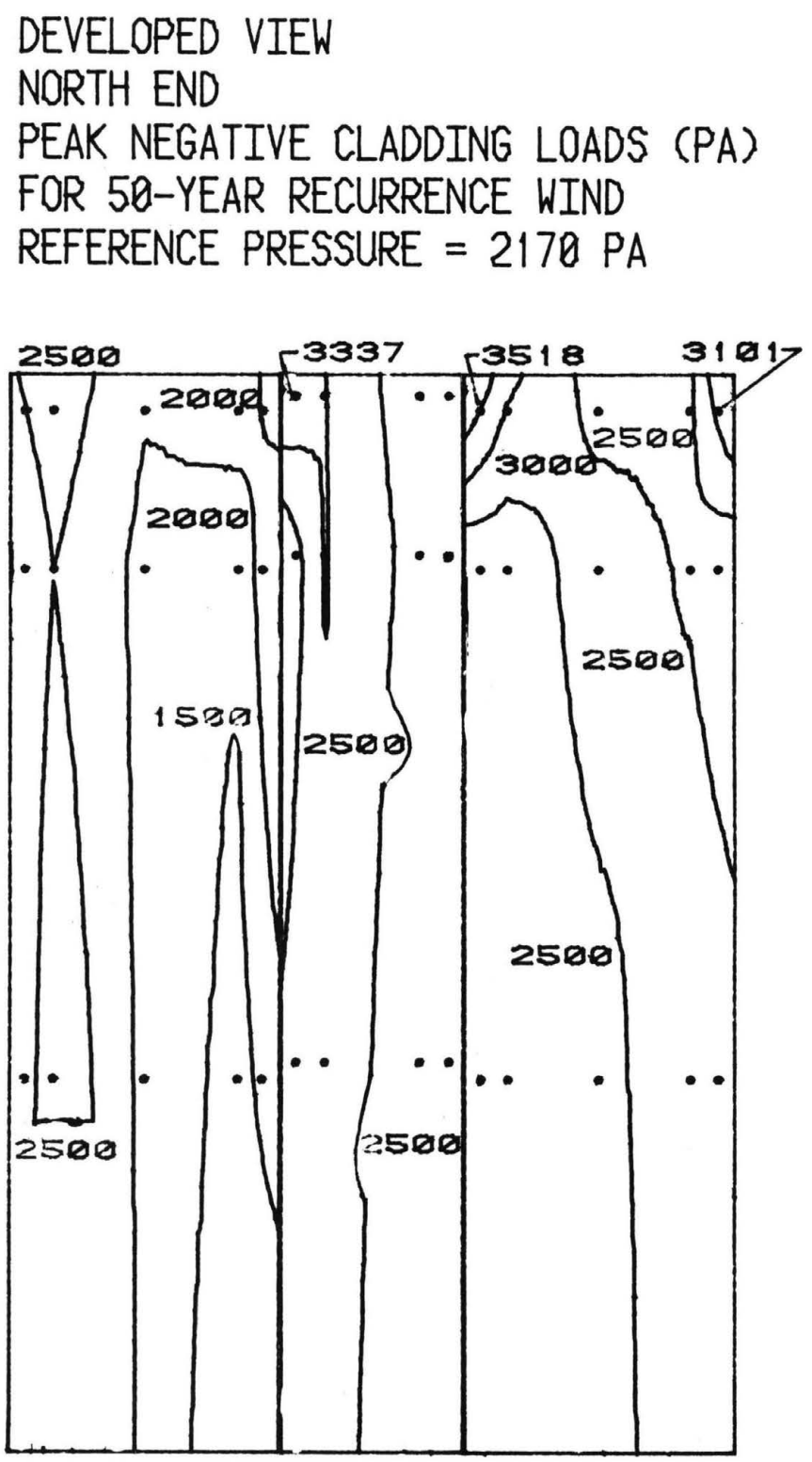

Figure 10a. Peak Pressure Contours on the Building for Cladding Loads

WEST TOWER

SOUTHWEST ELEVATION
PEAK NEGATIVE CLADDING LOADS (PA)
FOR 50-YEAR RECURRENCE WIND
REFERENCE PRESSURE = 2170 PA

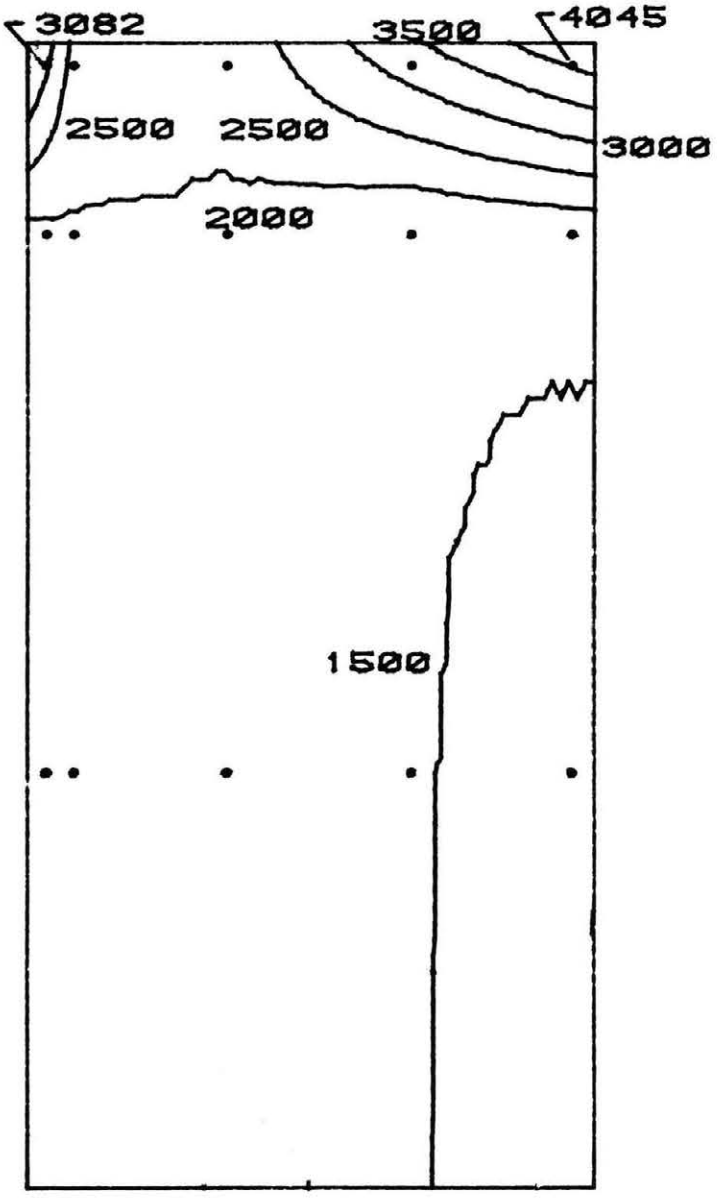

Figure 10b. Peak Pressure Contours on the Building for Cladding Loads

WEST TOWER

WEST ELEVATION
PEAK NEGATIVE CLADDING LOADS (PA)
FOR 50-YEAR RECURRENCE WIND
REFERENCE PRESSURE = 2170 PA

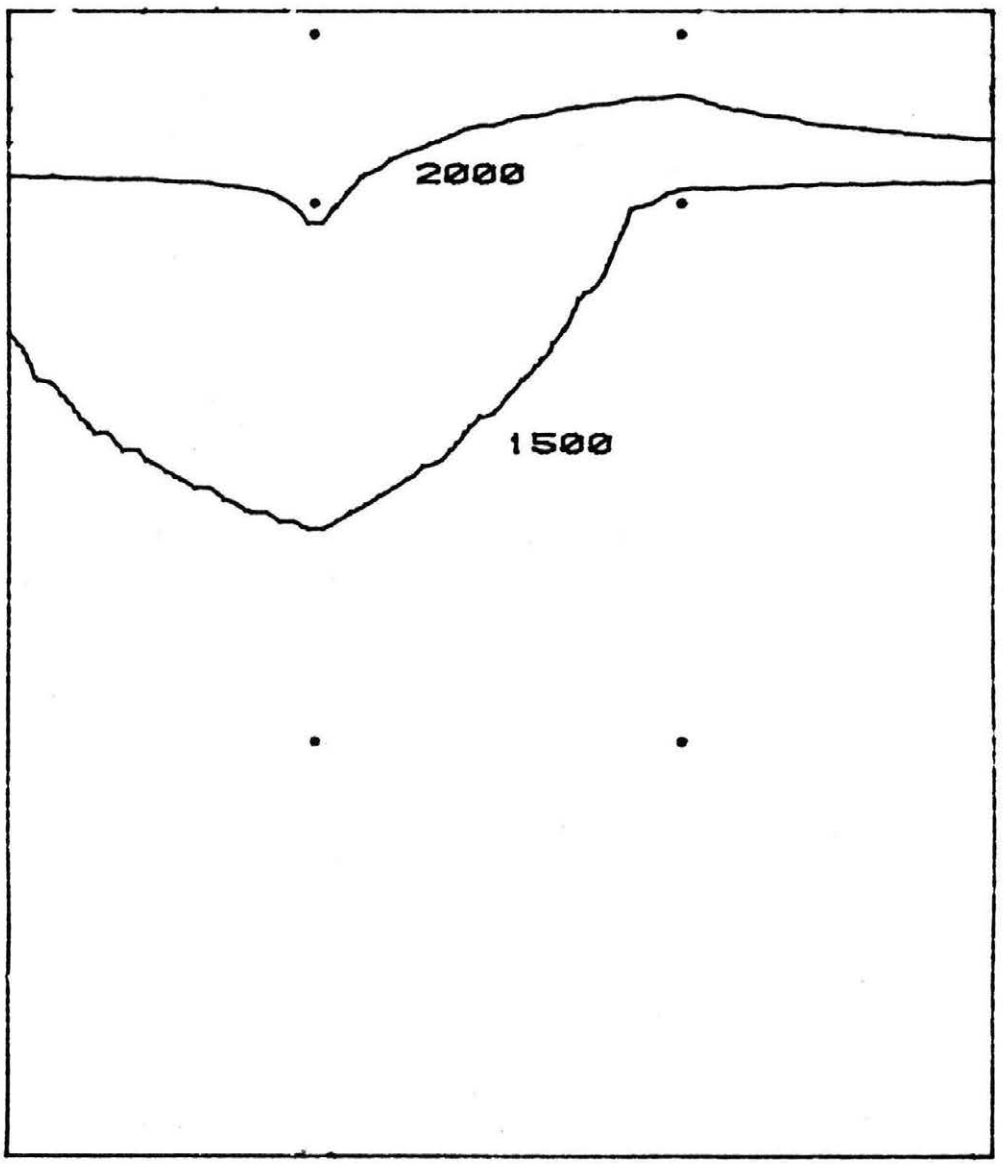

Figure 10c. Peak Pressure Contours on the Building for Cladding Loads

WEST TOWER

NORTHWEST ELEVATION
PEAK NEGATIVE CLADDING LOADS (PA)
FOR 50-YEAR RECURRENCE WIND
REFERENCE PRESSURE = 2170 PA

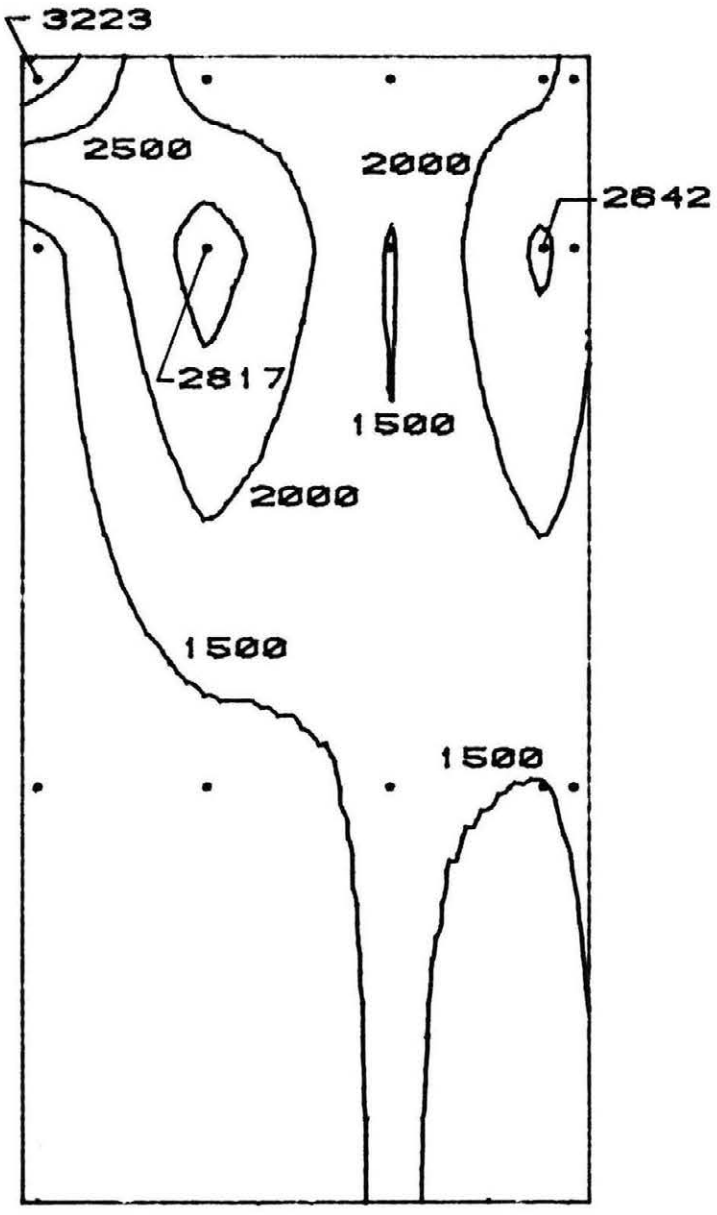

Figure 10d. Peak Pressure Contours on the Building for Cladding Loads

WEST TOWER

DEVELOPED VIEW
SOUTH END
PEAK NEGATIVE CLADDING LOADS (PA)
FOR 50-YEAR RECURRENCE WIND
REFERENCE PRESSURE = 2170 PA

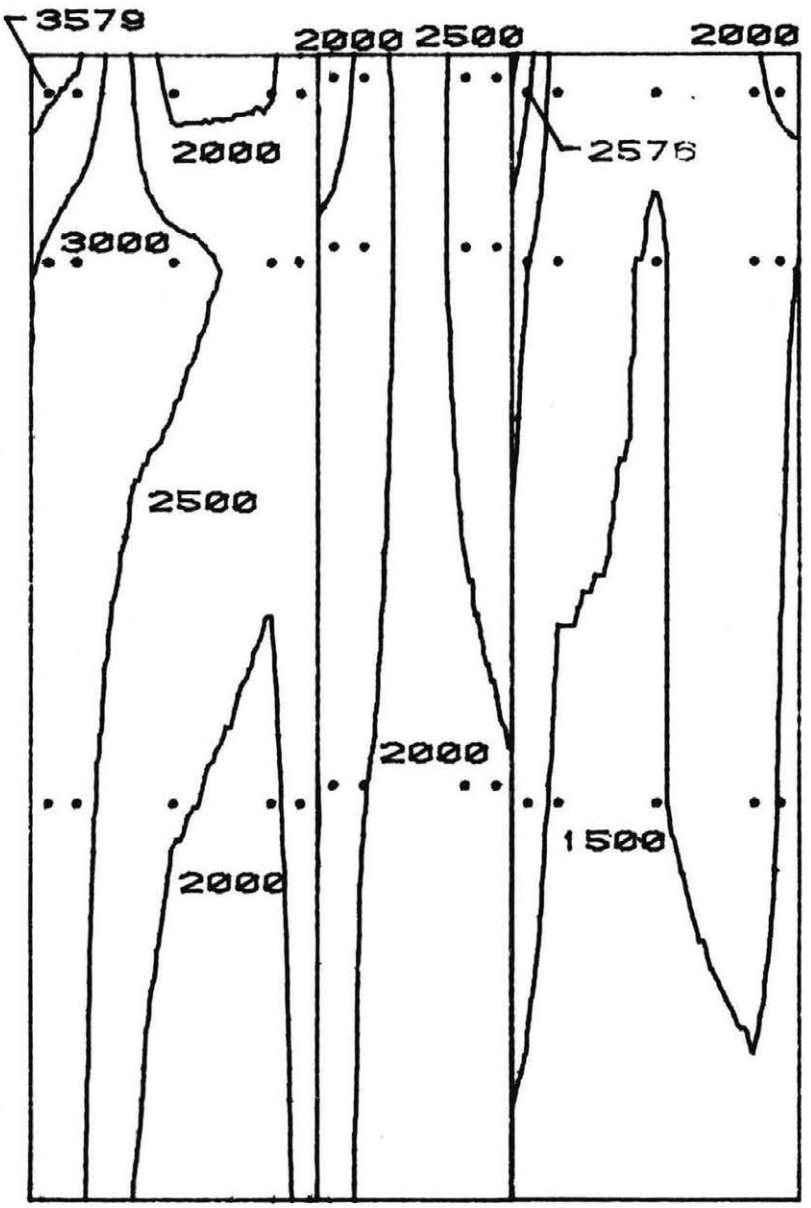

Figure 10e. Peak Pressure Contours on the Building for Cladding Loads

WEST TOWER

SOUTHEAST ELEVATION
PEAK NEGATIVE CLADDING LOADS (PA)
FOR 50-YEAR RECURRENCE WIND
REFERENCE PRESSURE = 2170 PA

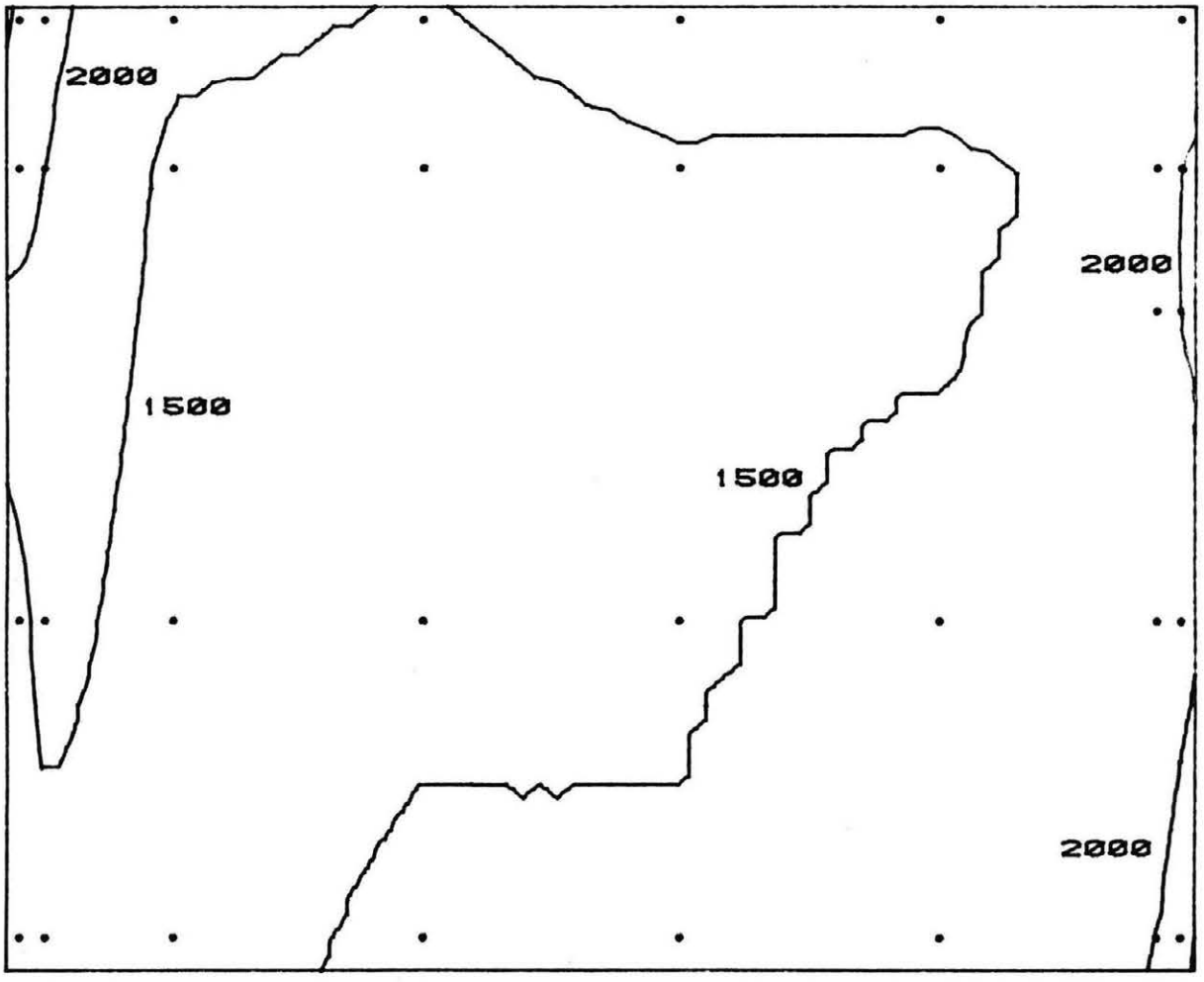

Figure 10f. Peak Pressure Contours on the Building for Cladding Loads

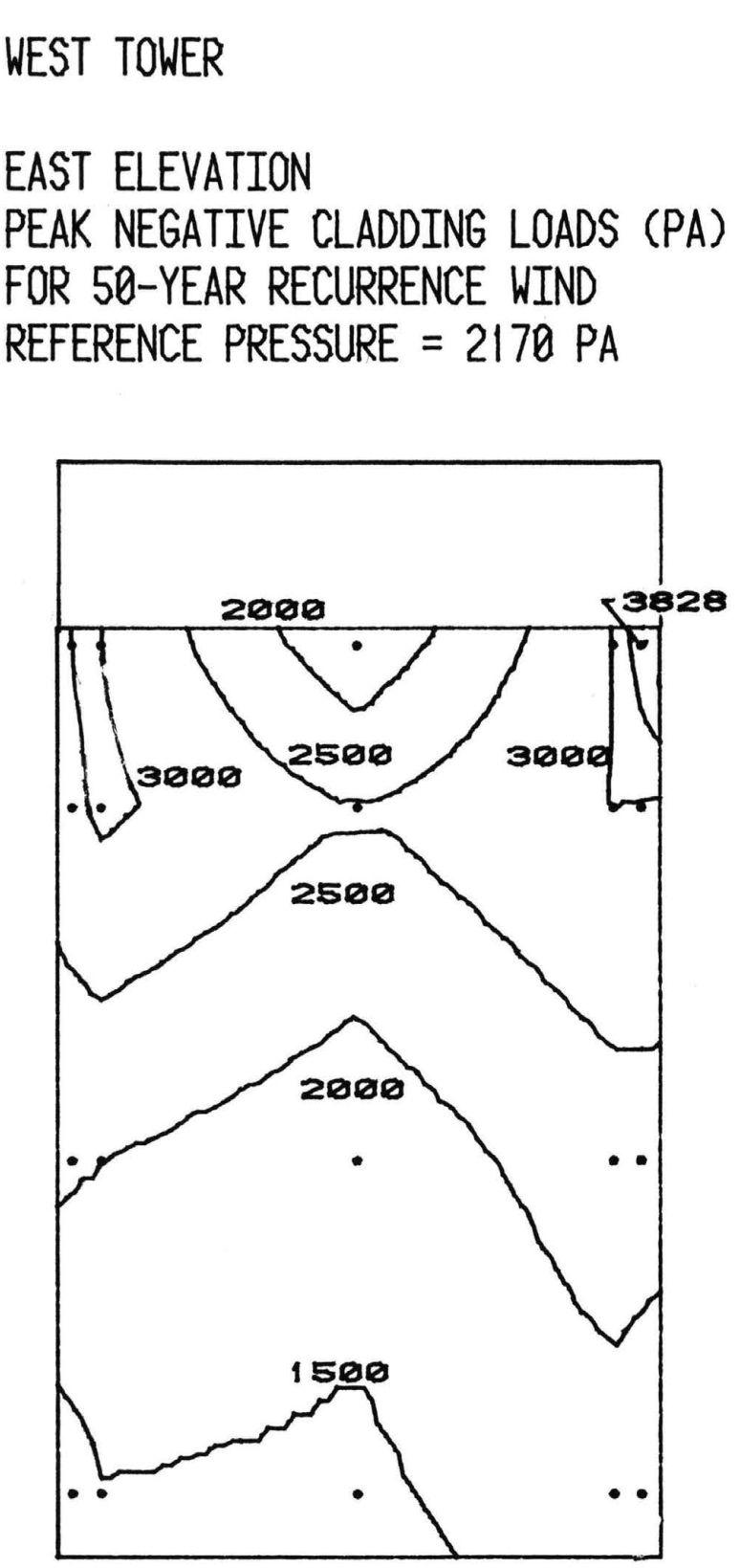

Figure 10g. Peak Pressure Contours on the Building for Cladding Loads

WEST TOWER

NORTHEAST ELEVATION
PEAK NEGATIVE CLADDING LOADS (PA)
FOR 50-YEAR RECURRENCE WIND
REFERENCE PRESSURE = 2170 PA

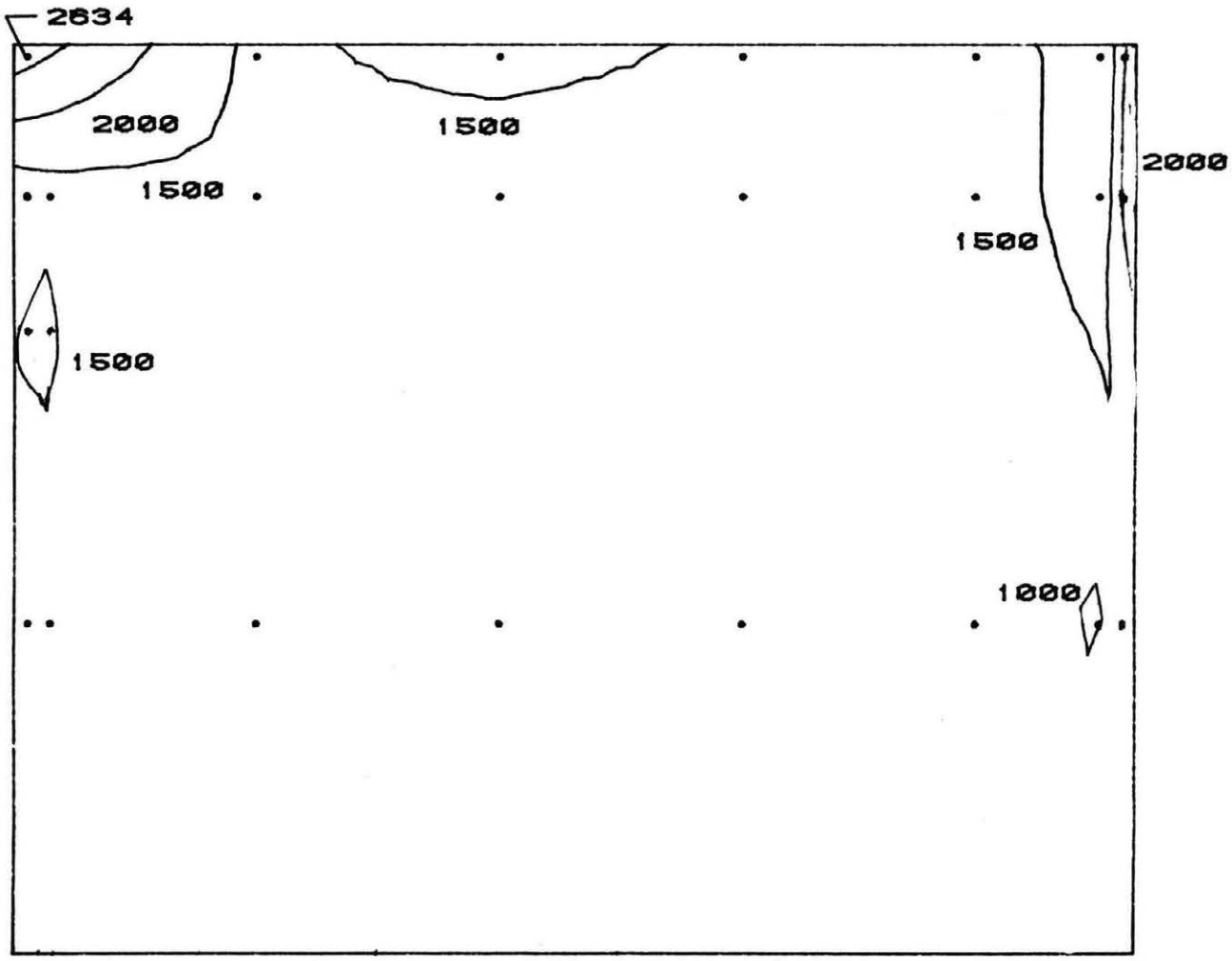

Figure 10h. Peak Pressure Contours on the Building for Cladding Loads

WEST TOWER

DEVELOPED VIEW
NORTH END
PEAK POSITIVE CLADDING LOADS (PA)
FOR 50-YEAR RECURRENCE WIND
REFERENCE PRESSURE = 2170 PA

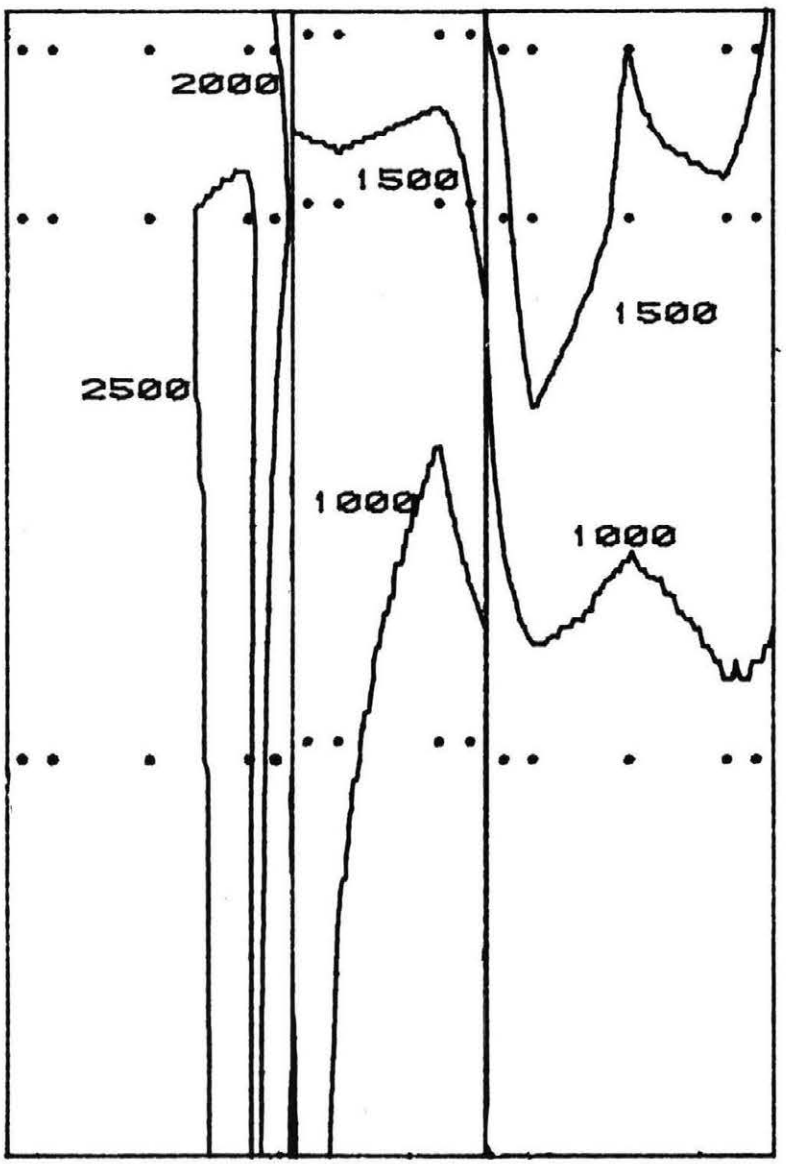

Figure 10i. Peak Pressure Contours on the Building for Cladding Loads

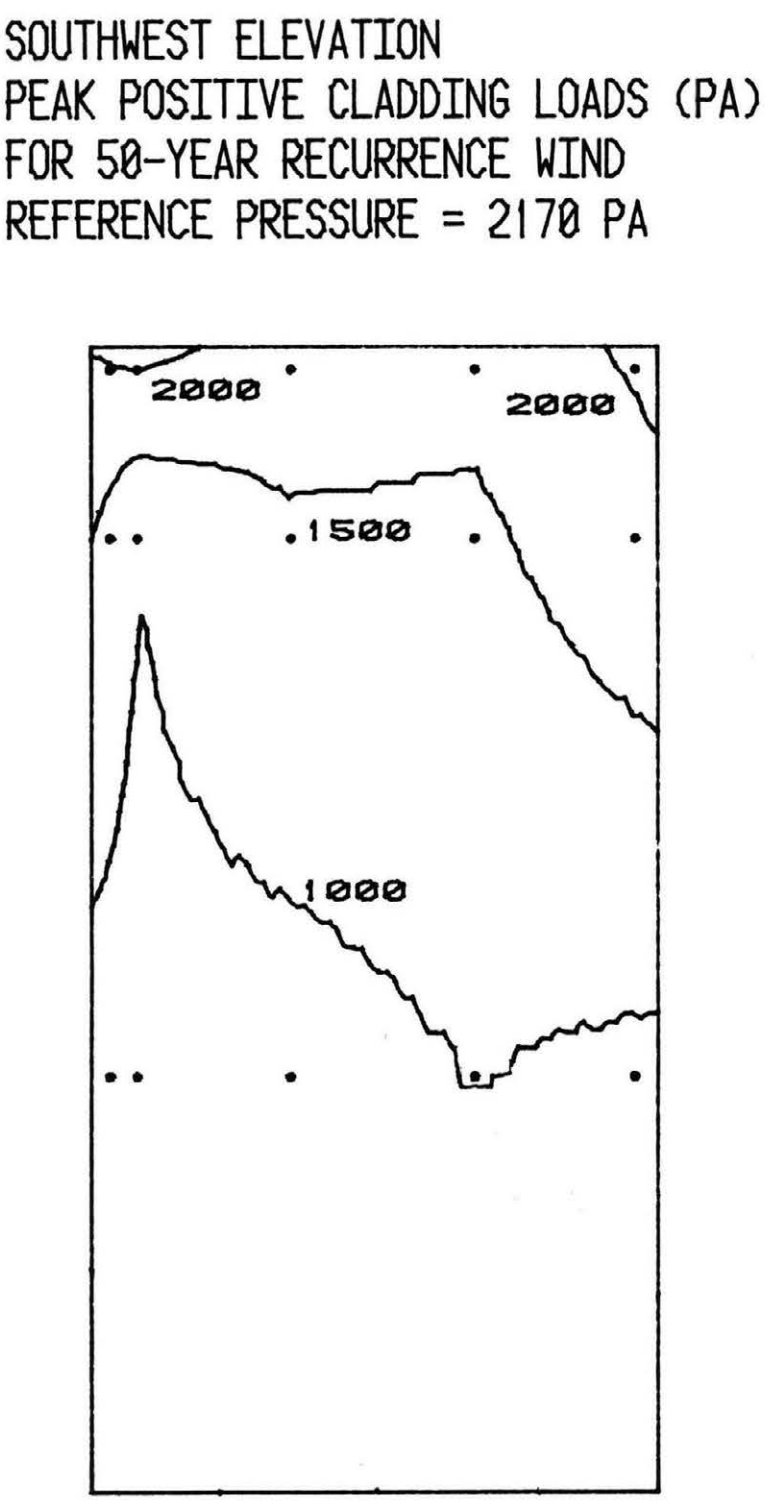

Figure 10j. Peak Pressure Contours on the Building for Cladding Loads

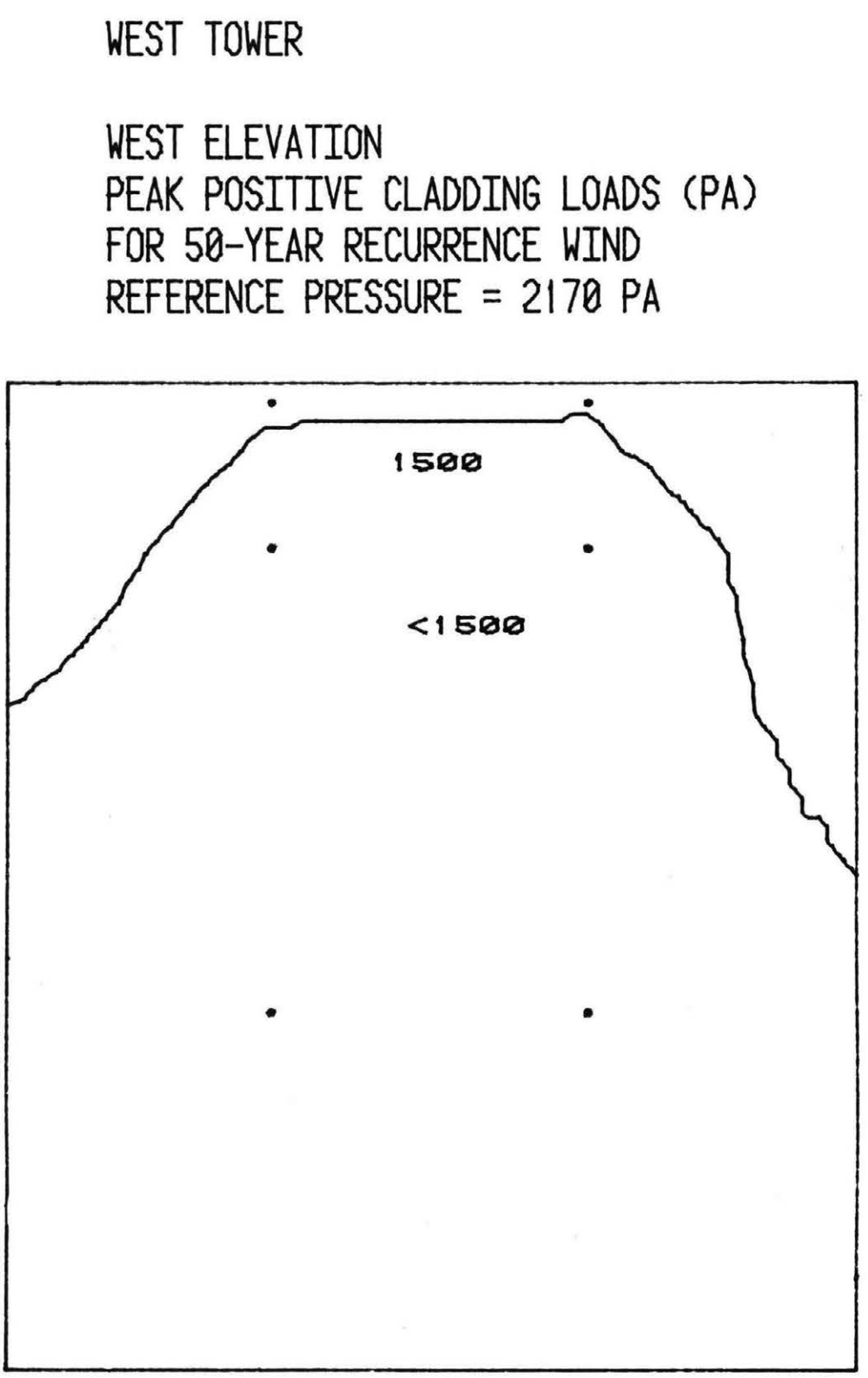

Figure 10k. Peak Pressure Contours on the Building for Cladding Loads

WEST TOWER

NORTHWEST ELEVATION
PEAK POSITIVE CLADDING LOADS (PA)
FOR 50-YEAR RECURRENCE WIND
REFERENCE PRESSURE = 2170 PA

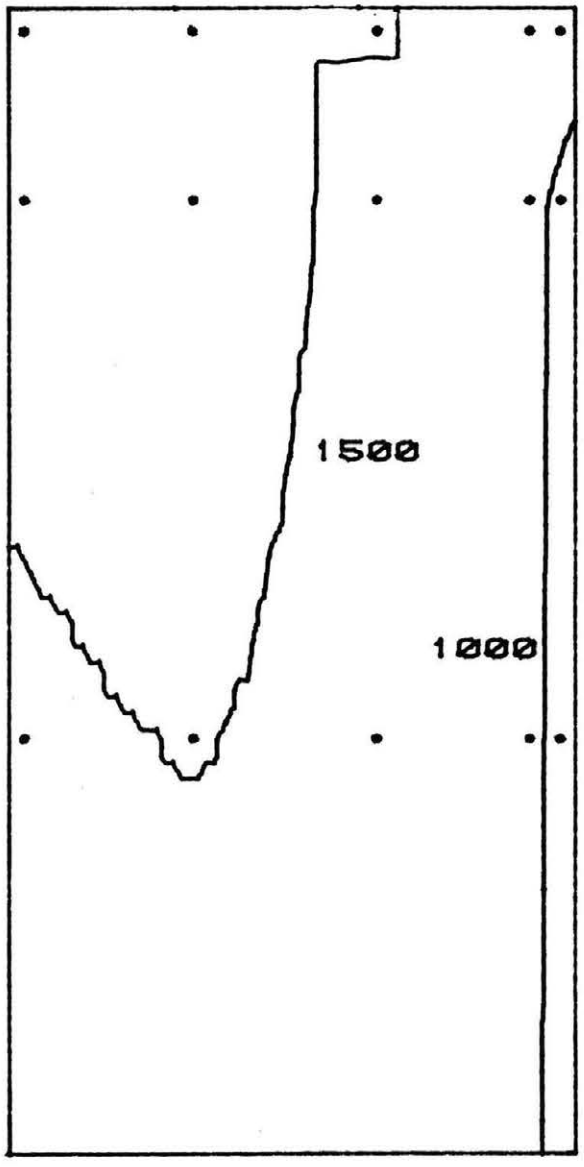

Figure 101. Peak Pressure Contours on the Building for Cladding Loads

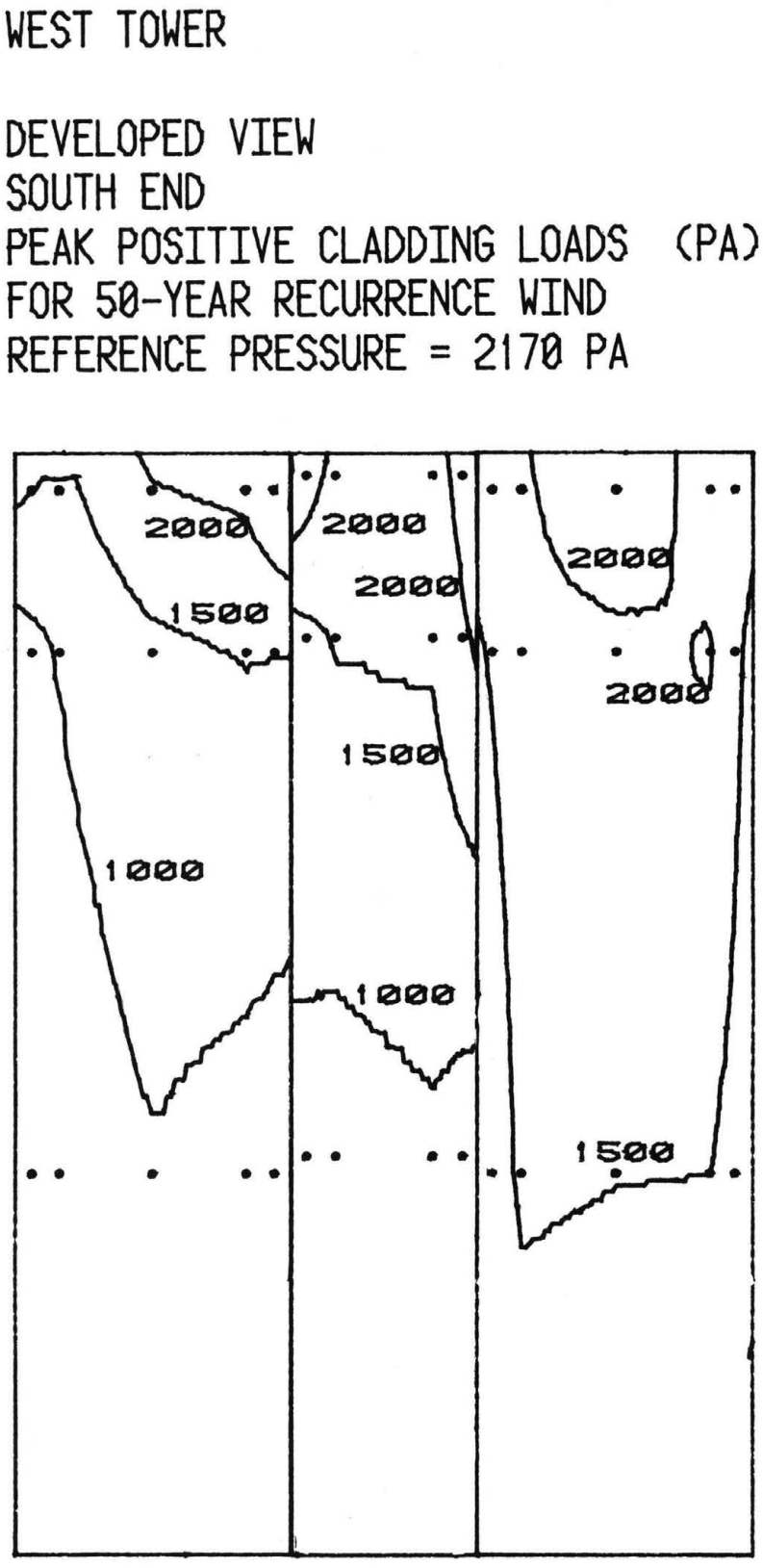

Figure 10m. Peak Pressure Contours on the Building for Cladding Loads

WEST TOWER

SOUTHEAST ELEVATION
PEAK POSITIVE CLADDING LOADS (PA)
FOR 50-YEAR RECURRENCE WIND
REFERENCE PRESSURE = 2170 PA

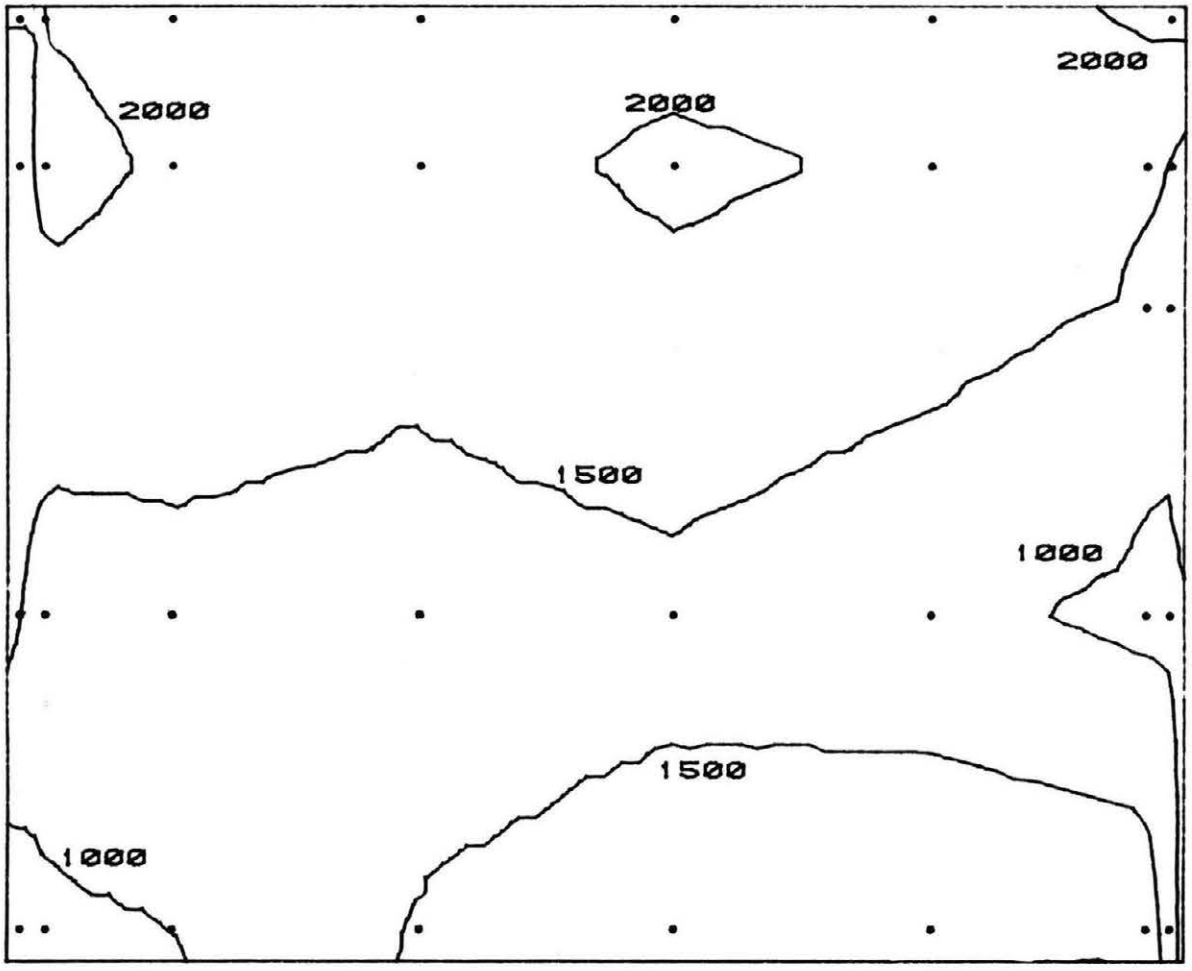

Figure 10n. Peak Pressure Contours on the Building for Cladding Loads

WEST TOWER

EAST ELEVATION
PEAK POSITIVE CLADDING LOADS (PA)
FOR 50-YEAR RECURRENCE WIND
REFERENCE PRESSURE = 2170 PA

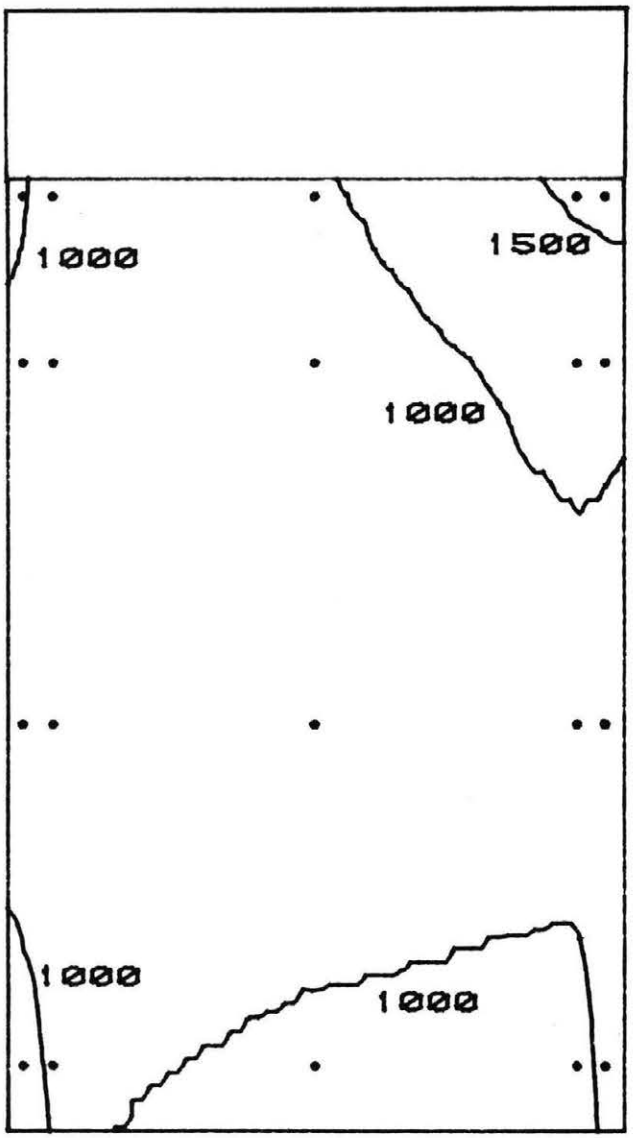

Figure 10o. Peak Pressure Contours on the Building for Cladding Loads

WEST TOWER

NORTHEAST ELEVATION
PEAK POSITIVE CLADDING LOADS (PA)
FOR 50-YEAR RECURRENCE WIND
REFERENCE PRESSURE = 2170 PA

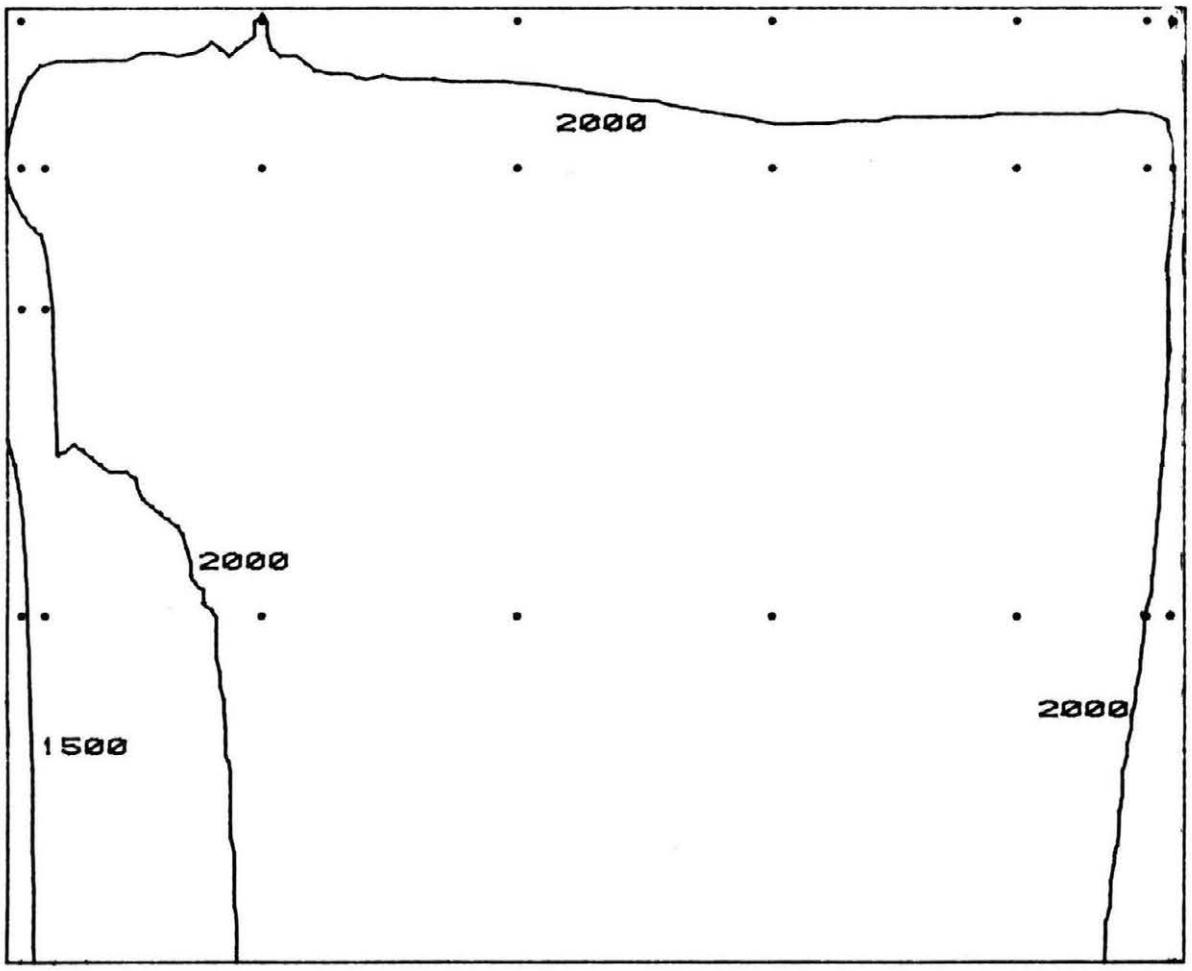

Figure 10p. Peak Pressure Contours on the Building for Cladding Loads

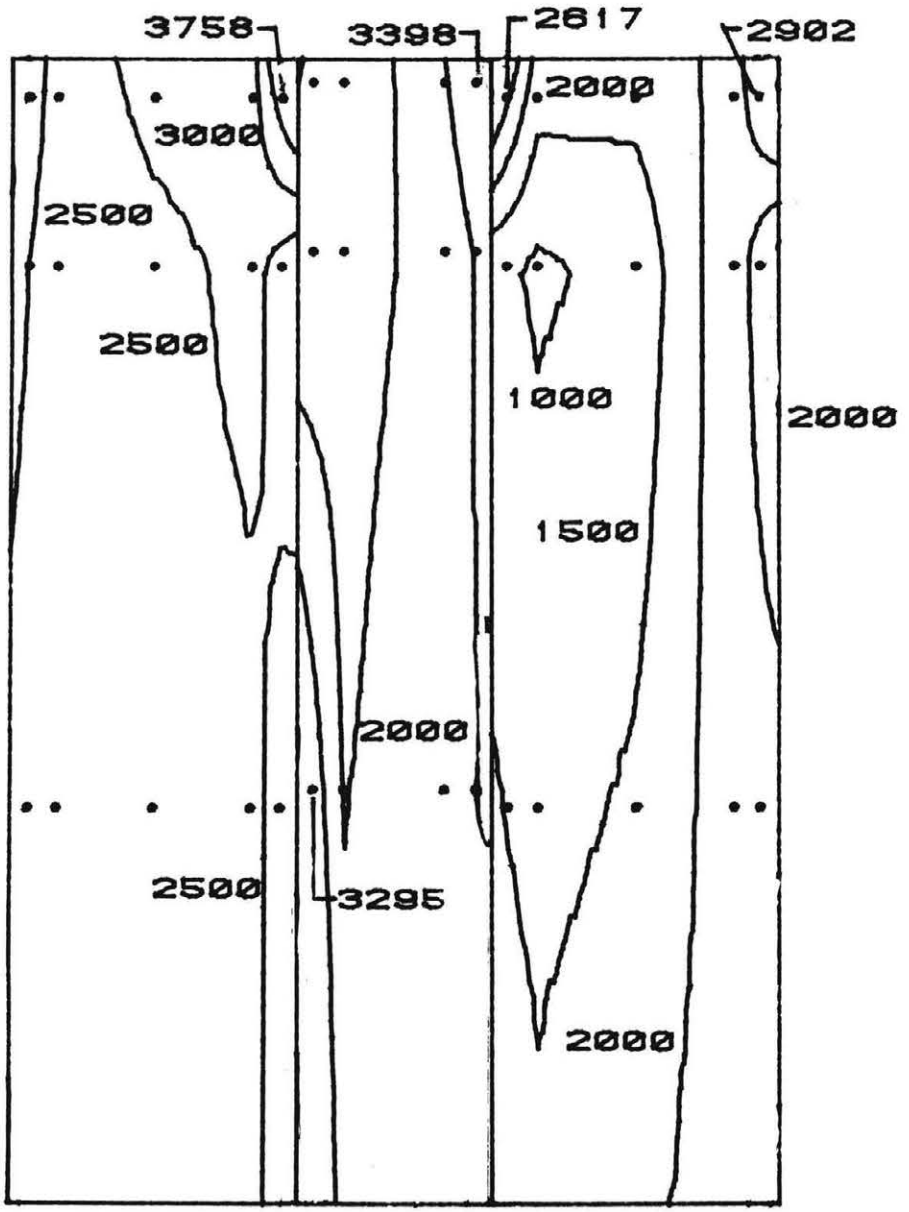

Figure 10q. Peak Pressure Contours on the Building for Cladding Loads

EAST TOWER

NORTHWEST ELEVATION
PEAK NEGATIVE CLADDING LOADS (PA)
FOR 50-YEAR RECURRENCE WIND
REFERENCE PRESSURE = 2170 PA

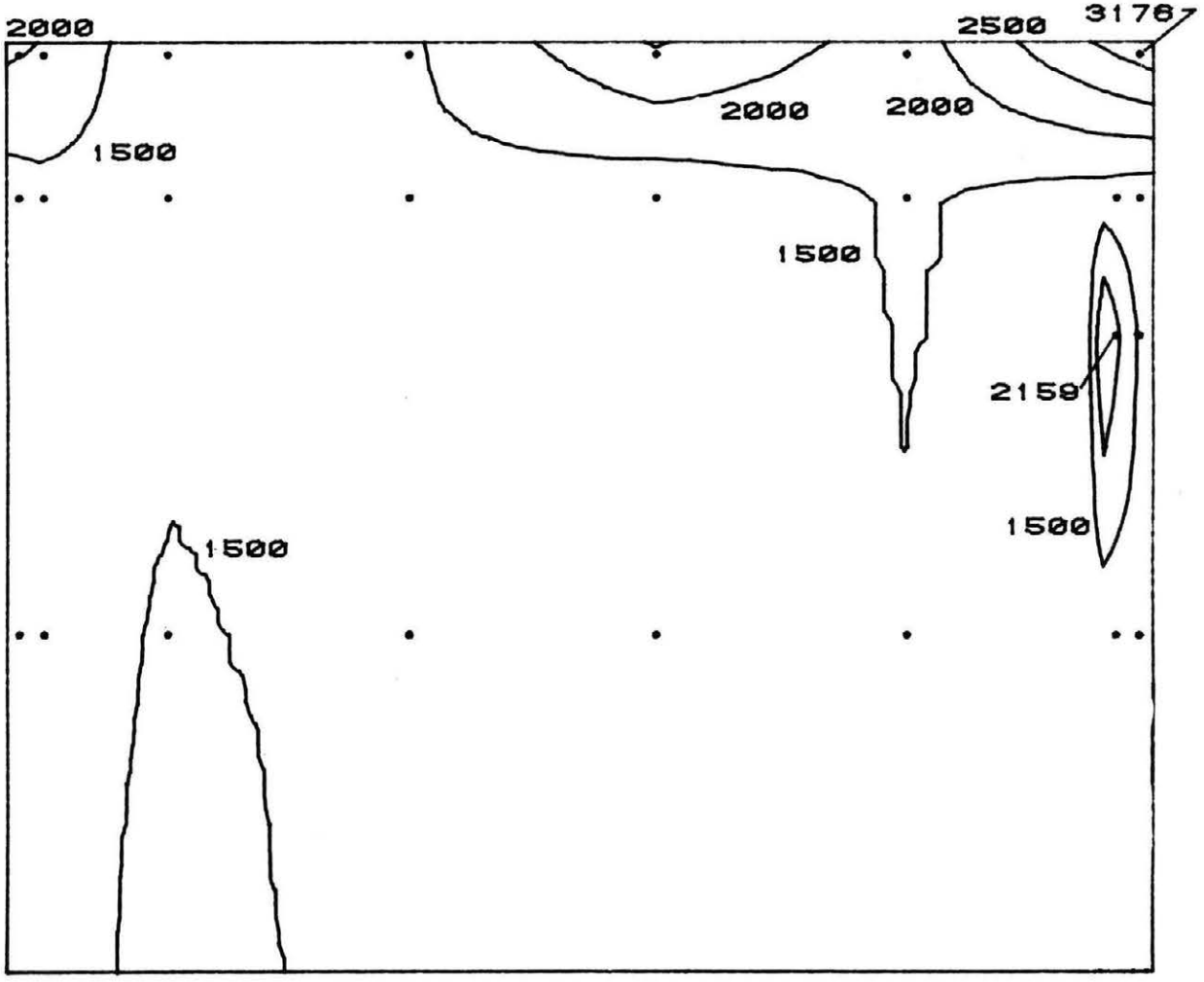

Figure 10r. Peak Pressure Contours on the Building for Cladding Loads

EAST TOWER

WEST ELEVATION
PEAK NEGATIVE CLADDING LOADS (PA)
FOR 50-YEAR RECURRENCE WIND
REFERENCE PRESSURE = 2170 PA

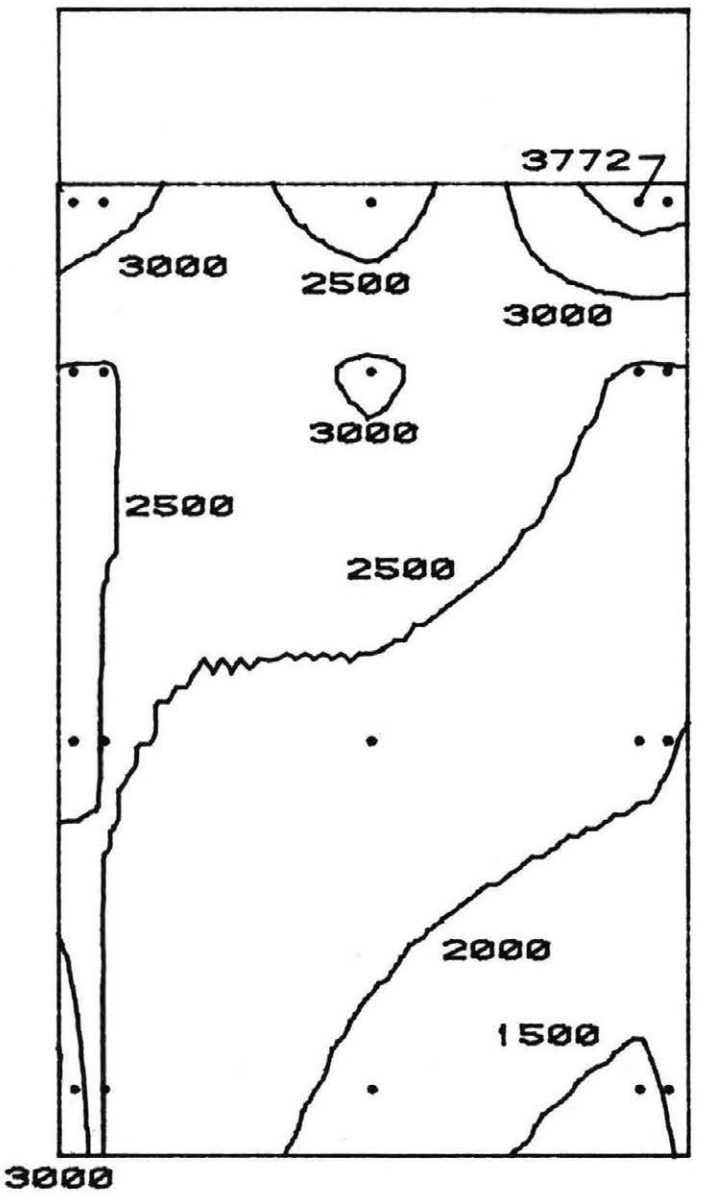

Figure 10s. Peak Pressure Contours on the Building for Cladding Loads

EAST TOWER

SOUTHWEST ELEVATION
PEAK NEGATIVE CLADDING LOADS (PA)
FOR 50-YEAR RECURRENCE WIND
REFERENCE PRESSURE = 2170 PA

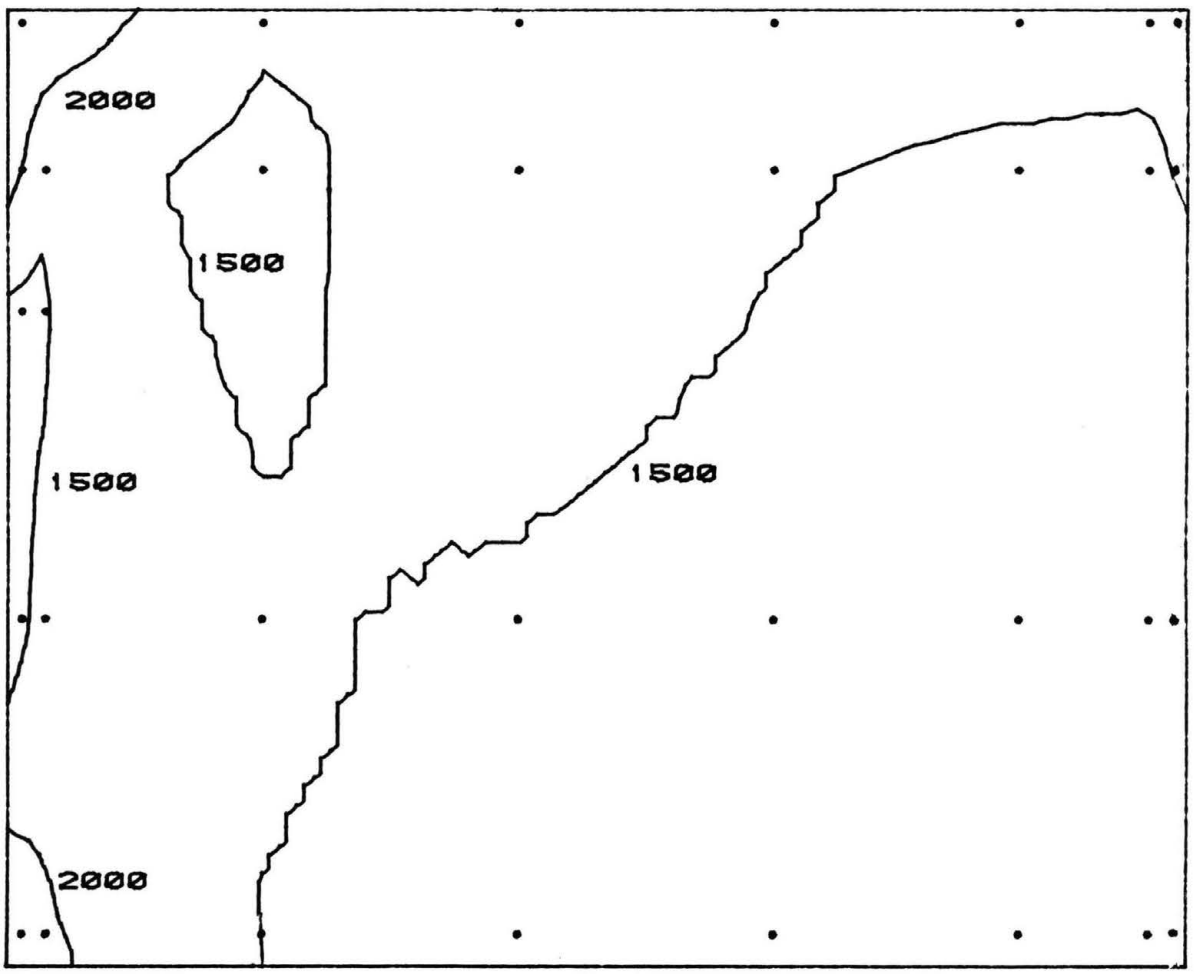

Figure 10t. Peak Pressure Contours on the Building for Cladding Loads

EAST TOWER

DEVELOPED VIEW
SOUTH END
PEAK NEGATIVE CLADDING LOADS (PA)
FOR 50-YEAR RECURRENCE WIND
REFERENCE PRESSURE = 2170 PA

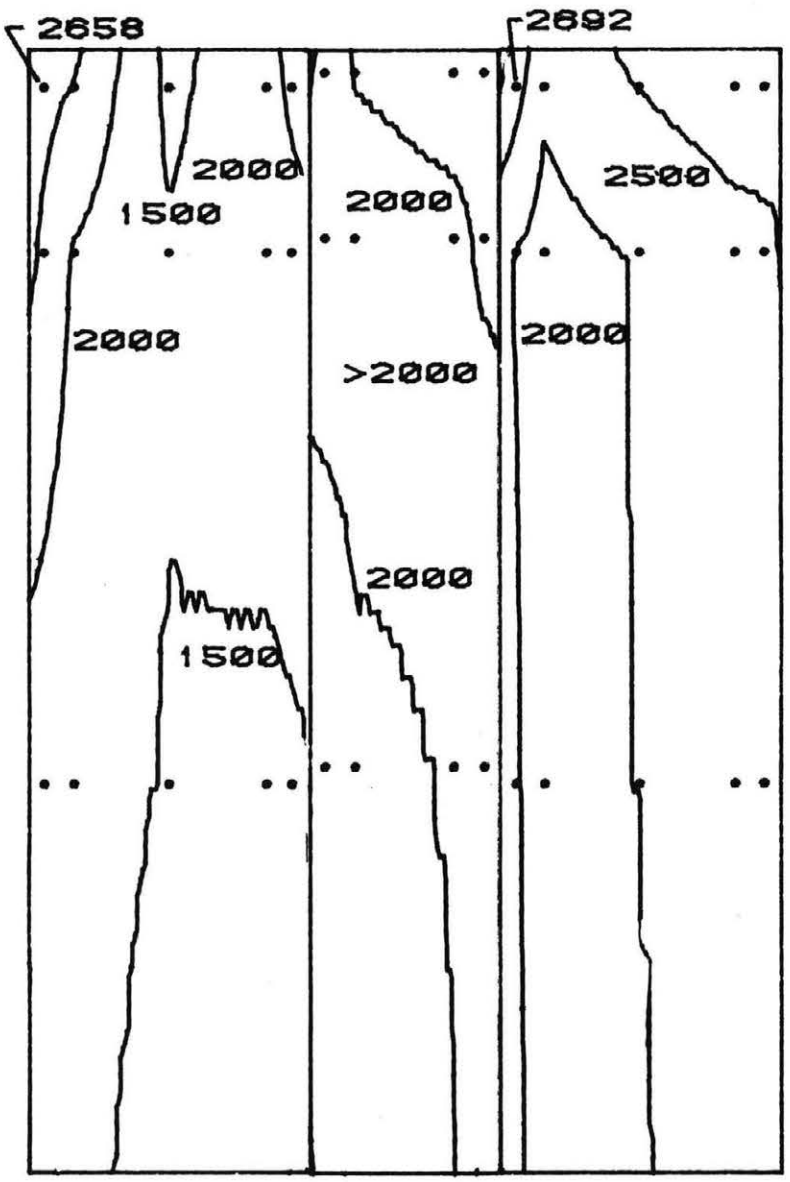

Figure 10u. Peak Pressure Contours on the Building for Cladding Loads

EAST TOWER

NORTHEAST ELEVATION
PEAK NEGATIVE CLADDING LOADS (PA)
FOR 50-YEAR RECURRENCE WIND
REFERENCE PRESSURE = 2170 PA

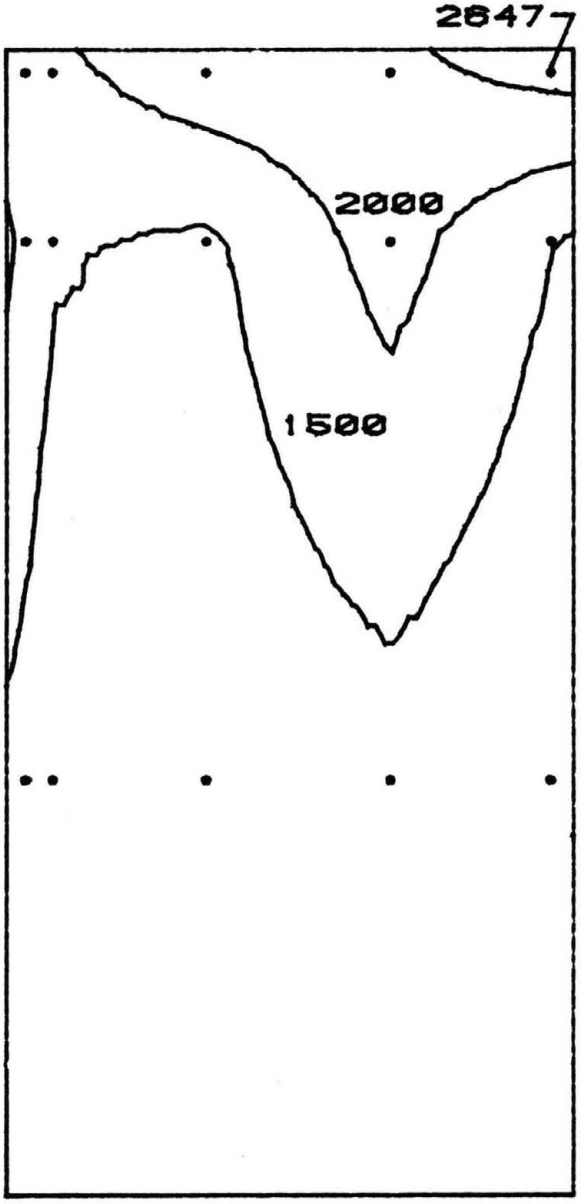

Figure 10v. Peak Pressure Contours on the Building for Cladding Loads

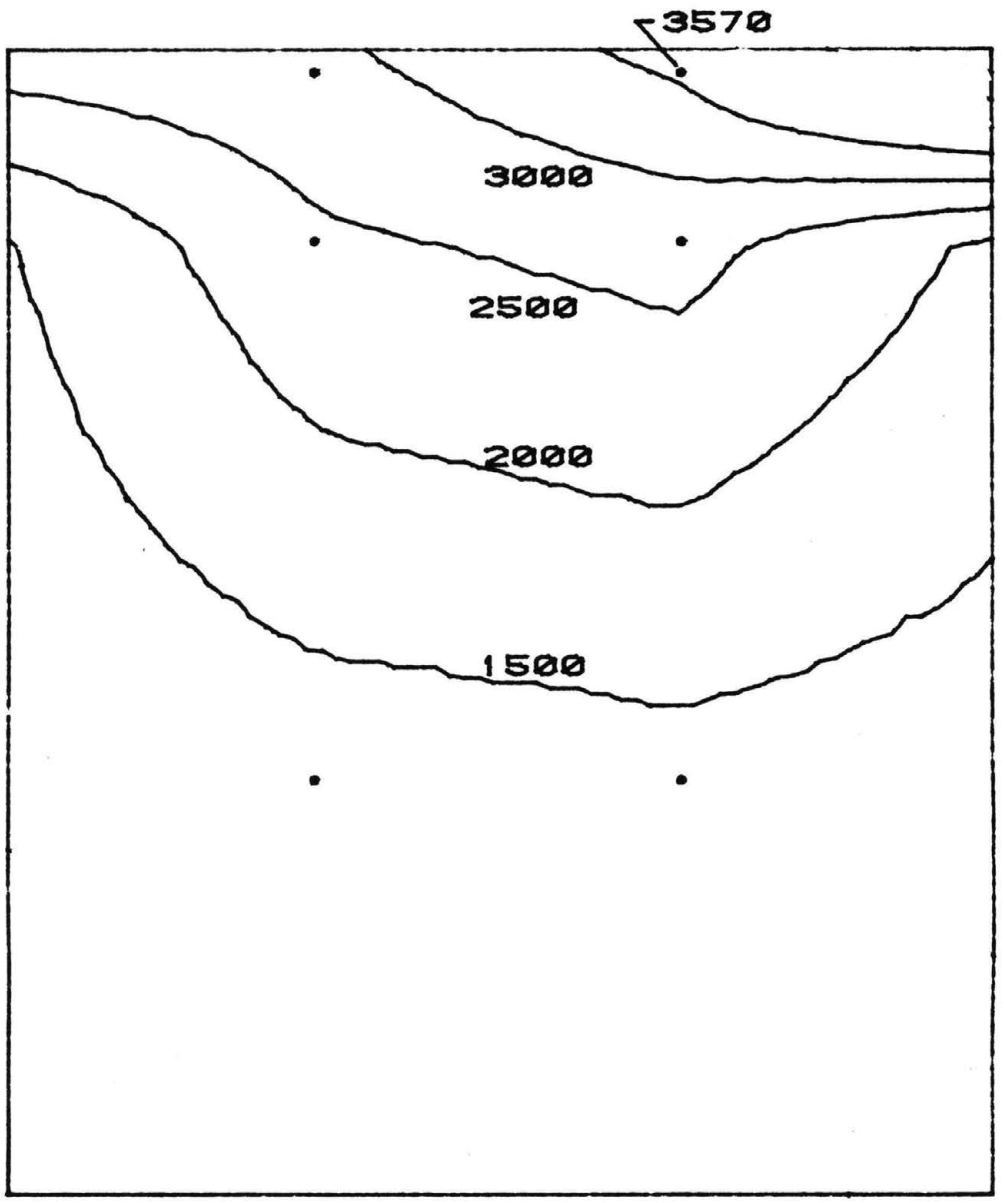

Figure 10w. Peak Pressure Contours on the Building for Cladding Loads

EAST TOWER

SOUTHEAST ELEVATION
PEAK NEGATIVE CLADDING LOADS (PA)
FOR 50-YEAR RECURRENCE WIND
REFERENCE PRESSURE = 2170 PA

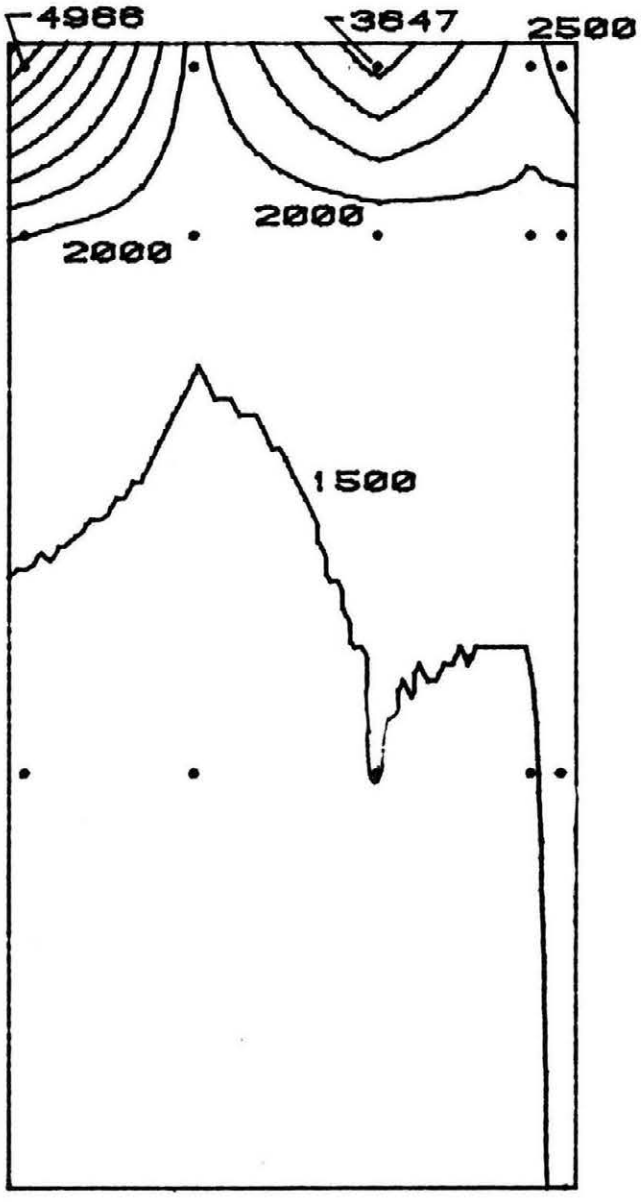

Figure 10x. Peak Pressure Contours on the Building for Cladding Loads

EAST TOWER

DEVELOPED VIEW
NORTH END
PEAK POSITIVE CLADDING LOADS (PA)
FOR 50-YEAR RECURRENCE WIND
REFERENCE PRESSURE = 2170 PA

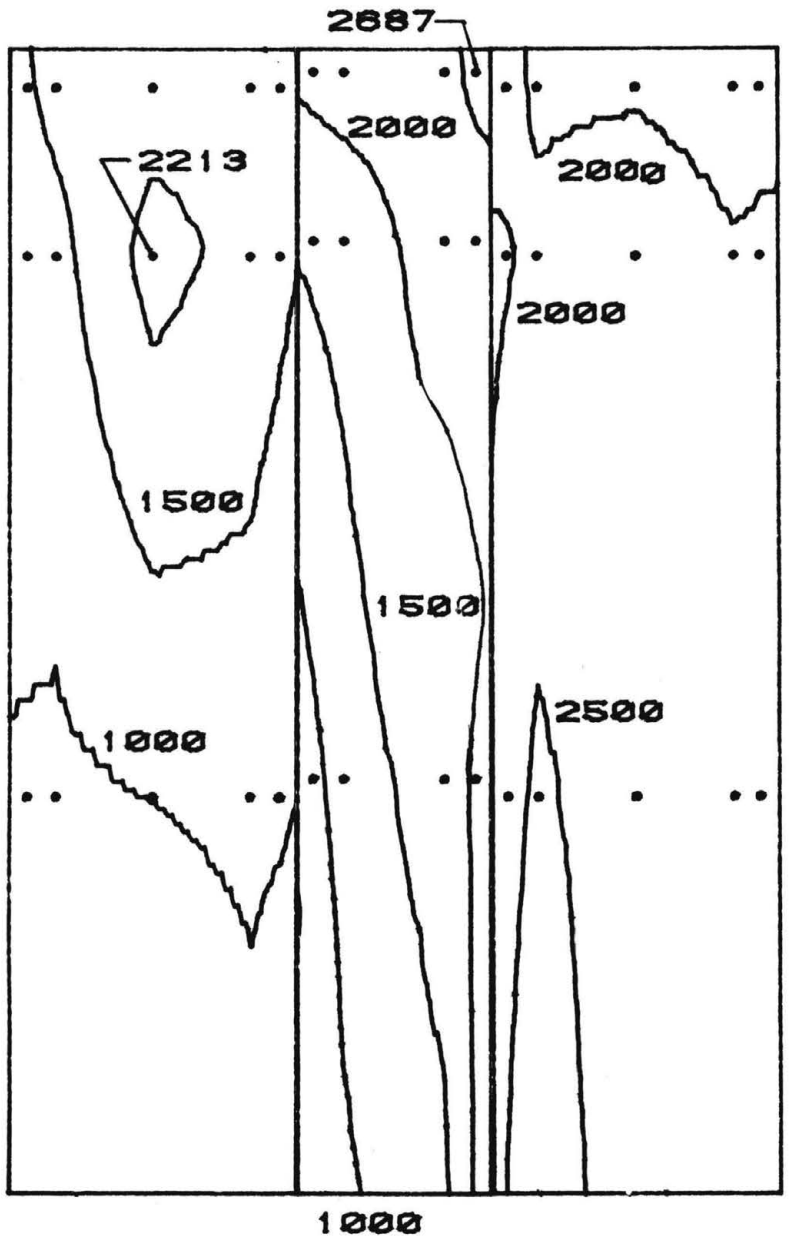

Figure 10y. Peak Pressure Contours on the Building for Cladding Loads

EAST TOWER

NORTHWEST ELEVATION
PEAK POSITIVE CLADDING LOADS (PA)
FOR 50-YEAR RECURRENCE WIND
REFERENCE PRESSURE = 2170 PA

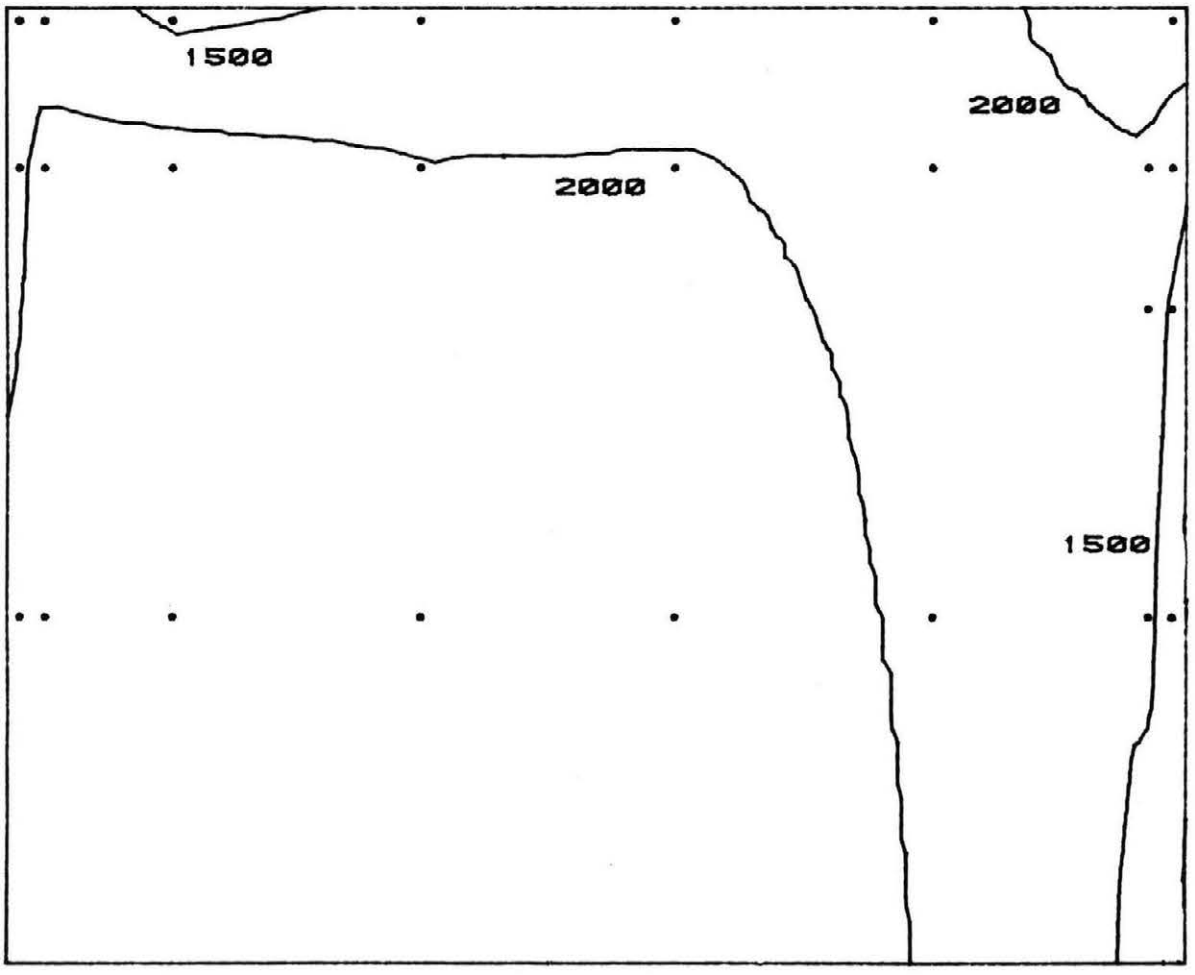

Figure 10z. Peak Pressure Contours on the Building for Cladding Loads

EAST TOWER

WEST ELEVATION
PEAK POSITIVE CLADDING LOADS (PA)
FOR 50-YEAR RECURRENCE WIND
REFERENCE PRESSURE = 2170 PA

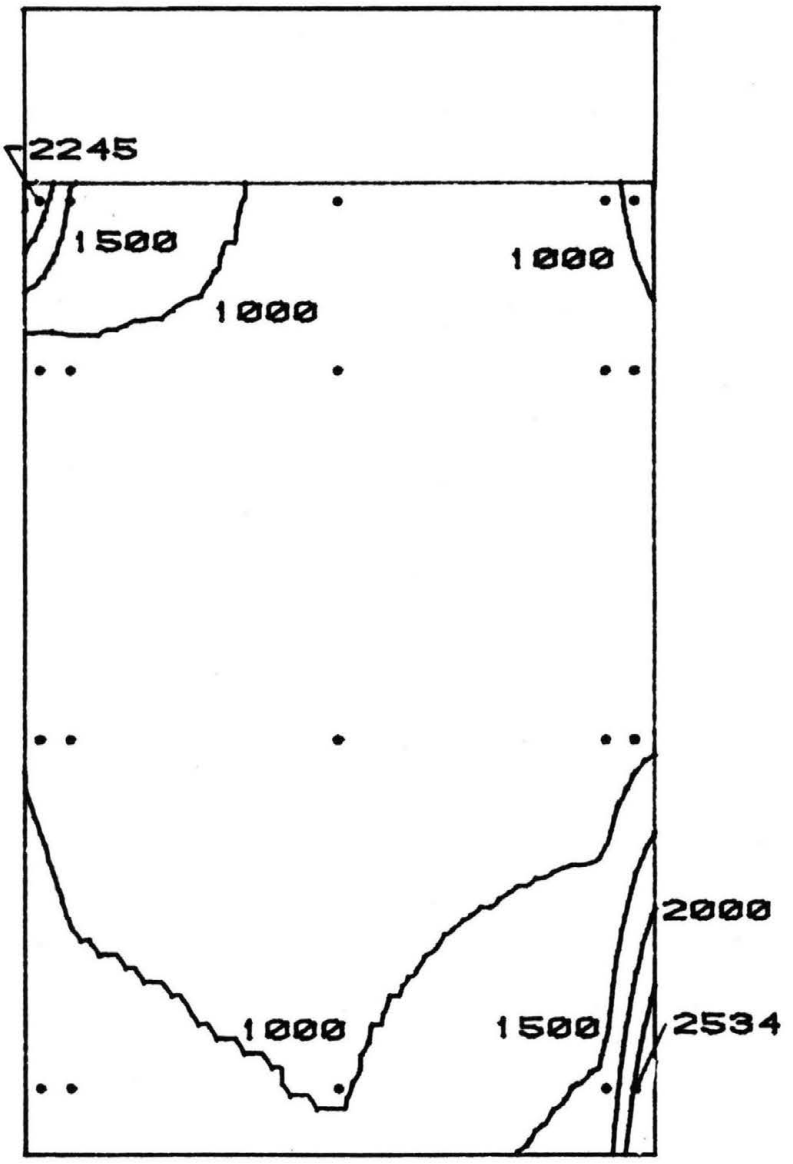

Figure 10A. Peak Pressure Contours on the Building for Cladding Loads

EAST TOWER

SOUTHWEST ELEVATION
PEAK POSITIVE CLADDING LOADS (PA)
FOR 50-YEAR RECURRENCE WIND
REFERENCE PRESSURE = 2170 PA

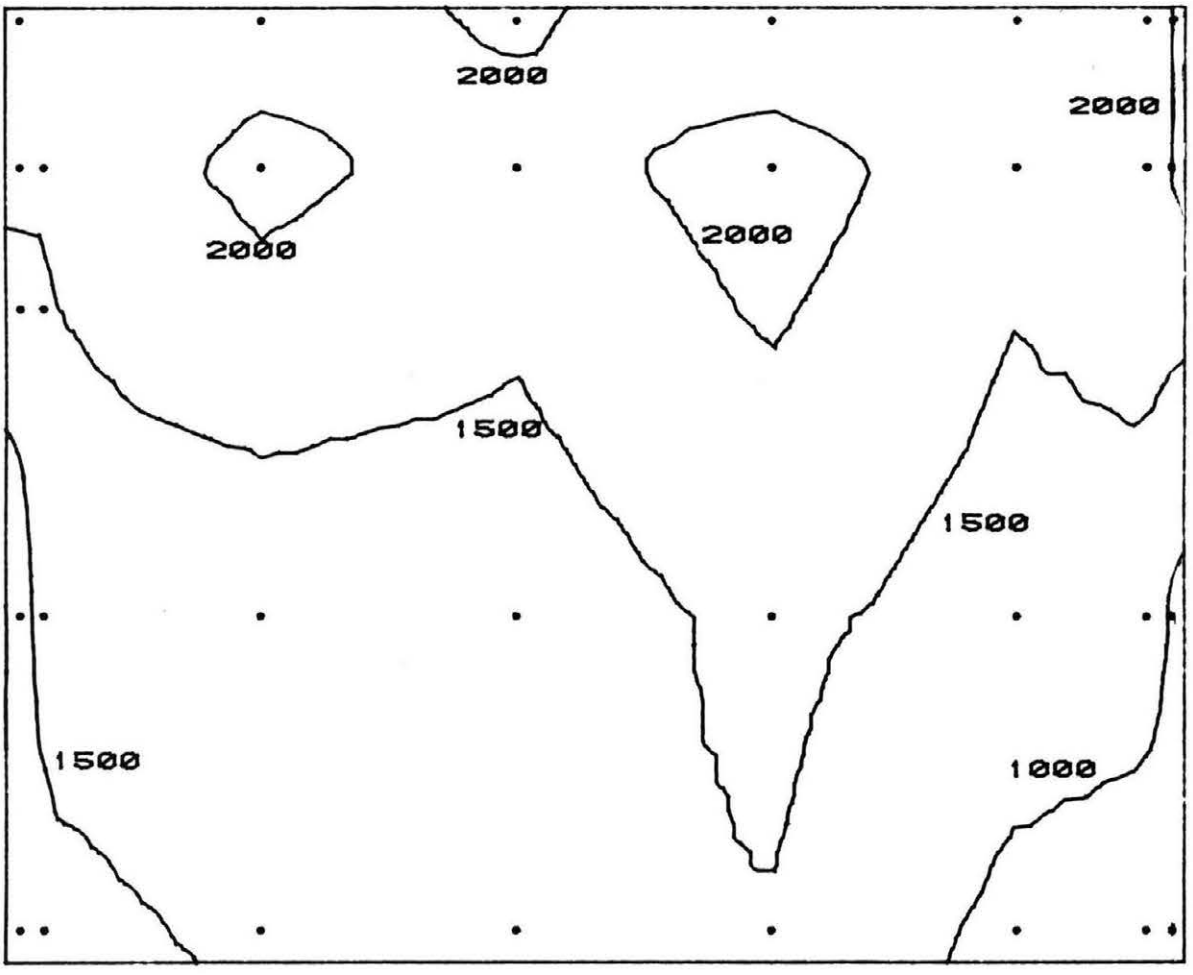

Figure 10B. Peak Pressure Contours on the Building for Cladding Loads

EAST TOWER

DEVELOPED VIEW
SOUTH END
PEAK POSITIVE CLADDING LOADS (PA)
FOR 50-YEAR RECURRENCE WIND
REFERENCE PRESSURE = 2170 PA

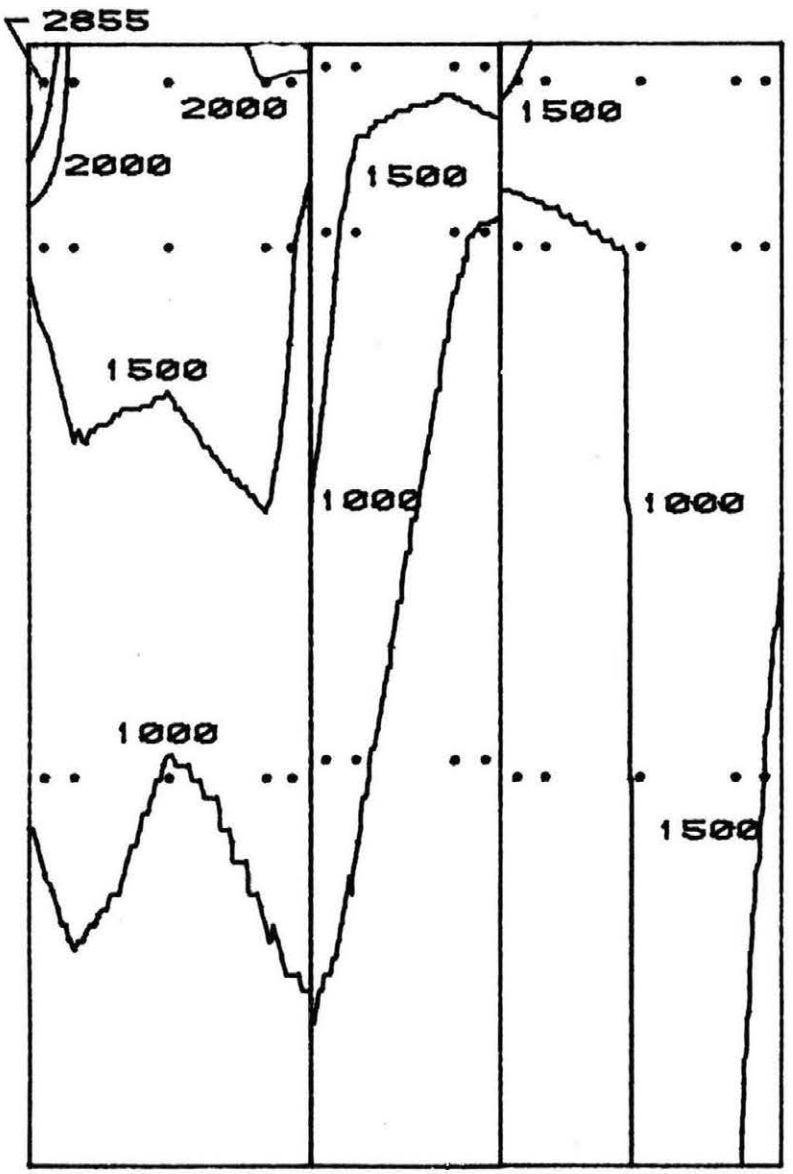

Figure 10C. Peak Pressure Contours on the Building for Cladding Loads

EAST TOWER

NORTHEAST ELEVATION
PEAK POSITIVE CLADDING LOADS (PA)
FOR 50-YEAR RECURRENCE WIND
REFERENCE PRESSURE = 2170 PA

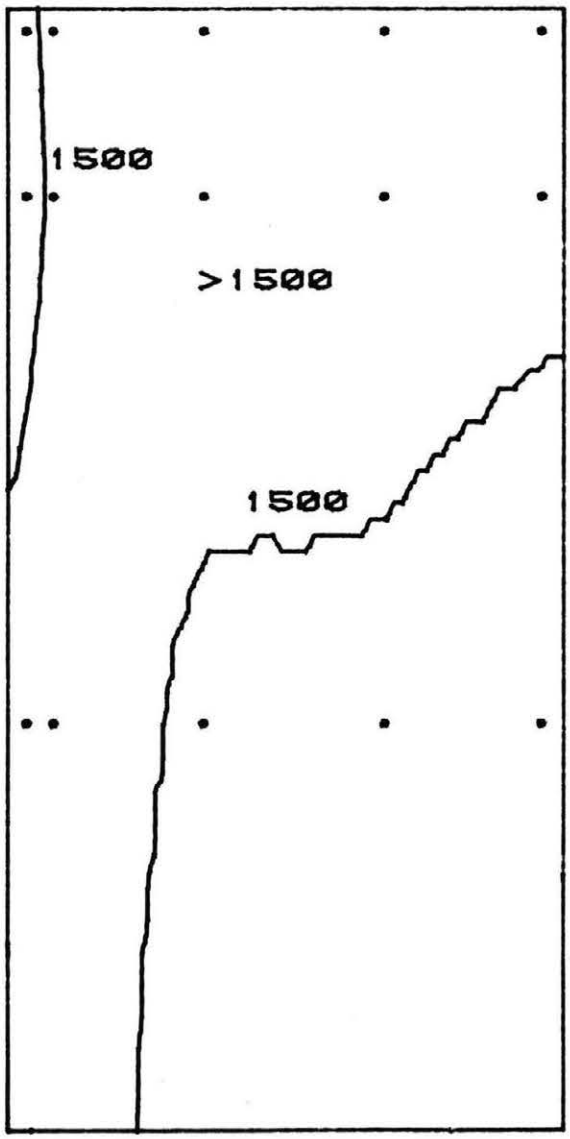

Figure 10D. Peak Pressure Contours on the Building for Cladding Loads

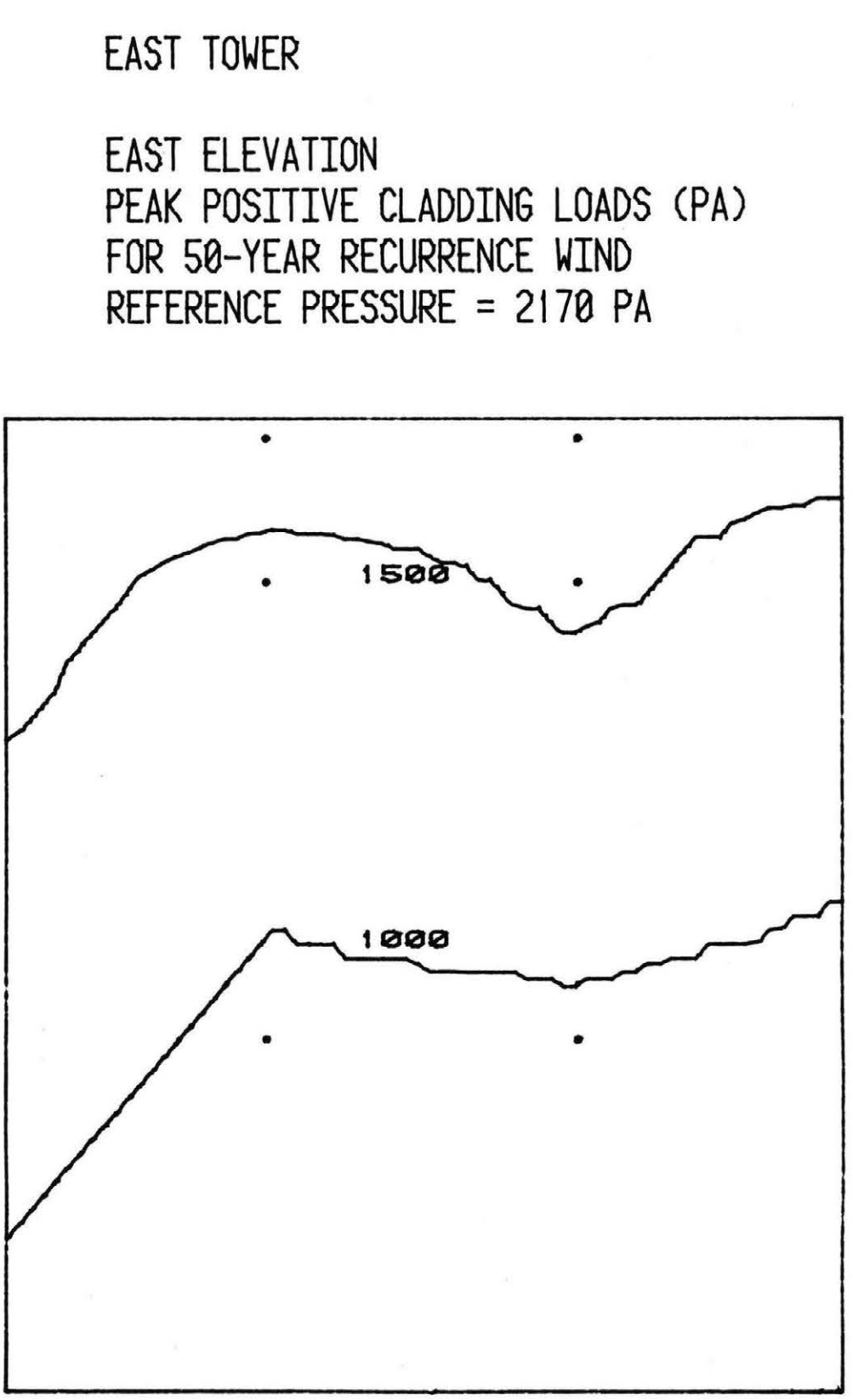

Figure 10E. Peak Pressure Contours on the Building for Cladding Loads

EAST TOWER

SOUTHEAST ELEVATION
PEAK POSITIVE CLADDING LOADS (PA)
FOR 50-YEAR RECURRENCE WIND
REFERENCE PRESSURE = 2170 PA

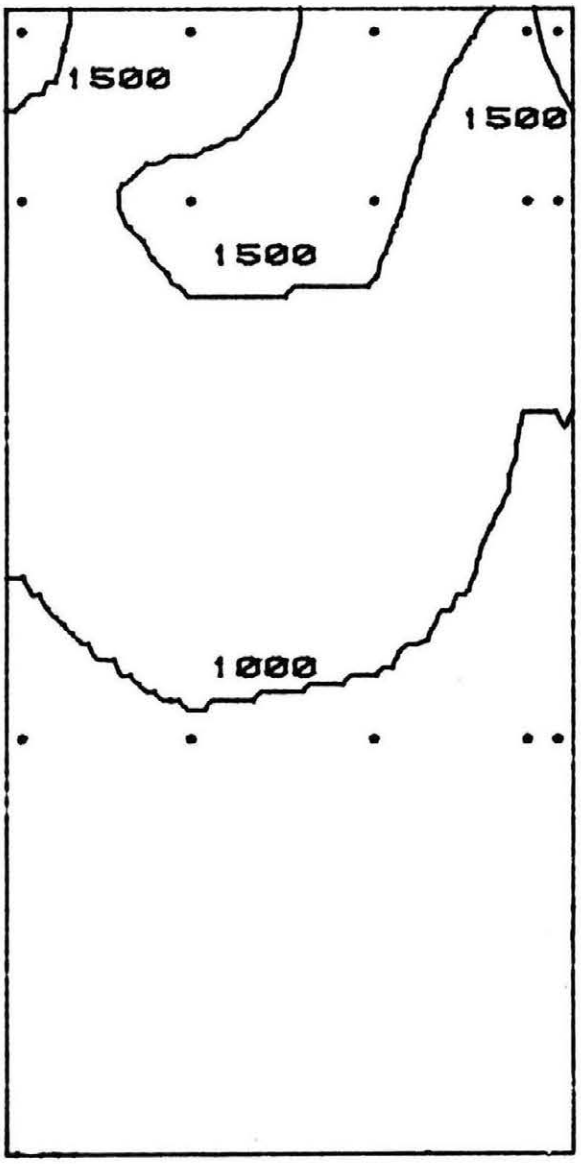

Figure 10F. Peak Pressure Contours on the Building for Cladding Loads

BASE

NORTH ELEVATION
PEAK NEGATIVE CLADDING LOADS (PA)
FOR 50-YEAR RECURRENCE WIND
REFERENCE PRESSURE = 2170 PA

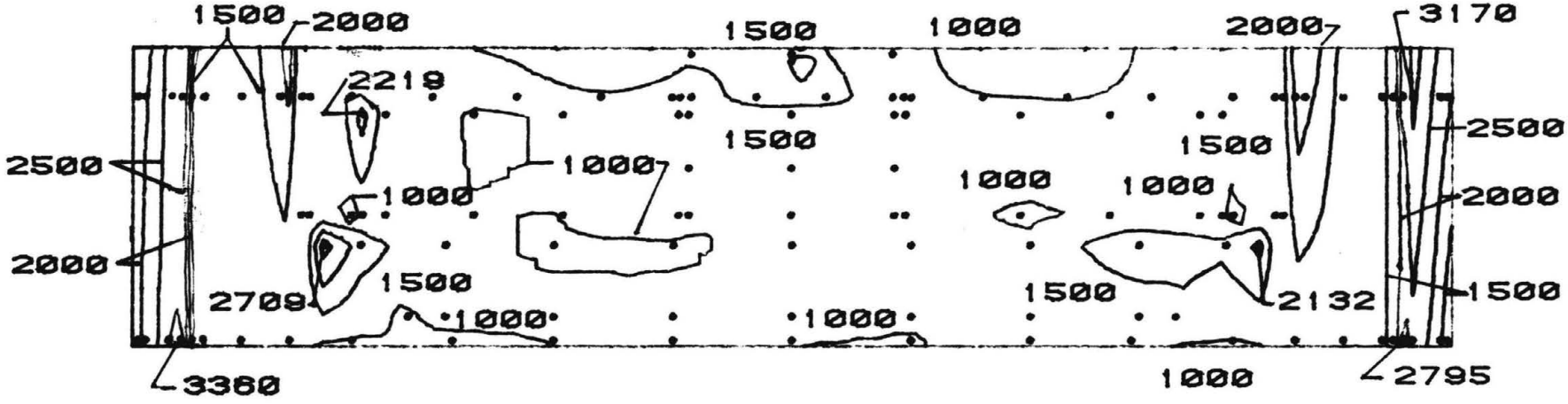

Figure 10G. Peak Pressure Contours on the Building for Cladding Loads

BASE

WEST ELEVATION
PEAK NEGATIVE CLADDING LOADS (PA)
FOR 50-YEAR RECURRENCE WIND
REFERENCE PRESSURE = 2170 PA

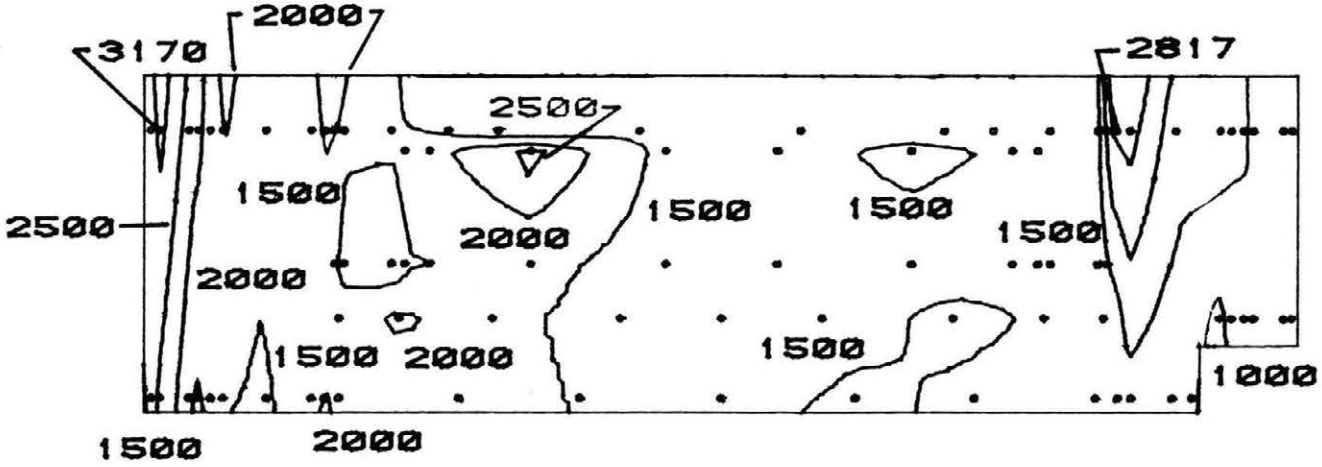

Figure 10H. Peak Pressure Contours on the Building for Cladding Loads

BASE

SOUTH ELEVATION
PEAK NEGATIVE CLADDING LOADS (PA)
FOR 50-YEAR RECURRENCE WIND
REFERENCE PRESSURE = 2170 PA

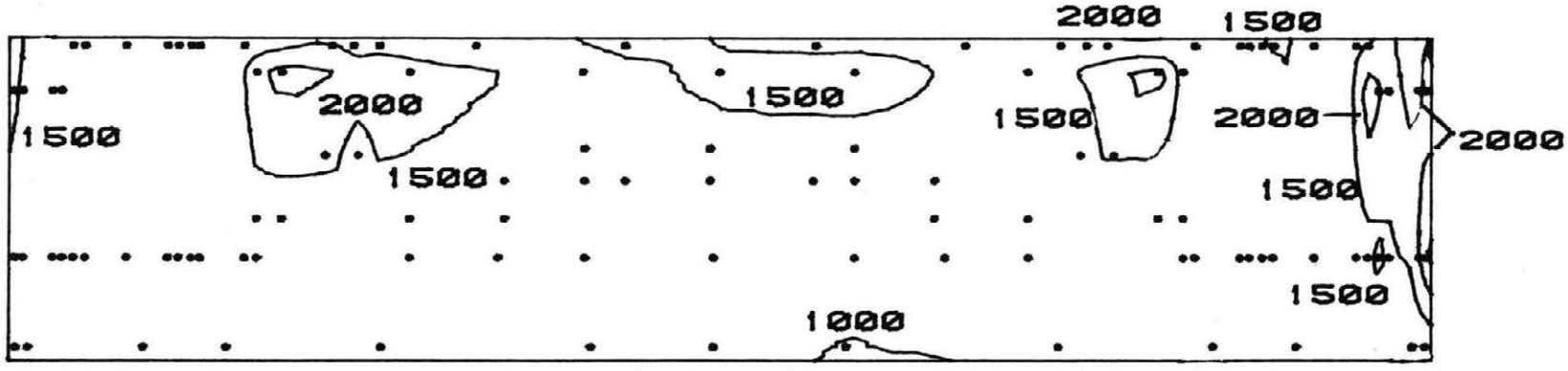

Figure 10I. Peak Pressure Contours on the Building for Cladding Loads

BASE

EAST ELEVATION
PEAK NEGATIVE CLADDING LOADS (PA)
FOR 50-YEAR RECURRENCE WIND
REFERENCE PRESSURE = 2170 PA

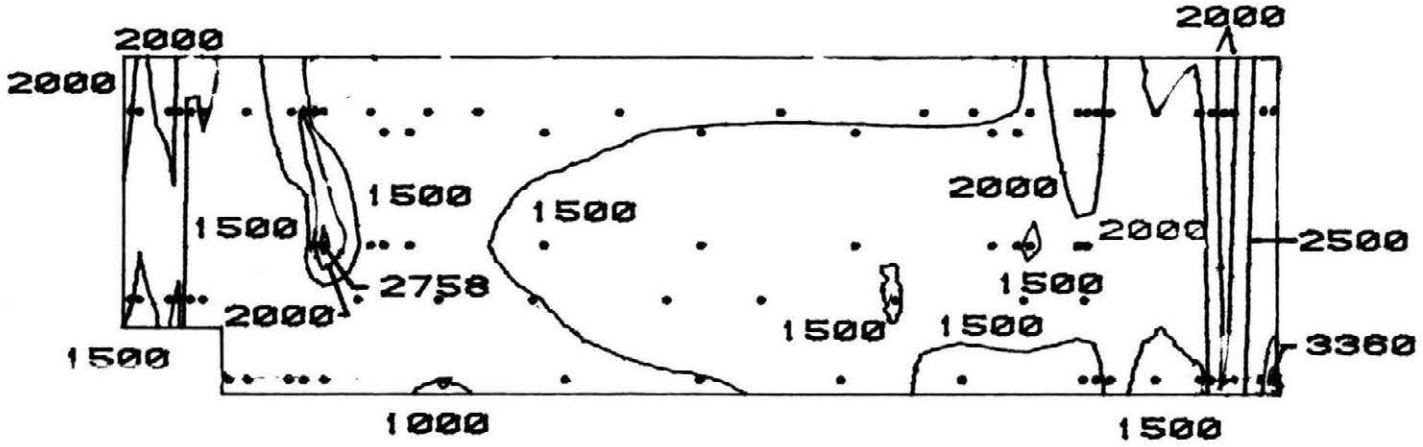

Figure 10J. Peak Pressure Contours on the Building for Cladding Loads

BASE

NORTH ELEVATION
PEAK POSITIVE CLADDING LOADS (PA)
FOR 50-YEAR RECURRENCE WIND
REFERENCE PRESSURE = 2170 PA

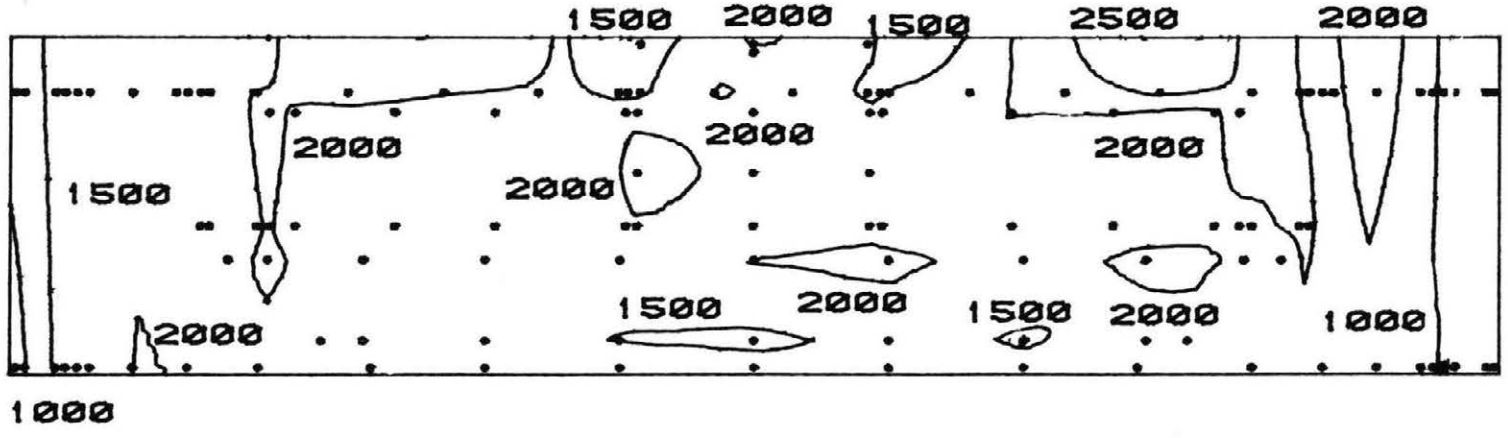

Figure 10K. Peak Pressure Contours on the Building for Cladding Loads

BASE

WEST ELEVATION
PEAK POSITIVE CLADDING LOADS (PA)
FOR 50-YEAR RECURRENCE WIND
REFERENCE PRESSURE = 2170 PA

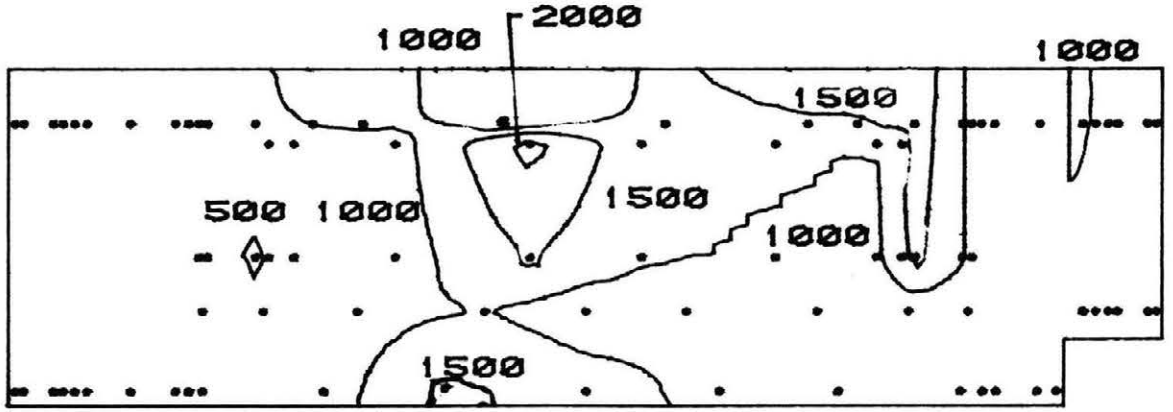

Figure 10L. Peak Pressure Contours on the Building for Cladding Loads

BASE

SOUTH ELEVATION
PEAK POSITIVE CLADDING LOADS (PA)
FOR 50-YEAR RECURRENCE WIND
REFERENCE PRESSURE = 2170 PA

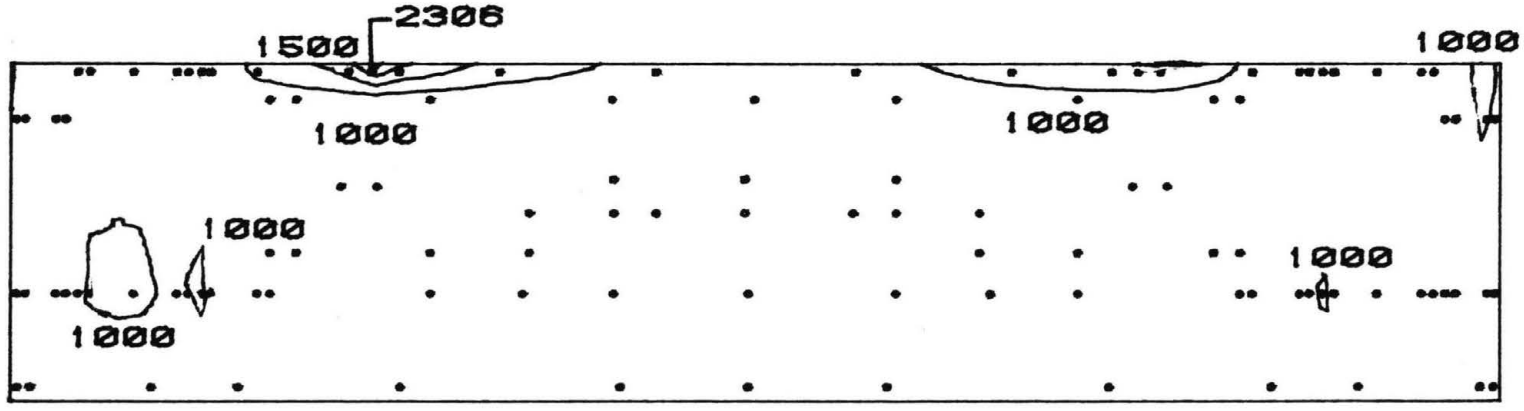

Figure 10M. Peak Pressure Contours on the Building for Cladding Loads

BASE

EAST ELEVATION
PEAK POSITIVE CLADDING LOADS (PA)
FOR 50-YEAR RECURRENCE WIND
REFERENCE PRESSURE = 2170 PA

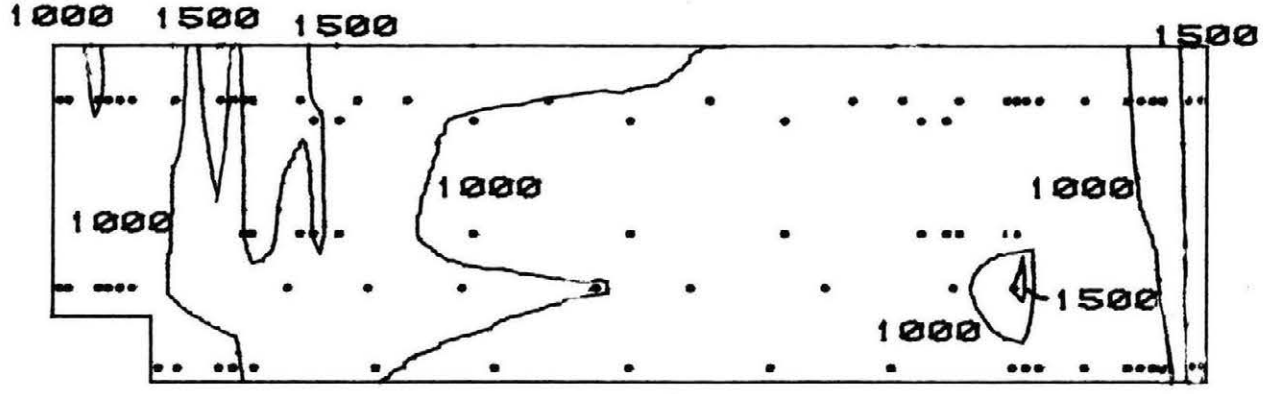

Figure 10N. Peak Pressure Contours on the Building for Cladding Loads

PROJECT #5040 TAIKOO SHING CITYPLAZA (WEST TOWER), HONG KONG

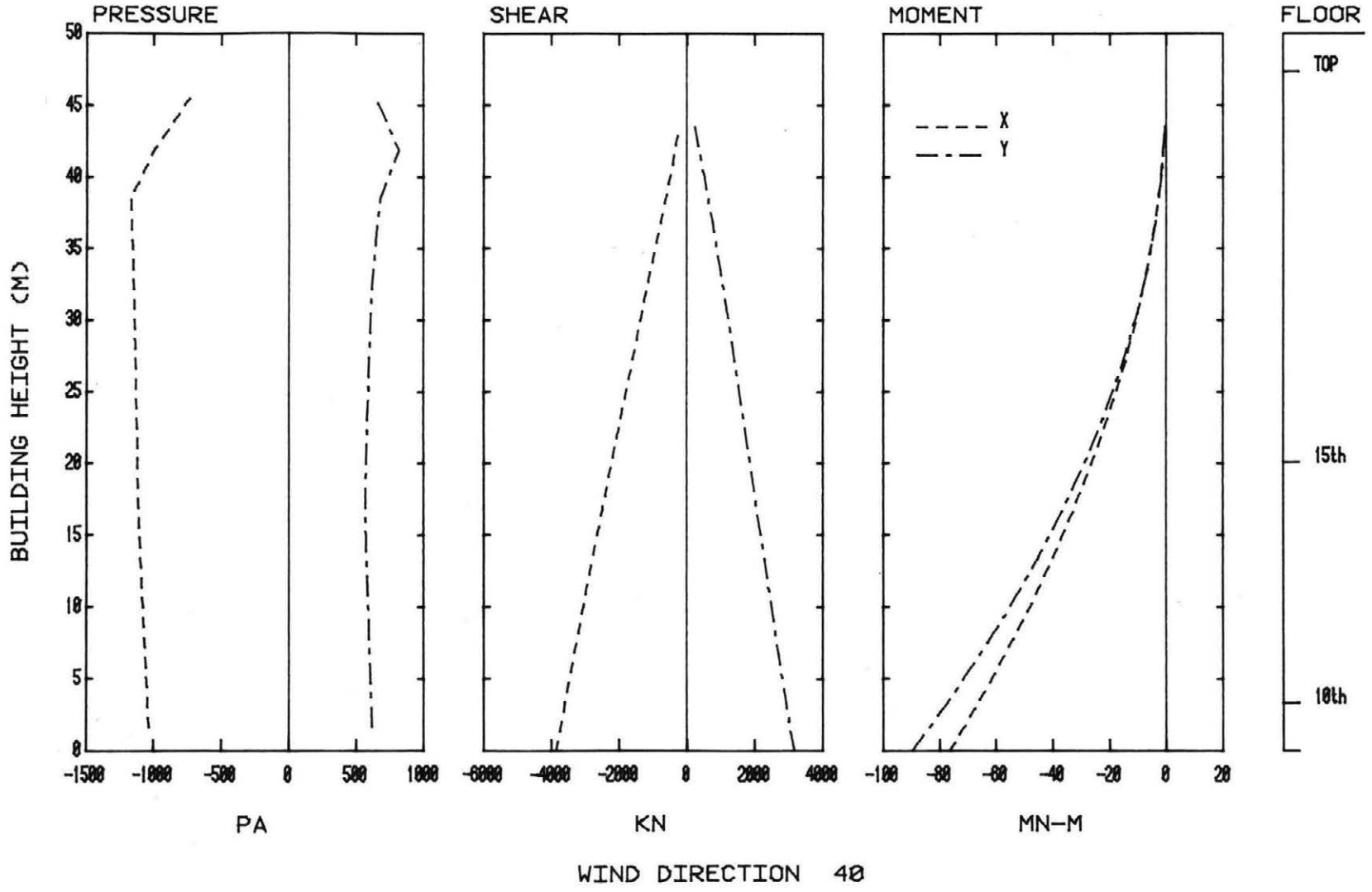

Figure 11. Load, Shear, and Moment Diagrams for Selected Wind Directions

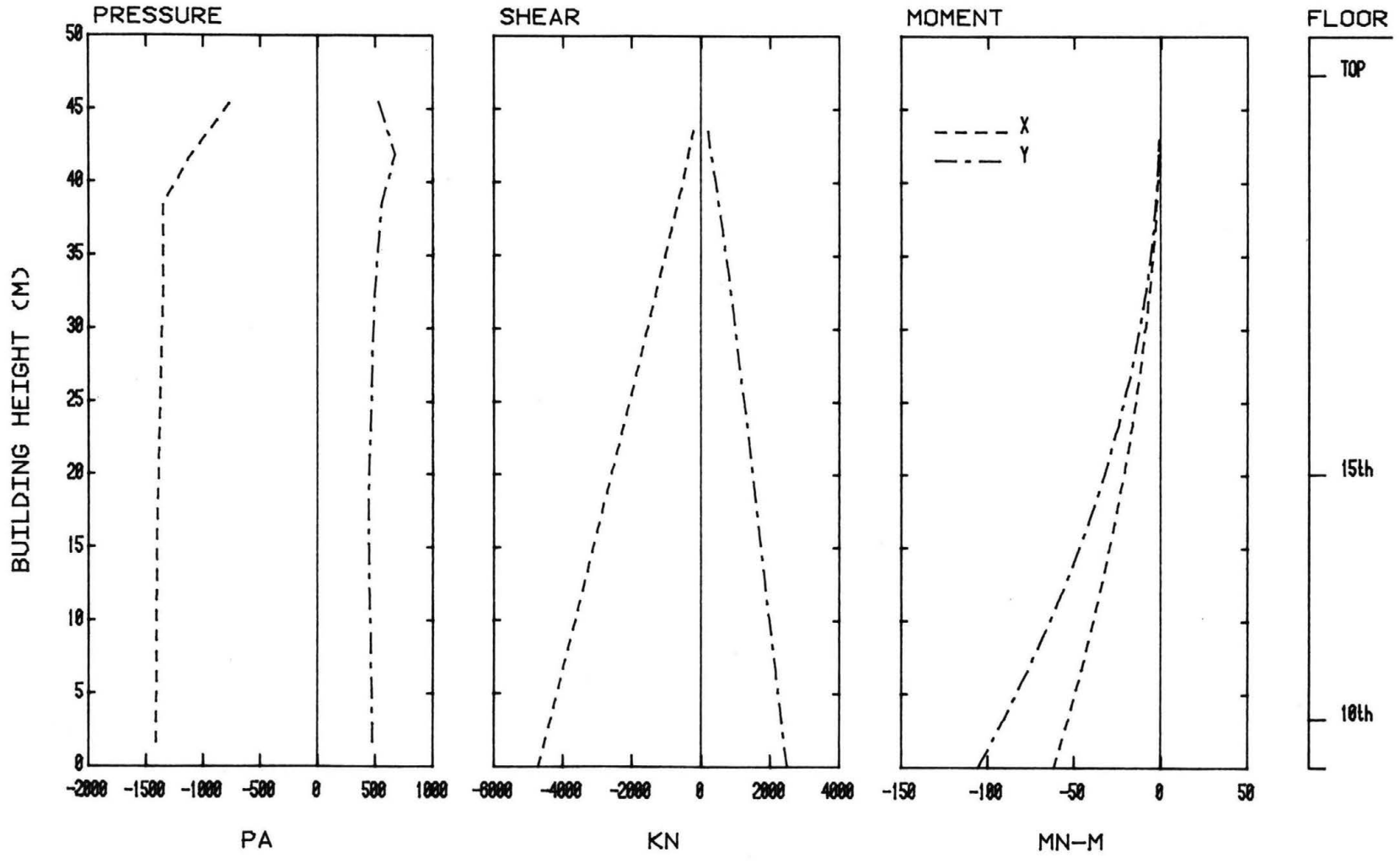

Figure 11. Load, Shear, and Moment Diagrams for Selected Wind Directions

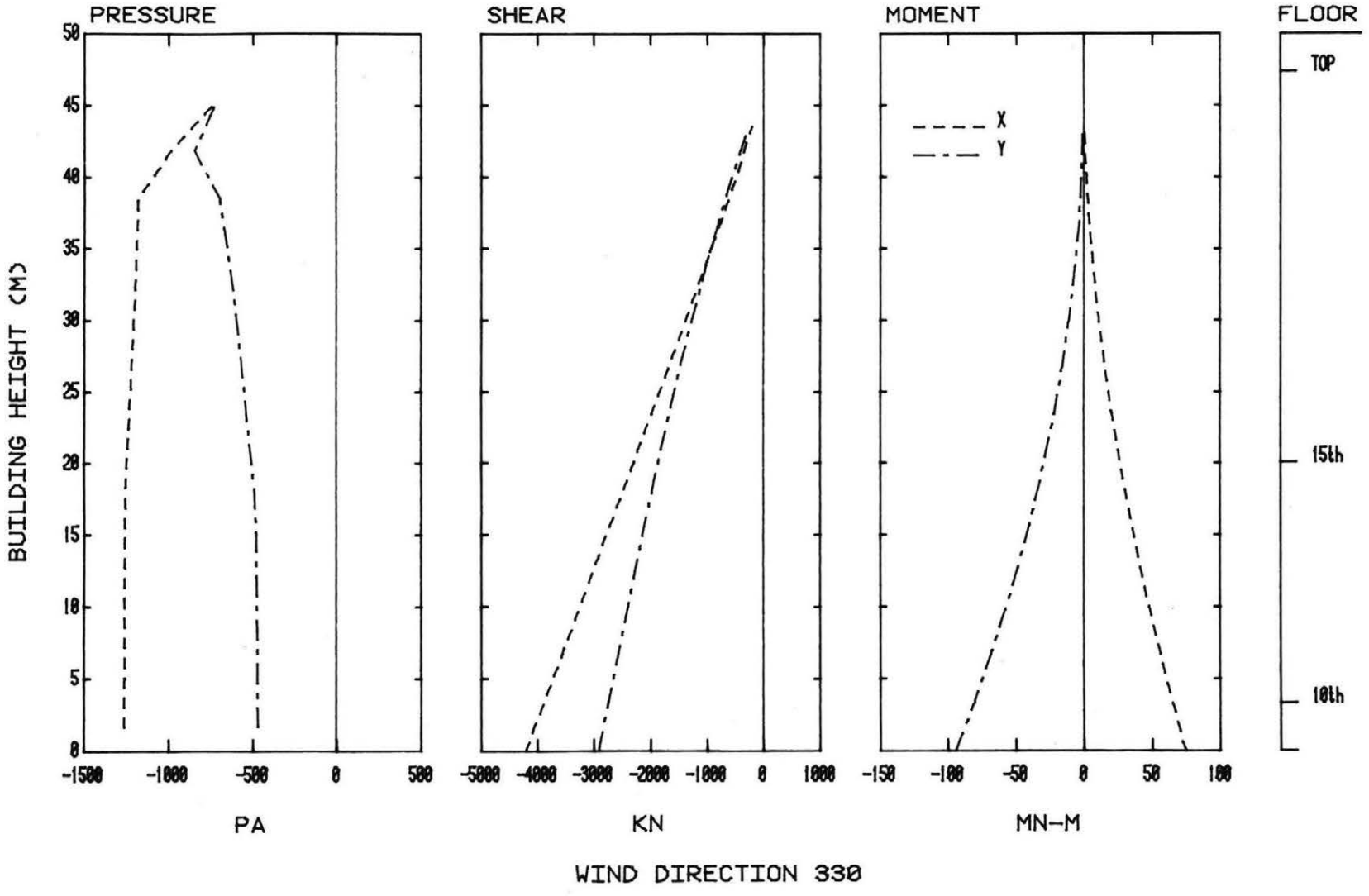

Figure 11. Load, Shear, and Moment Diagrams for Selected Wind Directions

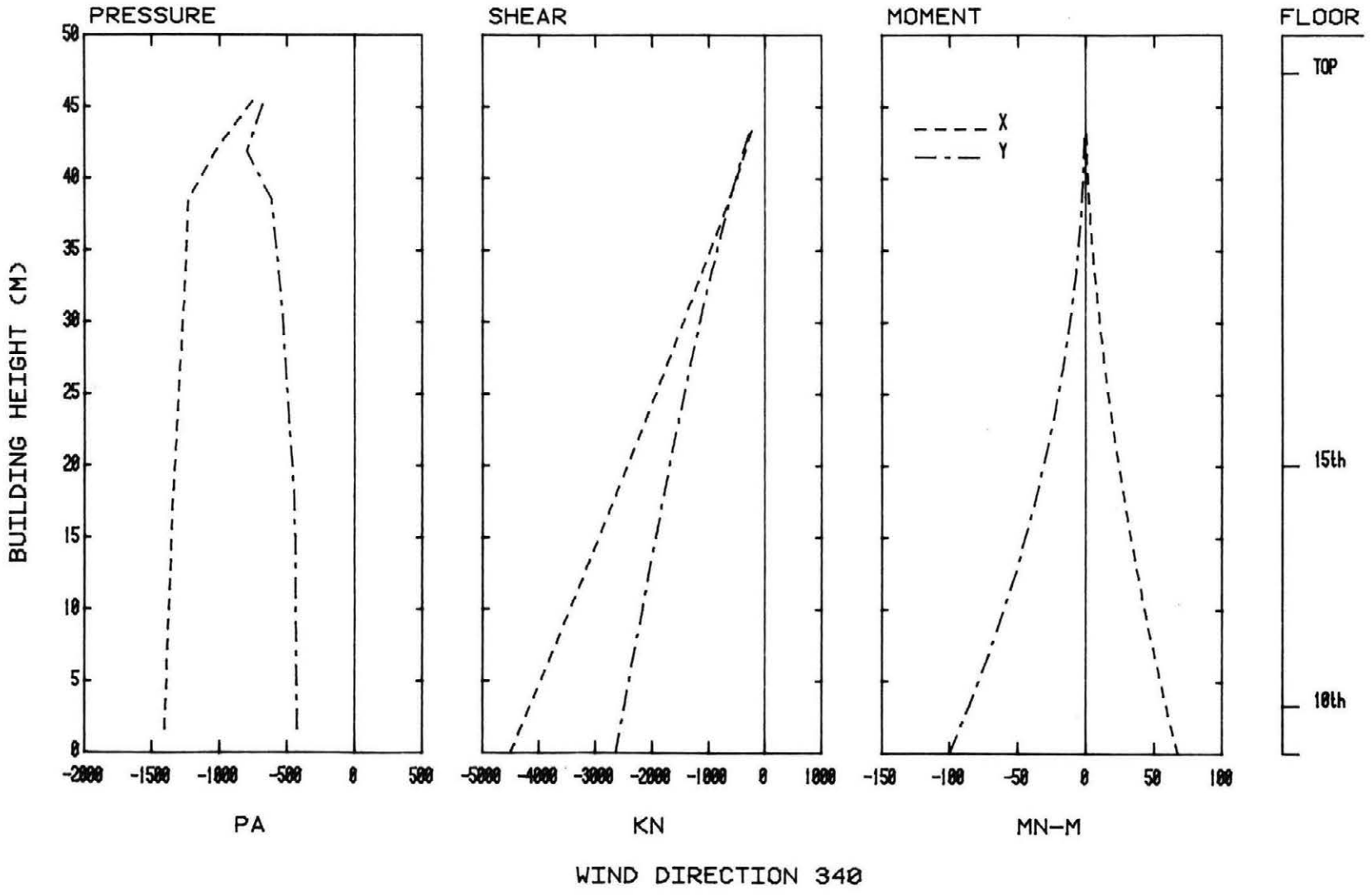

Figure 11. Load, Shear, and Moment Diagrams for Selected Wind Directions

PROJECT #5040 TAIKOO SHING CITYPLAZA (BASE), HONG KONG

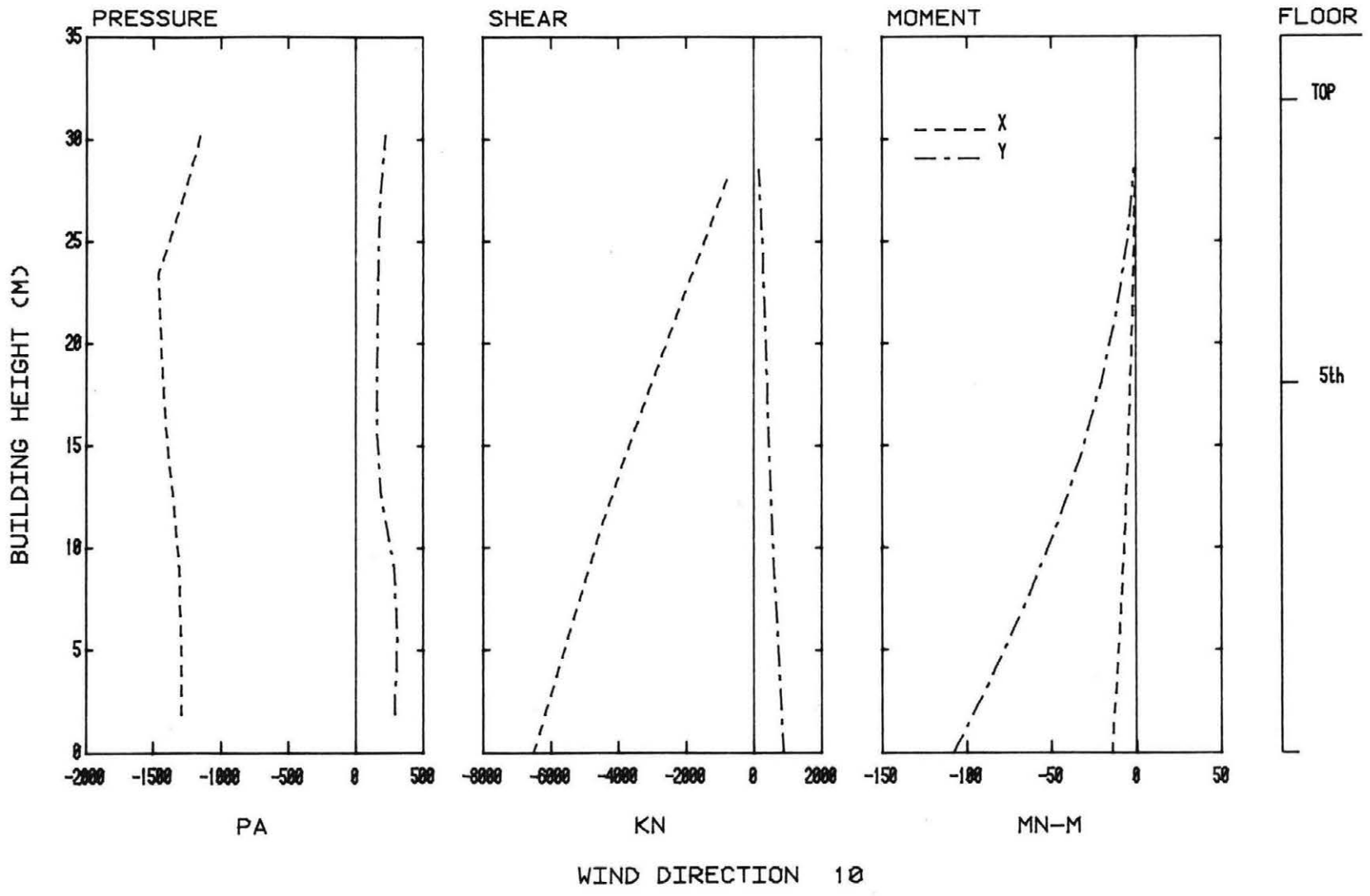

Figure 11. Load, Shear, and Moment Diagrams for Selected Wind Directions

PROJECT #5040 TAIKOO SHING CITYPLAZA (BASE), HONG KONG

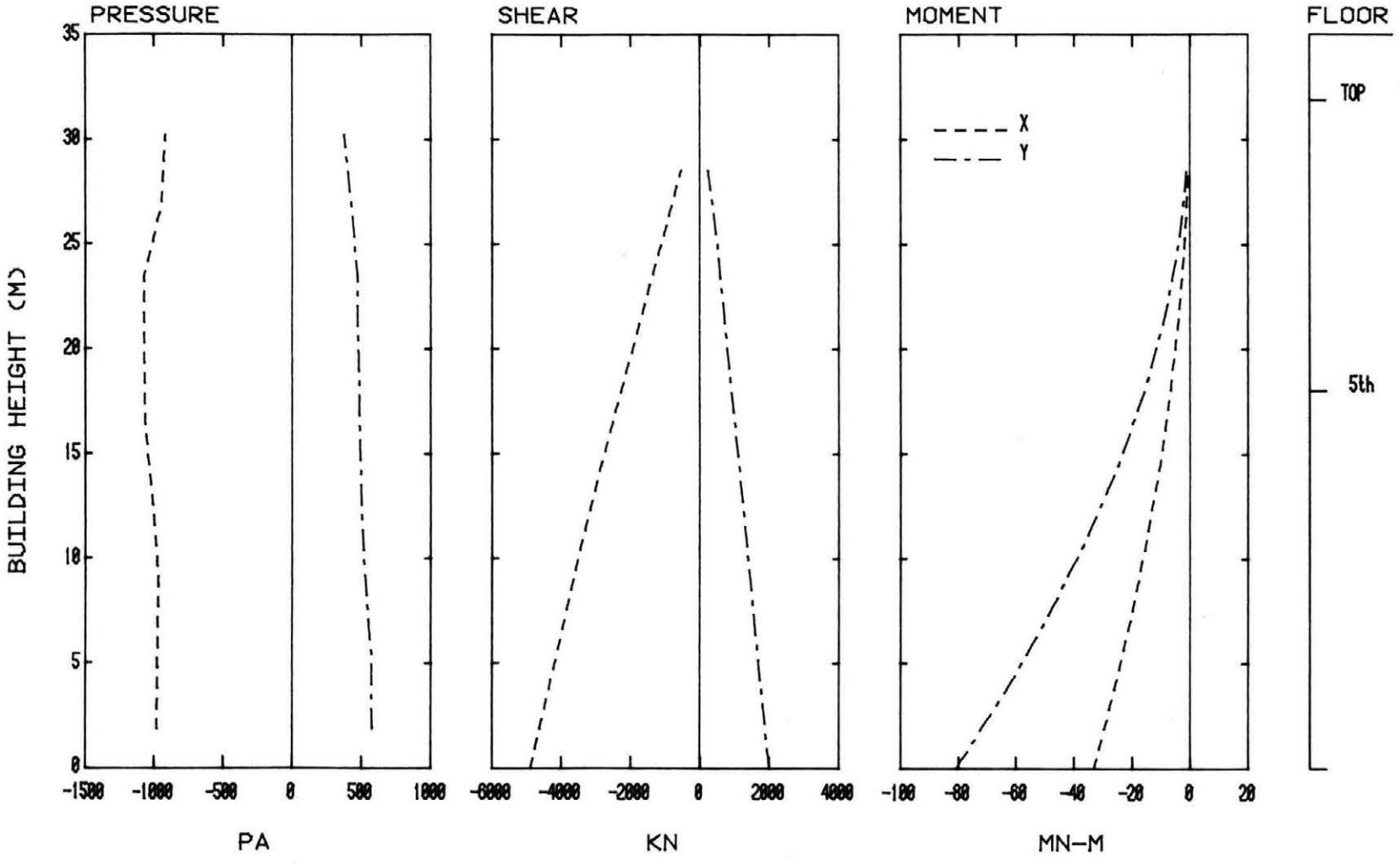

Figure 11. Load, Shear, and Moment Diagrams for Selected Wind Directions